2019-08-08

Investigating the Consequences of DRP1 and Fis1 Mediated Mitochondrial Fission in Colitis: in Pursuit of a Novel Therapeutic Target for IBD

Goudie, Luke

UNIVERSITY OF CALGARY

Investigating the Consequences of DRP1 and Fis1 Mediated Mitochondrial Fission in Colitis: in Pursuit of a Novel Therapeutic Target for IBD

by

Luke Goudie

A THESIS

SUBMITTED TO THE FACULTY OF GRADUATE STUDIES

IN PARTIAL FULFILLMENT OF THE REQUIREMENTS FOR THE

DEGREE OF MASTER OF SCIENCE

GRADUATE PROGRAM IN BIOMEDICAL ENGINEERING

CALGARY, ALBERTA

AUGUST, 2019

Abstract

Since the 1980s, it has been hypothesized that inflammatory bowel disease (IBD) may be tied to insufficient energy production within the intestinal epithelium. In support of this theory, mitochondrial dysfunction has been noted in both IBD patient biopsies and the commonly used dextran sodium sulfate (DSS) murine colitis model. While relatively unexamined in human IBD or animal colitis contexts, evidence obtained from neurological and cardiovascular disease models has shown that unbalanced mitochondrial dynamics, favouring excessive mitochondrial fission, can promote mitochondrial dysfunction and disease. Furthermore, targeted inhibition of two mediators of this maladaptive process, dynamin related protein-1 (DRP1) and mitochondrial fission protein-1 (Fis1), by the novel peptide: P110, has shown therapeutic benefit in both neurodegenerative and cardiovascular disease models. Therefore, previous observations of mitochondrial dysfunction in IBD patients and murine colitis models may be tied to excessive mitochondrial fission, with inhibition of this process by P110 highlighting a potential target for IBD. To test this hypothesis, this study sought to: i) develop protocols for the assessment of mitochondrial function within a murine intestinal epithelial cell line ($IEC^{4.1}$), ii) apply these protocols and other techniques to identify the consequences of DSS±P110 on $IEC^{4.1}$ mitochondrial function, morphology and polarization state and iii) systemically deliver P110 in DSS and DNBS murine colitis models to determine if inhibition of excessive mitochondrial fission could exert anti-colitic benefit. Utilizing the developed O2k protocols, we found that DSS induced functional defects in $IEC^{4.1}$ mitochondria, with P110 co-treatment mitigating some of the observed mitochondrial functional defects. Prophylactic and systemic administration of P110 was found to reduce macroscopic characteristics of both DSS and DNBS colitis in mice. Interestingly, these

macroscopic improvements occurred despite limited changes to the assessed inflammatory markers, suggesting similar disease burden between DSS/DNBS+P110 and their disease counterparts. Results obtained from both the cellular and murine colitis models provides evidence that DRP1-Fis1 mediated mitochondrial fission is a feature of these colitis models and that targeting this interaction with P110 yields anti-colitic benefit. Therefore, this interaction could similarly be occurring in IBD patients and prove to be a novel target for future IBD therapeutics.

Preface

The thesis is formatted as a manuscript-based thesis, with Chapters 3, 4 & 5 containing work that is in preparation for publication submission or currently undergoing review.

Chapter 3 is currently being prepared for submission. Goudie, L., McKay, D.M, Shearer, J. Assessment of mitochondrial function in intestinal epithelial cells: a novel tool to explore mitochondrial involvement in inflammatory bowel disease.

Chapter 4 & 5 contain work that is presently submitted. Mancini, N.L., † Goudie, L., † Xu, W., Rajabi, A.A., Jayme, T.S., Sabouny, R., Wang, A., Ferraz, J., Shutt, T., Shearer, J., McKay, D.M. Systemic delivery of a selective inhibitor of mitochondrial fission to treat colitis.

† Authors contributed equally to work

Acknowledgments

I would like to make special mention to those who have been instrumental in their guidance and support of this project.

For taking the chance on a student with limited research experience and accolades, I would like to thank Dr. Jane Shearer. You are a champion of the student experience, allowing independence in project direction, and guidance when those roads reach dead ends. You understand the importance of life behind research and ensure time off is available for students that need it. I owe much of my personal and experiential growth to you as my mentor and will always appreciate the opportunity you provided me of being a student in the Shearer lab.

I would also like to thank Dr. Derek McKay for co-supervising this project. You have been a great mentor, keeping me honest with my workload and providing me several opportunities to practice and promote my project. I am particularly appreciative of your inclusion of me into your lab, allowing me access to experienced students and lab personnel that allowed this project to reach its full potential

For imparting knowledge of mitochondrial processes and function I would like to thank my committee member: Dr. Tim Shutt. Your advice has provided several interesting directions for this project and allowed me to write this thesis from a more holistic perspective.

In addition to my supervisory committee, there are a few professors and post-doctoral colleagues I would like to recognize. Dr. Mark Ungrin for highlighting important details when experimenting with therapeutics and for forcing a welcome change on how I scrutinize and interpret my data. Dr. Wayne Giles for his help and support in my initial pursuit of doing graduate

studies. Dr. Lisa Daroux-Cole for the opportunity to help teach her course and be a guest lecturer. Dr. Fernando Lopes for helping troubleshoot ideas with me on experiments and the opportunity to lecture in your course. Dr. Younghee Ahn for providing guidance on Seahorse mitochondrial analysis.

Finally, I would like to thank previous and existing members of both the Shearer and McKay labs, who have collectively made a difference in my experience as a student through companionship and guidance. From the Shearer lab; Chris Newell, Warren Xu, Dr. Chunlong, Robbyn Madden, Paul Brown, Karen Blote, Anna Thacker, Melanie Trudeau, and Yegor Korchemagin. From the McKay lab: Nicole Mancini, Timothy Jayme, Adam Shute, Susan Wang, Sruthi Rajeev, Andrea Nunez, and Toshio Arai. I would also like to thank students and faculty from: Biomedical Engineering, Kinesiology, the Gastrointestinal Research Group and the Inflammation Research Network, as well as my funding sources: Crohns Colitis Canada, Natural Sciences and Engineering Research Council, Faculty of Graduate Studies and Biomedical Engineering program.

To:

My family, for their unconditional support.

My wife, for fueling my motivation.

My friends, for their companionship.

Table of Contents

List of Tables

List of Illustrations, Figures and Graphics

Lists of Symbols, Abbreviations and Nomenclature

Abbreviation/Symbols	Definition
ADP	Adenosine diphosphate
AMP	Antimicrobial peptides
ATP	Adenosine triphosphate
BAPTA-AM	1,2-bis-(2-aminophenoxy)ethane-N,N,N',N'-tetraacetic acid tetra(acetoxymethyl) ester
Ca^{2+}	Calcium
CCCP	Carbonyl cyanide-m-chlorophenylhydrazine
CD	Crohn's disease
ETF	Electron transferring flavoprotein complex
CI	NADH dehydrogenase
CII	Succinate dehydrogenase
CIII	Ubiquinone bc1-complex
CIV	Cytochrome c oxidase
CoA	Coenzyme A
CO_2	Carbon dioxide
CPT1	Carnitine palmitoyltransferases 1
CPT2	Carnitine palmitoyltransferases 2
DAMPs	Damage associated molecular patterns
DC	Dendritic cell
DMEM	Dulbecco's modified eagle medium
DNA	Deoxyribonucleic acid
DNBS	Dinitrobenzene sulfonic acid
Dnm2	Dynamin 2
DRP1	Dynamin related protein-1
DSS	Dextran sodium sulfate
ER	Endoplasmic reticulum
ETC	Electron transport chain

$FAD/FADH_2$	Flavin adenine dinucleotide
FCCP	Carbonyl cyanide-*4*-(trifluoromethoxy) phenylhydrazone
Fis1	Mitochondrial fission protein 1
FITC	Fluorescein isothiocyanate
GTP	Guanosine triphosphate
H&E	Hematoxylin and eosin
H_2O_2	Hydrogen peroxide
IBD	Inflammatory bowel disease
IEC	Intestinal epithelial cell
IgA	Immunoglobulin-A
IMM	Inner mitochondrial membrane
IMS	Intermembrane space
ISC	Intestinal stem cells
kDa	Kilodalton
LCFA	Long chain fatty acid
MAPK	Mitogen-activated protein kinases
MAX_{OX}	Maximum oxidative phosphorylation
Mff	Mitochondrial fission factor
Mfn1	Mitofusin 1
Mfn1 KO	Mitofusin 1 knockout
Mfn2	Mitofusin 2
MiD49	Mitochondrial dynamics protein kDa 49
MiD51	Mitochondrial dynamics protein kDa 51
MiR05	Mitochondrial respiration solution 05
MPO	Myeloperoxidase
mPTP	Mitochondrial permeability transition pore
mtDNA	Mitochondrial deoxyribonucleic acid
mtROS	Mitochondrial reactive oxygen species
NaBut	Sodium butyrate

NAD^+/NADH	Nicotinamide adenine dinucleotide
$NADP^+$/NADPH	Nicotinamide adenine dinucleotide phosphate
NF-KB	Nuclear factor kappa light chain of activated B-cells
NK	Natural killer cells
NLR	Nuclear binding oligomerization domain-like receptor
NLRP3	NLR pyrin containing domain 3
OCTN1	Organic cation transporter 1
OCTN2	Organic cation transporter 2
OPA1	Optic atrophy protein 1
OMM	Outer mitochondrial membrane
OXPHOS	Oxidative phosphorylation
O2k	Oxygraph-2k
O_2	Oxygen
PalmC	Palmitoylcarnitine
PBS	Phosphate buffered solution
PINK-1	PTEN induced putative kinase 1
PMF	Proton motive force
PRR	Pattern recognition receptor
PTEN	Phosphatase and tensin homologue
P_i	Inorganic phosphate
RCR	Respiratory control ratio
RLR	Retinoic acid inducible gene 1 like receptor
ROS	Reactive oxygen species
SCFA	Short chain fatty acid
SEM	Standard error of the mean
SOD	Superoxide dismutase
SUIT-002	Substrate uncoupler inhibitor titration protocol-002

TAT^{47-57}	HIV-1 transactivator of transcription, amino acid sequence 47-57
TCA cycle	Tricarboxylic acid cycle
TMPD	N,N,N′,N′-tetramethyl-p-phenylenediamine
TNBS	Trinitrobenzene sulfonic acid
TLR	Toll-like receptor
UC	Ulcerative colitis
$\Delta\psi m$	Membrane potential

This fire stolen from heaven, this torch of Prometheus, does not only represent an ingenious and poetic idea, it is a faithful picture of the operations of nature, at least for animals that breathe…… the torch of life lights itself at the moment the infant breathes for the first time, and it does not extinguish itself except at death

Lavioser, A. (1862). Oeuvres de Lavoiser, Imprimerie Imperiale, Paris

Chapter 1: Introduction

1.1. Background

Inflammatory bowel disease (IBD) covers a range of chronic gastrointestinal disorders that evolve from an exaggerated immune response to either commensal or pathogenic intestinal microbes. The relapse-remitting nature of IBD symptoms, potentially severe complications and presence of extraintestinal manifestations, highlight only part of the burden IBD exerts on patients. IBD presentation can vary widely, but typically patients experience diarrhea, weight loss, bloody stool, abdominal discomfort, and fatigue[1]. In aggressive cases, patients can experience narrowing of the bowels or abnormal tunneling from the bowel to the skin[2]. These complications, deemed "strictures" and "fistulas" respectively, often require surgery and can have post-operative recurrence rates as high as 44 - 55% after 10 years[2,3]. Patients with severe cases, that do not respond to medication or surgery, often undergo colon removal by colectomy, forever changing their quality of life[4,5]. Symptoms may also manifest outside of the underlying bowel disease, affecting almost every organ of the body and in some cases, present a greater threat to the patients well-being[6]. These "extraintestinal manifestations" can be found in approximately 1/3 of IBD patients[6]. IBD patients also bear a significantly greater risk of colon cancer[7].

The high comorbidities, chronic nature, and heterogeneity of both symptoms and treatment make IBD a particularly expensive disease. Within Canada, IBD treatment and management exhibits a large financial toll on the public health care system. Studies examining the prevalence of Canadian IBD cases from 2005 - 2012 have suggested that approximately 0.5 - 0.67% of the Canadian population have IBD[8,9]. In 2012, direct costs associated with IBD patients were predicted to be approximately 1.2 billion dollars for the Canadian public healthcare system[8]. In addition to these costs, management and treatment of extraintestinal manifestations or complications could

mean the direct healthcare cost of IBD is much higher. Recent data also suggests that the prevalence of pediatric IBD cases is increasing, requiring longer care and management than the typical disease onset within the second and third decade[10]. In Alberta specifically, estimates suggest that by the year 2025, the number of IBD patients could increase by up to 70%[11].

Attempts to resolve aberrant inflammation in IBD patients typically requires immunosuppressive treatments in order to induce remission and limit tissue damage. The utilization of monoclonal antibody treatments, in particular, has allowed for significant progress to be made during IBD treatment. However, patients can be immediately unresponsive to monoclonal antibody treatments or become refractory with continuous administration[3,5]. Other immunosuppressive agents for IBD, (corticosteroids, thiopurines) can also prove ineffective at the start of treatment or become ineffective over time[3,5]. Additionally, complications like infection or disease susceptibility can be introduced with these immunosuppression agents, ie: osteoporosis and corticosteroids[6]. Therefore, examining potential targets and pathways that operate alternative to current immunosuppressive treatments, could yield novel therapeutics for the management and/or treatment of IBD[12].

Since both mitochondrial function and dysfunction affect reactive oxygen species (ROS) production, cellular bioenergetics and cell death pathways, targeting mitochondria and mitochondrial associated processes may present a good candidate for therapeutic interventions. Indeed, recent evidence suggests that inhibiting excessive mitochondrial division, otherwise known as mitochondrial fission, could provide therapeutic potential in inflammatory diseases like IBD. Inhibition of two mediators of excessive mitochondrial fission: dynamin-related protein-1 (DRP1) and mitochondrial fission protein-1 (Fis1), by the peptide P110, has been found to exert therapeutic benefits within several animal disease models representative of the following human

diseases: multiple sclerosis, Parkinson's, Huntington's, myocardial infarction, amyotrophic lateral sclerosis and pulmonary arterial hypertension[13-18]. P110 has also demonstrated therapeutic benefit *in-vitro* with cells isolated from patients that had either amyotrophic lateral sclerosis, Huntington's or Alzheimer's[17-19]. More specifically, P110 was able to limit mitochondrial dysfunction based on improvements in mitochondrial function, ROS production, and cell death[17,18]. Interestingly, several of these same mitochondrial related consequences have been reported in IBD patients and animal colitis models, suggesting that P110, could prove useful in limiting colitis[20].

1.2. Purpose of Research

The successful use of P110, as a therapeutic in heart and brain animal models, provides evidence that mitochondrial fission is an inherent feature in the development and progression of certain disease pathologies[13-19]. However, there remains a paucity of research examining mitochondrial dynamics and mitochondrial function within the context of colitis and IBD. Therefore, this project hopes to determine if inhibition of excessive mitochondrial fission could present a novel therapeutic pathway for the treatment of murine colitis and ultimately serve as a potential treatment option for human IBD.

1.3. Aims

1. To develop a protocol for the assessment of functional changes within specific mitochondrial complexes and pathways for the murine intestinal epithelial cell line: $IEC^{4.1}$.

2. To determine if DSS induces mitochondrial dysfunction in the $IEC^{4.1}$ cell line and if inhibition of DRP1 and Fis1 mediated fission can reduce mitochondrial dysfunction as assessed by changes in mitochondrial function, morphology and membrane potential.

3. To identify if systemic delivery of P110 reduces colitis manifestation in both dextran sodium sulfate (DSS) and dinitrobenzene sulfonic acid (DNBS) mouse models of colitis according to macroscopic disease analysis and readouts of inflammation.

1.4. Hypotheses

i) With the *in-vitro* model, we hypothesize that DSS will induce mitochondrial dysfunction and that inhibition of excessive mitochondrial fission by P110 will ameliorate DSS induced damage to mitochondrial networks.

ii) With the *in-vivo* model, we hypothesize that P110 administration will reduce colitis manifestation within both DSS and DNBS mouse models.

1.5. Thesis Composition

This thesis is composed of 7 Chapters. Chapter 1 provides a brief outline of the significance of the research project and both the aims and hypothesis guiding the project. Chapter 2 reviews literature on mitochondrial physiology and function, intestinal physiology and mitochondrial involvement, inflammatory bowel disease and molecular inhibition of excessive mitochondrial fission. Chapter 3 covers the development of the respirometric techniques utilized within the thesis. Chapter 4 details evidence of both DSS and P110's effect on mitochondrial function in an *in-vitro* murine epithelial cell model. Chapter 5 examines the therapeutic use of P110 *in-vivo* through two commonly employed murine colitis models. Chapter 6 discusses how the results support or disprove the underlying hypothesis of the thesis. Chapter 7 provides a summary of key findings, highlights the limitations of the study and discusses future directions.

1.6. Statement of Contribution

In Chapter 4, Mancini, N. L. performed the mitochondrial morphology quantification and scoring. In Chapter 5, both Mancini, N. L., and Xu, W., helped in conducting animal trials, histology preparation and data collection (weight change, colon length, blood smear).

Chapter 2
Literature Review

2.1. Mitochondrial Physiology and Function

2.1.1. Mitochondrial Anatomy

Within the mitochondria, the separation of distinct compartments by membranes is essential for proper mitochondrial function. Two membranes: the outer mitochondrial membrane (OMM) and inner mitochondrial membrane (IMM) mediate the separation of mitochondrial compartments into the intermembrane space (IMS) and mitochondrial matrix (Figure 2.1)[21]. The semi-permeable OMM allows for the diffusion of ions and small molecules from the cytosol to the IMS, while also preventing the release of larger proteins like cytochrome c from the IMS[21]. The OMM also tethers the mitochondria to the endoplasmic reticulum (ER) thereby providing a bridge for calcium (Ca^{2+}) signaling between the two organelles[22]. In contrast to the OMM, the IMM is mostly impermeable, only allowing the transfer of specific metabolites and ions through protein complexes and transporters[21]. Another difference is that the IMM is highly convoluted, containing several invaginations called cristae (Figure 2.1)[21]. At these cristae, several key membrane complexes oxidize metabolic intermediates to release protons and electrons, forming an electron transport chain (ETC) (Figure 2.1)[21]. These intermediates: nicotinamide adenine dinucleotide (NAD^+ oxidized, NADH reduced) and flavin adenine dinucleotide (FAD oxidized, $FADH_2$, reduced) are generated through the "citric acid cycle"[21].

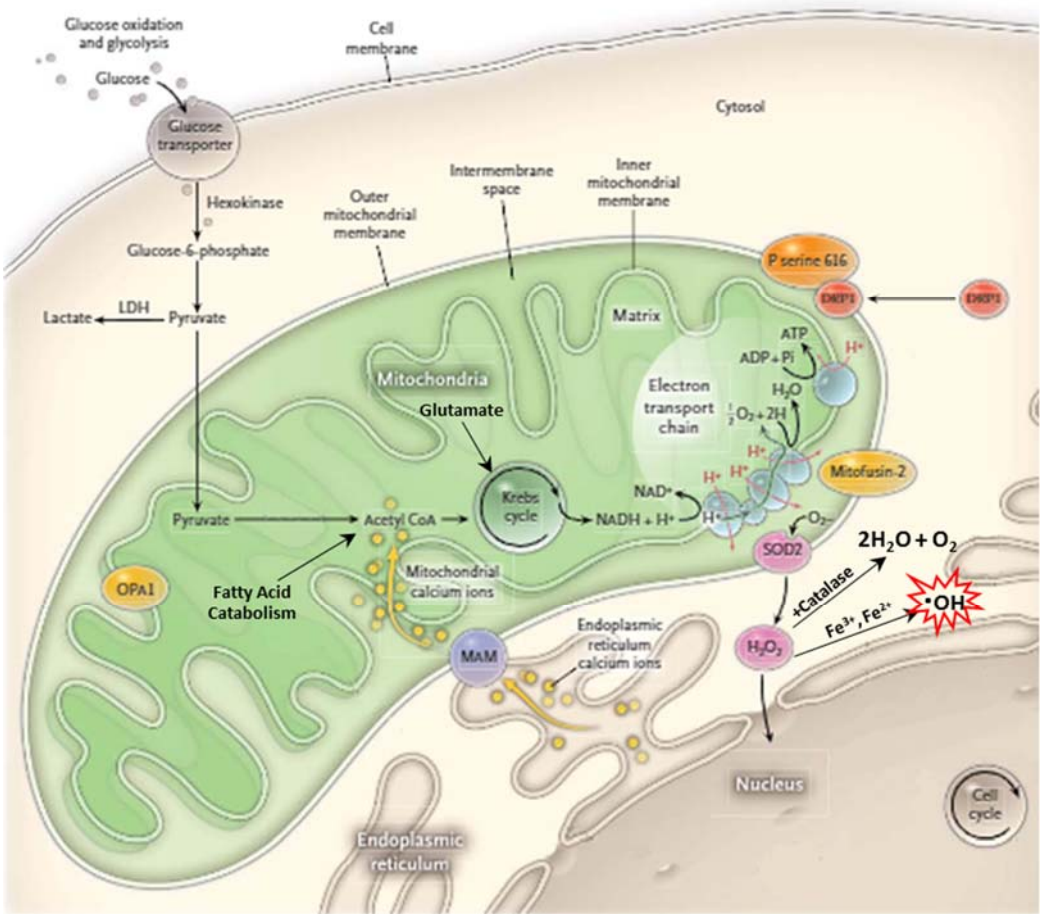

Figure 2.1: Anatomical representation of mitochondria with key processes. Adapted from Longo & Archer (2013). *The New England Journal of Medicine*[23].

2.1.2. Glycolysis

Glycolysis is an evolutionary conserved metabolic process necessary for the initial oxidation of glucose[24]. In eukaryotic cells, the process is unique because it can occur both in the presence (aerobic glycolysis) and absence of oxygen (anaerobic glycolysis/fermentation). For both aerobic and anaerobic glycolysis, NAD^+, glucose and adenosine triphosphate (ATP) molecules are invested to produce pyruvate, NADH, protons and additional ATP[25]. Upon completion of the reaction, NAD^+ is regenerated by different mechanisms for aerobic and anaerobic glycolysis[24]. During aerobic glycolysis, NADH can transfer its electrons and protons

to cytosolic oxaloacetate or dihydroxyacetone forming malate or glycerol-3-phosphate[25]. The malate and glycerol-3-phosphate can then enter the mitochondria and be oxidized by mitochondrial NAD^+ or FAD to make either NADH or $FADH_2$[25]. For anaerobic glycolysis, no mitochondrial intervention is required and instead, NAD^+ is regenerated by reducing pyruvate into lactate[25]. The flexibility of glycolysis to operate under both anaerobic and aerobic conditions is key to meeting the energetic demands of tissues, like skeletal muscle, that often shift into states of anoxia.

2.1.3. Beta Oxidation

The oxidation of fats and fatty acids is a critical bioenergetic pathway for numerous tissues, generating a significant amount of energy and metabolites[26,27]. This mitochondrial based process, known as "beta oxidation", is important for maximizing the transfer of potential chemical energy from fats to energy intermediates like NADH and $FADH_2$. In order for cytosolic long chain fatty acids (LCFA) to enter the mitochondrial IMS, these fatty acids must be modified into their fatty acyl-coenzyme A (acyl-CoA) moieties, by the action of acyl-CoA synthase and one ATP molecule (Figure 2.2)[26,27]. Removal of CoA and replacement with carnitine by carnitine palmitoyltransferases (CPT1) is also required for mitochondrial import from the IMS to the mitochondrial matrix (Figure 2.2)[26,27]. Through the action of carnitine acyl transporters, the fatty acylcarnitine molecules may pass into the mitochondrial matrix for beta oxidation (Figure 2.2)[26,27]. Within the mitochondrial matrix, an inner CPT (CPT2) removes the carnitine and adds the CoA back, forming a fatty acyl CoA molecule (Figure 2.2)[26,27].

In contrast to LCFA, short chain fatty acids (SCFA) that range from 1-6 carbons, have been shown to enter the cytosol by either non-ionic diffusion or through the exchange of protons

and ions (Cl^-, HCO_3, Na^+)[28]. SCFAs may then be converted into their acyl-CoA moieties within the mitochondria matrix, requiring no carnitine transport for mitochondrial import[29].

Fatty acyl CoA molecules are then oxidized within the mitochondrial matrix in a cyclic manner by several enzymes specific to the fatty acyl CoA chain length (Figure 2.2)[26,30]. Each cyclic oxidation of the original fatty acyl CoA molecule generates a two-carbon acetyl-CoA chain and one NADH (Figure 2.2)[26,30]. These acetyl-CoA molecules can then be utilized during the tricarboxylic acid (TCA) cycle (Figure 2.3)[26,30]. Additionally, during the first step of these cyclic reactions, electrons and protons are released and transferred to the electron transferring flavoprotein complex (ETF) and subsequently onto coenzyme Q_{10} for use in the ETC (Figure 2.2)[26,28].

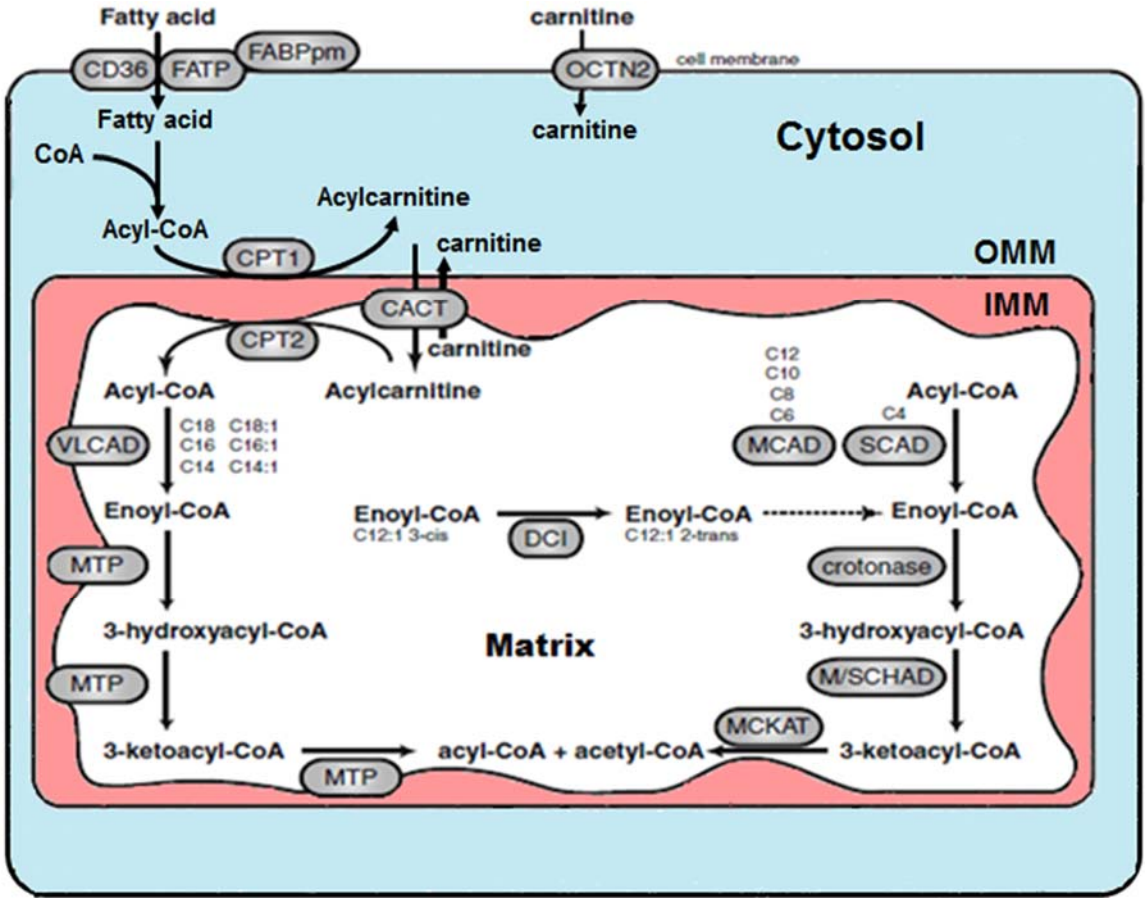

Figure 2.2: Diagrammatic representation of mitochondrial LCFA import and beta-oxidation. Adapted from Houton & Wanders. (2010). *Journal of Inherited Metabolic Disorders*[30]. FATP: fatty acid transport proteins, CACT: carnitine acylcarnitine translocase, VLCAD: very long chain acyl-CoA dehydrogenase, MTP: mitochondrial trifunctional protein, MCAD: medium chain acyl-CoA dehydrogenase, SCAD: short chain acyl-CoA dehydrogenase, DCI: dodecanoyl-CoA delta isomerase, M/SCHAD: medium/short chain hydroxyacyl-CoA dehydrogenase, MCKAT: medium chain 3-ketoacyl-CoA thiolase.

2.1.4. Oxidative Phosphorylation

The TCA or citric acid cycle provides a crucial convergent point in the metabolism of carbohydrates, proteins, and fats, generating NADH and $FADH_2$ for the ETC[31]. Many different metabolites from previous catabolic processes, including acetyl-CoA and α-ketoglutarate, provide the fuel for the TCA cycle[31]. Entry of acetyl-CoA to the TCA cycle from either beta oxidation or glycolysis leads to the formation of citrate by its reaction with water and oxaloacetate (Figure 2.3)[31]. Several other reactions then transform and oxidize this citrate molecule, releasing electrons and protons necessary for the reduction of NAD^+ and FAD into NADH and $FADH_2$ (Figure 2.3)[31]. Other products from the TCA cycle include carbon dioxide (CO_2), guanosine triphosphate (GTP) and most importantly oxaloacetate, which can be recycled back into the TCA cycle (Figure 2.3)[31]. The oxidation of citrate derivatives and transfer of protons to intermediates like NADH and $FADH_2$ is critical for the operation of the ETC and the end goal of oxidative phosphorylation (OXPHOS).

The ETC includes five mitochondrial membrane-bound complexes: NADH dehydrogenase (CI), succinate dehydrogenase (CII), ubiquinone bc1-complex, (CIII), cytochrome c oxidase (CIV) and ATP synthase within the mitochondrial cristae (Figure 2.4)[21,32,33]. These complexes catalyze reactions involving NADH and $FADH_2$ to release protons into the IMS, generating a proton gradient and potential energy to power ATP synthase. CI oxidizes NADH to release and transfer both protons and electrons onto ubiquinone (Figure 2.4) [21,32,33]. During this transfer, CI also undergoes a conformational change to "pump" 4 protons into the IMS[32]. At CII, the oxidation of $FADH_2$ produces another fully reduced ubiquinone molecule, but with no proton pumping action (Figure 2.4)[21,32,33]. The two fully reduced ubiquinone molecules from CI and CII now enter CIII to be oxidized, passing electrons onto cytochrome c

molecules and releasing protons into the IMS (Figure 2.4)[21,32,33]. At CIV, 4 electrons from 4 reduced cytochrome c molecules pass through to the mitochondrial matrix and react with molecular oxygen and 4 protons to produce water (Figure 2.4)[32,33]. Similar to CI, CIV then undergoes a conformational change and pumps 4 protons into the IMS[32]. With the generation of a proton gradient by CI, CII, CIII & CIV, potential electrochemical energy can be used to power the final mitochondrial complex, ATP synthase.

ATP synthase catalyzes the energetically unfavorable reaction of adenosine diphosphate (ADP) and inorganic phosphate (P_i) into ATP with protons from the IMS[34]. This "coupling" of the proton gradient to ATP production by ATP synthase is central to mitochondrial function and cell health. The potential energy of proton diffusion from the strongly positive and proton dense IMS to the comparatively negative mitochondrial matrix can be defined as proton motive force (PMF)[35,36]. This PMF is utilized by ATP synthase to generate the rotary action of its subunits and joining of ADP and P_i together to form ATP[35,38]. By coupling the IMS proton gradient with ATP production, approximately 15 times more ATP is generated than anaerobic glycolysis alone[39]. Studies have shown that pharmacological dissipation of the IMS proton gradient using carbonyl cyanide-*4*-trifluoromethoxy-phenylhydrazone (FCCP) dramatically reduces ATP production, promotes the production of ROS and initiates programmed cell death[40-41]. The coupling of protons to ATP production is not only paramount to proper mitochondrial function but also the reduction of mitochondrial dysfunction. Alterations in the IMS proton gradient are closely tied to changes in mitochondrial membrane potential.

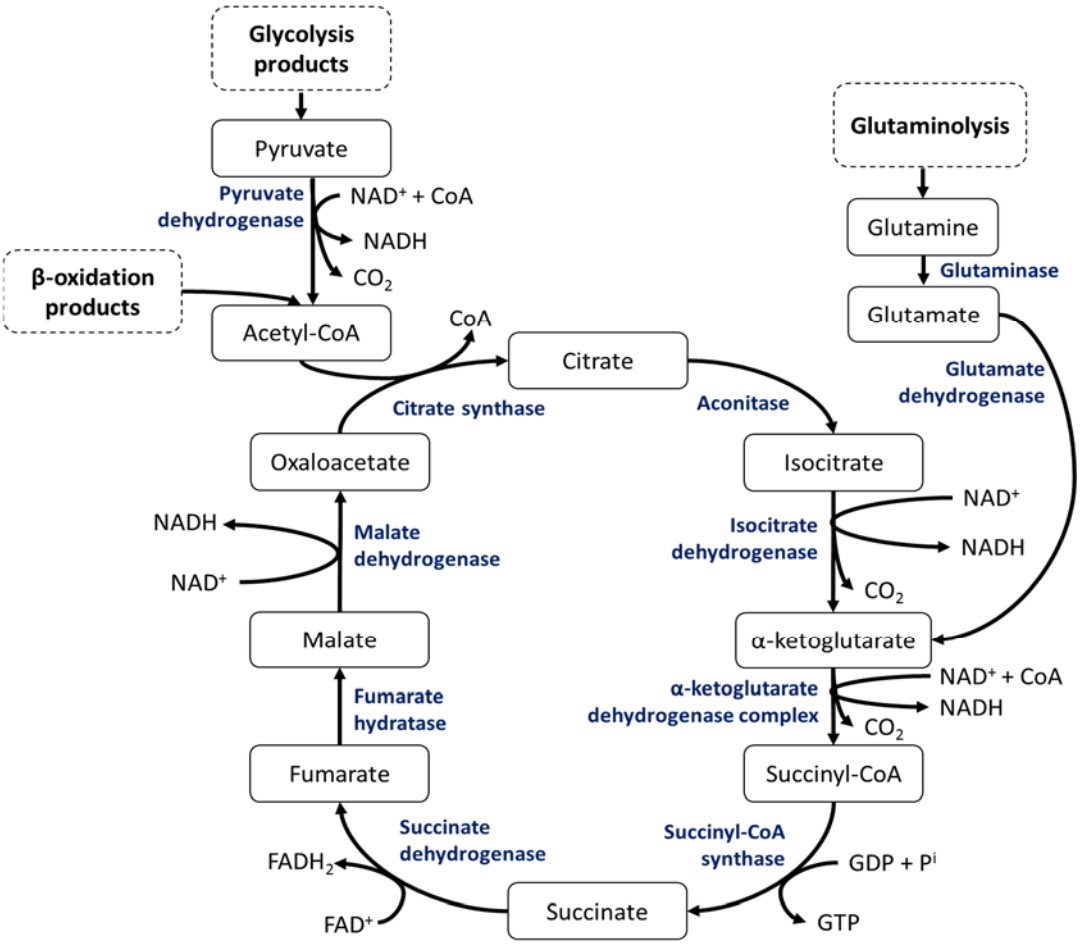

Figure 2.3: Diagrammatic summary of metabolites and enzymes within the TCA cycle. Enzymes catalyzing reactions are highlighted in blue. Adapted from Anderson et al. (2018). *Protein Cell*[42].

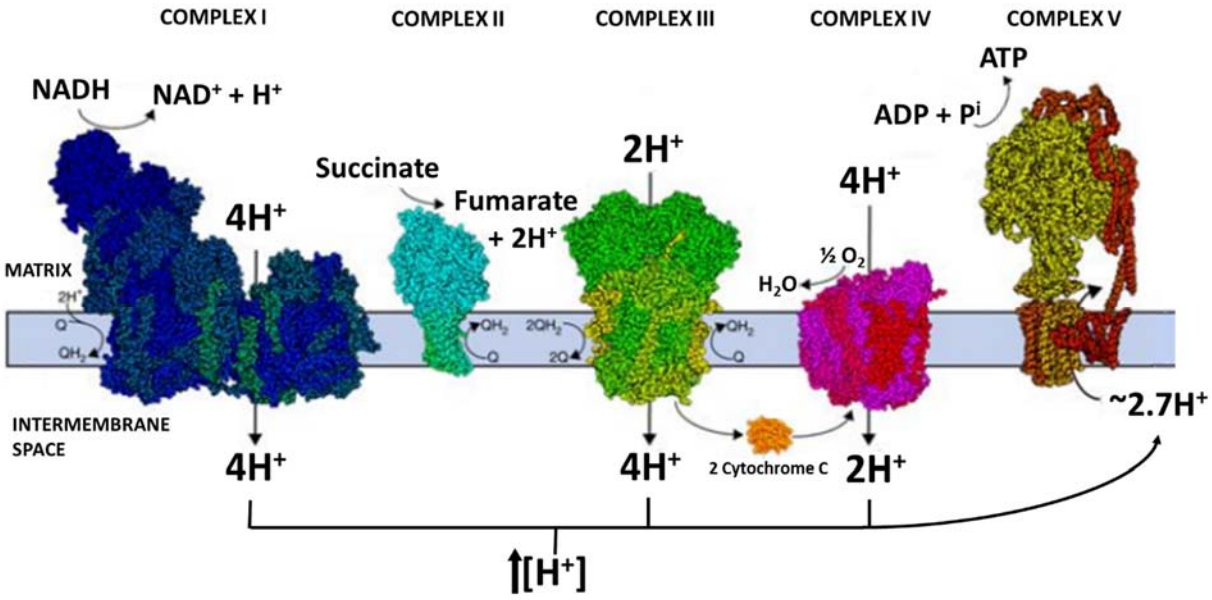

Figure 2.4: Diagrammatic representation of the ETC. Adapted from Letts and Sazanov (2017). *Nature Structural and Molecular Biology*[43].

2.1.5. Mitochondrial Membrane Potential

The electrochemical difference of ions between the mitochondrial matrix and IMS determines the membrane potential ($\Delta\psi_m$) within the mitochondria. Alterations in mitochondrial $\Delta\psi_m$ hold important physiological consequences for mitochondrial OXPHOS and mitochondrial quality control processes. Generation of a sufficient $\Delta\psi_m$ by OXPHOS and mitochondrial complex proton pumping is key to fueling ATP synthase and subsequently driving ATP synthesis. This process is not entirely efficient since a small number of protons passively diffuse through the IMM to the mitochondrial matrix, a consequence often referred to as "proton leak"[44-46]. If protons are allowed to freely move across the IMM, for example: upon the introduction of chemical uncouplers like FCCP or IMM damage, the electrochemical gradient dissipates, $\Delta\psi_m$ decreases and mitochondria become "depolarized"[47,48]. In contrast, the inhibition of ATP synthase by oligomycin

prevents proton transfer into the mitochondrial matrix, increasing the $\Delta\psi_m$ from proton accumulation and shifting mitochondria into a "hyperpolarized" state[49]. Prolonged states of hyperpolarization are detrimental to individual mitochondrion, often resulting in excessive ROS production, dramatic depolarization events, and the initiation of apoptosis by cytochrome c release[50-52]. To maintain quality control of mitochondrial networks, depolarized mitochondria are eliminated by a form of selective mitochondrial autophagy or "mitophagy" mediated by PTEN induced putative kinase-1 (PINK1) binding and ubiquitination of OMM proteins by the E3 ubiquitin ligase; Parkin[53,54]. Appropriate mitochondrial $\Delta\psi_m$ is necessary for ATP synthesis and deviations in both increasingly negative (depolarization) and positive (hyperpolarization) directions can be tied to mitochondrial dysfunction. Both depolarization and inhibition of ETC in dysfunctional mitochondria are also related to the significant production of ROS.

2.1.6. Reactive Oxygen Species

ROS are a group of highly reactive, oxygen-containing molecules that contain a single unpaired electron or "free radical". The neutralization of ROS members by both enzymatic (superoxide dismutase, catalase) and non-enzymatic (glutathione) antioxidant agents is important in maintaining cellular homeostasis. Most ROS originates by the passive leaking of electrons from mitochondrial CI, CIII, and CIV, by the incomplete reduction of molecular oxygen into superoxide radicals[55,56]. The rapid dismutation of reactive superoxide anions by superoxide dismutase (SOD) eliminates potential oxidative damage from these radicals and yields hydrogen peroxide (H_2O_2) [57]. H_2O_2 can then be safely changed to water and molecular oxygen by catalase, thereby eliminating potential oxidative reactions of H_2O_2 and transition metals[58]. However, if the production of H_2O_2 exceeds the catalase buffering capacity, H_2O_2 can react with transition metals (Fe, Cu) to form

hydroxyl radicals through the Fenton reaction[59]. Interactions by hydroxyl or superoxide radicals with macromolecules can create mutations or strongly mutagenic products (DNA adducts, advanced lipid peroxidation products) and disrupt protein structure/function (modification of cysteine residues, the formation of disulfide bridges and creation of protein aggregates)[59-64]. The non-enzymatic antioxidant, glutathione, plays an important role in reducing oxidative damage to macromolecules by transferring electrons to affected molecules, thereby reducing mutagenic products and restoring protein structure and function[65]. Cellular antioxidants like SOD, catalase, and glutathione allow some capacity to buffer against oxidative damage from ROS. In the event that ROS production becomes excessive, like for example from depolarized mitochondria, the dynamic processes of mitochondrial fusion and fission allow for segregation of these mitochondria from healthy networks and eventual degradation by mitophagy.

2.1.7. Mitochondrial Dynamics

The classical notion that mitochondrial networks behave in a static manner has been shifting in recent years, with increasing literature emphasizing the importance of the mitochondrial dynamic processes of fission and fusion. Both mitochondrial fission and fusion are highly regulated processes, mediated through the GTP utilizing members of the dynamin family. Mitochondrial fusion is mediated by both the OMM bound dynamin protein members: mitofusin-1 (Mfn1) and mitofusin-2 (Mfn2), and IMM bound dynamin protein member: optic atrophy protein-1 (OPA1)[66-69]. Different mediators for IMM and OMM fusion are necessary to mediate independent fusion of the OMM, prior to fusion of the IMM and formation of the mitochondria's double membrane structure[66-69]. In contrast, mitochondrial fission is mediated by only one dynamin protein: DRP1 and it's binding to several different receptors on the OMM[66-69]. These

fission receptors include mitochondrial fission factor (Mff), mitochondrial dynamics protein kDa-49 (MiD49), mitochondrial dynamics protein kDa-51 (MiD51) and Fis1[66-69]. Participation of these dynamin protein members and their targets for fusion and fission is important for maintaining the dynamic behavior of mitochondrial networks. These dynamic processes allow flexibility in tailoring responses of mitochondrial networks to a host of different stimuli[68].

2.1.7A. Mitochondrial Fusion

Several hypotheses have arisen for why mitochondrial fusion is essential in maintaining mitochondrial networks and cell homeostasis. Evidence has supported a role for mitochondrial fusion in improving mitochondrial ATP synthesis and allowing the transfer of both soluble and membrane-bound components between mitochondria. During starvation of cells, mitochondrial networks exhibit a hyperfused morphology, which could be interpreted as a method of increasing mitochondrial efficiency in a low nutrient environment[70]. In support of this, hyperfused mitochondrial networks have also been found to contain higher cellular ATP and a greater capacity for ATP production[71]. Mitochondrial fusion also helps in buffering against potential oxidative damage by mixing and redistributing both damaged mitochondrial DNA (mtDNA) and proteins that might otherwise accumulate and disrupt mitochondrial function[72,73]. Mitochondrial networks of skeletal muscle cells that cannot undergo mitochondrial fusion, exhibit a higher degree of point mutations in their mtDNA genome[74]. Chen et al. also identified that mitochondrial fusion helps preserve mitochondrial respiratory function in cells by limiting mtDNA mutations[74]. Other studies have made similar observations tying mitochondrial fusion to mtDNA preservation, mitochondrial respiratory function and ATP synthesis[75,76]. *In-vivo* genetic studies have also demonstrated the importance of mitochondrial fusion, since knockout of OPA1 leads to mouse embryonic lethality

by Day 9, while knockout of Mfn1 or Mfn2 only appears to have relevance in certain tissue specific contexts[77-79]. The opposing process of mitochondrial fission also plays an integral role in maintaining mitochondrial network quality and function.

2.1.7B. Mitochondrial Fission

Similar to mitochondrial fusion, mitochondrial fission plays an important role in maintaining mitochondrial network quality and function. Under homeostatic conditions, mitochondrial fission is mediated by the coordination of DRP1 with its receptors (Mff, MiD49, MiD51) and eventual termination by dynamin-2 (Dnm2). The first step of mitochondrial fission involves pre-constriction of the mitochondria by the ER at sites with replicating mtDNA (Figure 2.5). Cytosolic DRP1 is then recruited to sites marked by the ER along the mitochondria and associates with fission receptors Mff, MiD 49 or MiD51 to form a ring-like structure around the mitochondria (Figure 2.5)[66,80]. Assembly of supporting mechanical constructs between the mitochondria and ER then assist in driving and regulating mitochondrial fission (Figure 2.5)[66,80]. Hydrolysis of GTP by the DRP1 ring complex initiates further constriction and the recruitment of Dnm2, with complete mitochondrial scission occurring shortly afterwards (Figure 2.5)[66,80]. DRP1 mediated mitochondrial fission is essential in normal animal development since DRP1-null mice do not live past day 11 due to improper neural tube formation[81]. At the cellular level, downregulation of DRP1 by siRNA transfection in HeLa cells leads to increased ROS production, loss in mtDNA, decreased respiratory function and ultimately loss in cell proliferation[82]. These observations may be tied to the importance of DRP1 in mediating mitochondrial quality control through asymmetric fission. Asymmetric fission of depolarized mitochondria by DRP1 allows larger, functional daughter mitochondria to remain in the mitochondrial network, while the

depolarized, smaller daughter mitochondria undergo mitophagy[83]. The participation of DRP1 with its receptors in mitochondrial fission is necessary for both animal and cellular homeostasis. Excessive fission, however, represents a significant pathological threat, particularly in the context of energetically demanding tissues like the heart and brain.

Excessive mitochondrial fission promotes a shift in mitochondrial networks to a "fragmented" state, consisting of small, punctate mitochondria. Evidence suggests that these fragmented mitochondrial networks could be mediated by DRP1 hyperactivation and participate in the promotion of disease. Cardiomyocytes isolated from rats after ischemia-reperfusion injury demonstrated excessive mitochondrial fission, related to the exclusive binding of DRP1 to Fis1[15]. Further investigation of these isolated cardiomyocytes showed that they contained significantly less ATP, exhibited lower OXPHOS capacity and produced more ROS[15]. Neurodegenerative animal models representative of human diseases (multiple sclerosis, Parkinson's, Huntington's, amyotrophic lateral sclerosis) also show dramatic increases in DRP1 activation and a fragmented mitochondrial morphology[13,14,17,18]. Interestingly, Alzheimer's and Huntington's patient fibroblasts also exhibit dysfunctional and fragmented mitochondrial networks, coinciding with DRP1 hyperactivation and DRP1-Fis1 binding [18,19]. Fragmented mitochondrial networks related to the hyperactivation of DRP1 in numerous cardiovascular and neurodegenerative models, highlight a potential pathway for unbalanced mitochondrial fission and the promotion of disease. Similar to heart and brain tissues, intestinal tissues also exert high energetic costs due to constant cellular turnover in response to noxious intestinal stimuli[84-86]. However, the role of mitochondrial dynamics and its consequences on cellular energetics, homeostasis and dysfunction remains relatively unexamined within intestinal tissues and particularly in a disease context.

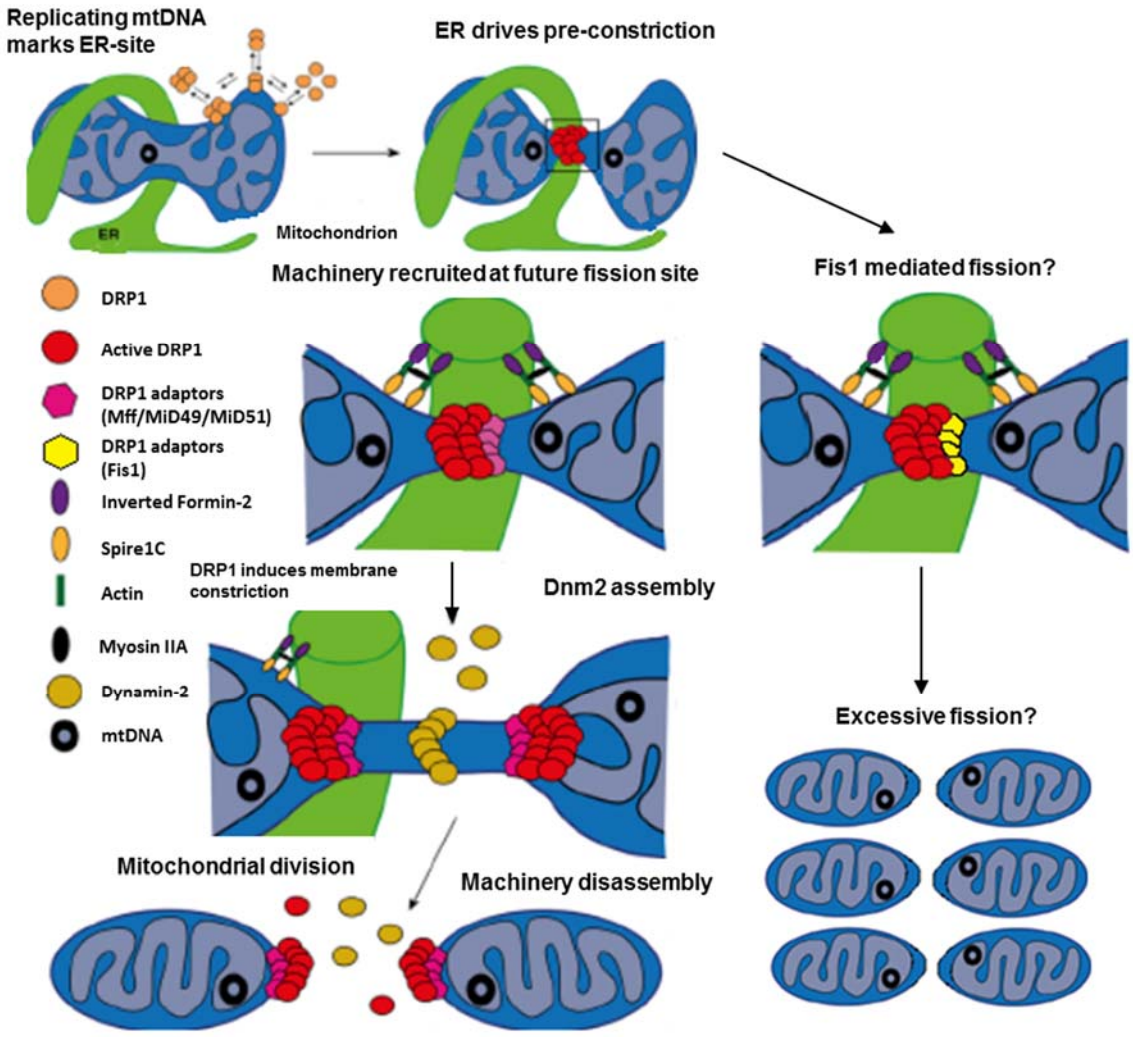

Figure 2.5: Model for the current understanding of homeostatic mitochondrial fission and a hypothesized model for how excessive fission may be mediated. Adapted from Tilokani et al. (2018). *Essays Biochem*[80].

2.2. Intestinal Physiology and Mitochondrial Involvement

2.2.1. Intestinal Anatomy

The intestinal tract is primarily responsible for the absorption of nutrients and water, as well as the elimination of waste products after digestion[84-86]. Reflecting the nature of its function, the characteristics and structure of colon tissues favor absorption and motility of digesta. Moving distally from the lumen, the intestine consists of four layers: mucosa, submucosa, muscularis, and serosa[84-86]. The mucosa is stratified into three layers: epithelium, lamina propria, and the muscular mucosae[84-86]. The epithelium is the site of intestinal absorption, containing a high degree of folding for increased surface area and absorption[84-86]. These folds or "crypts" contain intestinal stem cell (ISC) populations at their base, which differentiate into epithelial cells that migrate towards the lumen[84-86] (Figure 2.6). At the lamina propria, immunological cell populations communicate with epithelial cells and monitor for signs of infection[84-86] (Figure 2.6). Supporting vasculature, lymphatic vessels and nerve fibers for the mucosa are found at the submucosa[84-86]. Intestinal motility occurs through peristaltic contractions, facilitated by layers smooth muscles and nerves at the muscularis propria[84-86].

2.2.2. Intestinal Barrier Function and Host Defences

Near the mucosal layer of the intestine, and in particular the colon, trillions of microbes exert a constant pathogenic threat to their host. Mitigation of these luminal microbes is largely maintained by both absorptive (columnar) and secretory (goblet, Paneth) intestinal epithelial cells (IECs). Connections between IECs through desmosomes, tight junctions, adherens junctions, and gap junctions regulate paracellular permeability and serve as a physical barrier to intestinal microbes[87]. Beyond the IEC monolayer, goblet cell secretions of several different kinds of

glycoproteins, but predominantly Mucin-2, promote the formation of a thick mucus layer[87,88]. The mucus layer of the small intestine remains loose and semi-permeable to microbes, while in the colon it manifests as a dense, sterile, epithelial bound mucous layer, that is broken down by certain mucous digesting bacteria, forming an additional outer mucous layer[87,88] (Figure 2.6). This outer mucous layer helps promote the growth of commensal bacterial species which yield beneficial metabolites and afford their host colonization resistance to opportunistic and pathogenic microbes[87,88]. Within these mucous layers, gradients of both antimicrobial peptides (AMPs) and immunoglobulin-A (IgA) from Paneth cells and intestinal plasma cells respectively, provide a biochemical means of protection for the host[89,90] (Figure 2.6). Under homeostatic conditions, the mucosal layer typically provides a sufficient barrier to the microbial colonies residing in the intestine. Upon detection of a potential pathogenic challenge, the epithelium can also respond dynamically through activation of their pattern recognition receptors (PRR).

Migration of luminal microbial species towards the IEC monolayer promotes signaling of potential impending infection by PRRs. PRRs located on/in IECS involve the participation of members of Toll-like receptors (TLR), nuclear binding oligomerization domain-like receptor (NLR) and retinoic acid-inducible gene-1 like receptor (RLR) families, which signal either pro-inflammatory factors and/or tissue repair mechanisms upon detection of damage-associated molecular patterns (DAMPS) and/or pathogen-associated molecular patterns (PAMPS). DAMPs are molecular modes of communicating tissue damage or cell stress to the immune system, while PAMPs are evolutionarily conserved molecular sequences that the body has evolved to recognize as foreign microbes[91,92]. Upon recognition of these ligands, TLRs and NLRs activate intermediates within both the nuclear factor kappa light chain of activated B-cells (NF-KB) and mitogen-activated protein kinases (MAPK) pathways, to induce nuclear inflammatory transcription and

cytokine release[93]. In IECs, NF-KB nuclear transcription has been shown to trigger cytokine release and induction of cell survival pathways, while MAPK nuclear transcription is related to differentiation of crypt stem cell populations and proliferation of differentiated IECs[94,95]. Activation of PRRs and corresponding nuclear transcription ensures appropriate responses in not only IECs, but also in host immune cells.

PRR activation of both the epithelium and immune surveillance cells at the lamina propria initiates increasingly inflammatory and pathogen-specific responses in order to resolve potential infection. The unspecific but more rapid response of the innate branch consisting of: macrophages, dendritic cells (DC), mast cells, neutrophils, monocytes, basophils, eosinophils, and natural killer (NK) cells serve as an immediate answer and facilitates activation of adaptive immune cells. At the lamina propria, macrophages and DCs engulf microbes through phagocytosis and release cytokines to initiate systemic recruitment of immune cells[96-98]. Detection of these cytokines by neutrophils, monocytes, eosinophils, and basophils within the blood promotes their migration to intestinal tissues, where they carry out their effector functions (phagocytosis, degranulation). Intestinal mast cells can also release granules of histamine in a systemic manner to elicit changes in smooth muscle, endothelial cells, and neurons[99]. The last innate member: NK cells, initiates apoptosis in cells infected with intracellular pathogens to prevent their replication in host cells[100]. The aforementioned members of the innate immune branch are important in rapidly combatting early stages of infection. In the event that the infection persists, macrophages and DCs initiate adaptive immune responses by presenting immunogenic factors from phagocytosed pathogens to T-helper cells[98]. However, if the barrier function of IECs becomes compromised, the persistent migration of luminal microbes and their products may lead to excessive and potentially indiscriminate inflammation in order to resolve the infection.

2.2.3. Role of Mitochondria in Intestinal Homeostasis

Like all cellular functions, the "gatekeeper" role that IECs exhibit to the intestinal contents is dependent on sufficient energy production. Because of this dependency, mitochondria play an important role in maintaining intestinal barrier function and ultimately intestinal homeostasis. Colonocytes derive approximately 70% of their energy through the oxidation of the SCFA: butyrate, by beta-oxidation within the mitochondria[101]. Uncoupling of mitochondrial metabolism with carbonyl cyanide *m*-chlorophenyl hydrazone (CCCP), negatively alters both intestinal permeability and transepithelial resistance, leading to increased bacterial internalization[102]. Similarly, Wang et al. found that IECs treated with another uncoupler: 2-4 dinitrophenol, had an increased internalization of non-invasive *Escherichia coli*[103]. The opposite also holds true, that improvements in mitochondrial function help in maintaining colon homeostasis. Mitochondrial DNA (mtDNA) polymorphisms that improve OXPHOS capacity and subsequently intestinal ATP, protect mice from both DSS and trinitrobenzene sulfate induced colitis (TNBS)[104]. Proper mitochondrial function is necessary for IEC butyrate utilization, maintenance of the intestinal barrier and protection against chemically induced colitis. Mitochondria also play an important role in intestinal homeostasis by regulating the differentiation and/or proliferation of epithelial cells and ISCs.

Renewal of the intestinal epithelium occurs through the differentiation of crypt ISCs into IECs and their migration towards the lumen. Regulation of both ISC and IEC cell fate decisions has been shown to be greatly reliant on mitochondrial OXPHOS. Recent evidence has found that within small intestinal crypts, Paneth cells preferentially undergo anaerobic glycolysis to provide lactate for nearby ISCs[105]. This supply of lactate, once it is converted back into pyruvate, allows ISCs to undergo OXPHOS without risking substrate depletion[105]. Importantly, these high rates of

OXPHOS also yield the mtROS necessary for ISC MAPK redox signaling and subsequent crypt maturation[105]. Inhibition of either Paneth cell glycolysis by deoxyglucose or ISCs OXPHOS by oligomycin greatly affected the number of crypts in isolated mouse organoids[105]. A separate study also found that mitochondrial OXPHOS is necessary for ISC differentiation into IECs since inhibition of pyruvate transport into the mitochondria promoted the expansion of ISCs populations and limited differentiation[106]. After ISC differentiation, terminally differentiated IECs also exhibit a high degree of mitochondrial OXPHOS in order to metabolize butyrate and limit it's signaling effects on crypt ISCs[107]. The rapid renewal of the intestinal epithelium requires sufficient mitochondrial OXPHOS to mediate both bioenergetic and redox signaling requirements for ISC populations, with perturbed mitochondrial function potentially limiting stem cell replenishment of the epithelium. Therefore, mitochondrial dysfunction within the epithelium could play a role in the development of IBD.

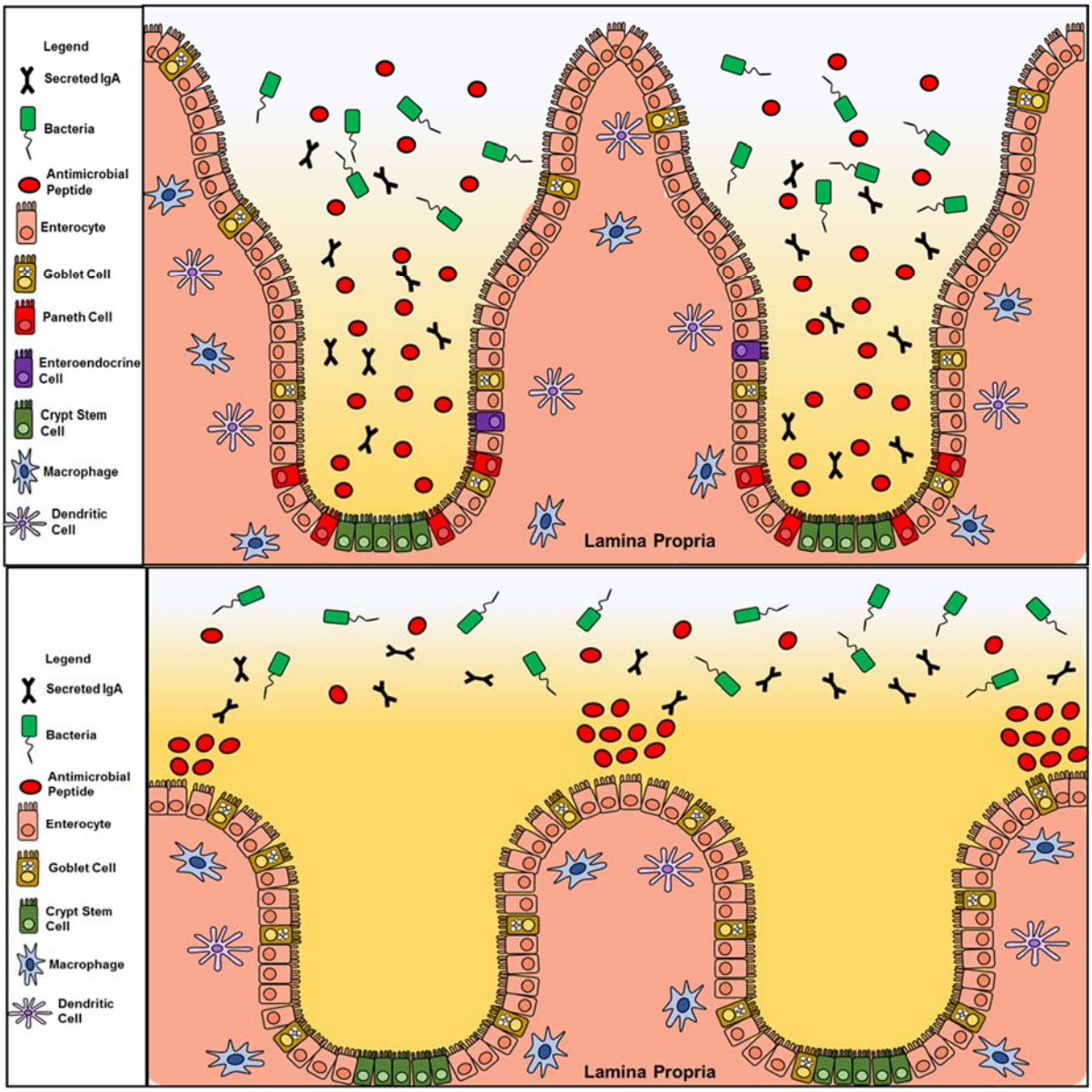

Figure 2.6: Simplistic representations of both the small (top) and large (bottom) intestine mucosal layers. Original figure by Luke Goudie.

2.3. Inflammatory Bowel Disease

2.3.1. Disease Characteristics

In order to identify disease course and appropriate treatment options for IBD, important distinctions must be made due to the disease's heterogenic presentation. Two well-recognized subtypes of IBD: Crohn's disease (CD) and ulcerative colitis (UC) can be identified by histological, endoscopic and symptomatic characteristics. The presence of focal, granulomatous, transmural patches throughout the GI tract is a defining feature of CD[108]. Additionally, CD specific symptoms typically include weight loss, inflammation around the anus or "perianal involvement" and fistulas[108]. Differing from CD, UC patients typically exhibit a continuous, superficial inflammation within just the colon[109]. Symptoms in UC patients are often similar to CD, with rectal bleeding and anemia occurring more frequently[109]. Patients demonstrating patterns of both UC and CD are often grouped into a third subtype called "indeterminant colitis"[7]. Amongst these subtypes, extraintestinal manifestations add additional complexity to disease presentation, diagnosis and patient burden[6] (Table 2.1). Early-onset cases of both CD and UC are also recognized as unique, owing to their often aggressive and invasive presentation[110]. Recognition of these IBD subtypes allows some predictions on disease behavior and course, despite IBD's heterogenicity. The identification of a large number of genetic and environmental risk factors can somewhat explain why IBD manifests so differently (Table 2.2).

To date, over 201 genetic risk loci and numerous environmental risk factors have been shown to confer varying degrees of susceptibility to IBD[111,112]. In these genetically susceptible individuals, exposure to certain environmental stimuli may shift epithelial-microbial and immunological dynamics into a pro-inflammatory state, unresolved inflammation and eventually IBD. Linking of polygenic risk variants to related pathways has shown that mutations in microbial

recognition (NOD2), clearance of phagocytosed bacteria by autophagy (ATG16L1, IRGM, LRRK2, NOD2) and intestinal barrier function (CDH1, HNF4α) are related to IBD development (Table 2.2)[113-123]. Exposure of individuals bearing these risk variants to environmental risk factors like antibiotics and infection could alter interactions between the gut microbiota, immune system, and epithelial cell monolayer, shifting the gut into a pro-inflammatory state. The indiscriminate elimination of microbes with antibiotics can reduce beneficial commensal species that confer "colonization resistance" to the host and increase the risk of infection by opportunistic or pathogenic bacteria[124,125]. Successful infection by bacterial species like adherent invasive *Escherichia coli* and *Ruminococcus gnavus* can further alter the gut microenvironment and have been shown to be associated with IBD development[126,127]. In addition to antibiotics and infection, several other environmental risk factors can affect IBD development (Figure 2.7)[128]. Both genetic susceptibility and certain environmental exposures like infection history and improper usage of antibiotics can affect the risk of IBD development[128]. To help identify the relationships of these risk factors and colitis, researchers often utilize murine colitis models.

Tissue Affected	Extraintestinal Manifestation (Prevalence)
Musculoskeletal	• Peripheral Arthropathies (5-20%) • Axial Arthropathies (2-22%)
Mucocutaneous	• Erythema nodosum (10-15%) • Pyoderma gangrenosum (1-5%) • Sweet syndrome • Aphthous stomatitis (up to 10%)
Ocular	• Scleritis (2-3%) • Uveitis (2-6%)
Hepatobiliary	• Primary sclerosing cholangitis (up to 7.5%) • Pancreatitis
Pulmonary	• Parenchymal disease
Renal and Urologic	• Glomerulonephritis; tubulointerstitial nephritis (4-23%)
Bone	• Osteopenia and osteoporosis (up to 40%)

Table 2.1: Extraintestinal manifestations associated with IBD and rates of prevalence if known. Adapted from Ott & Schölmerich, (2013). *Nature Reviews Gastroenterology & Hepatology*[6]

IBD Subtype	Gene	Protein	Role of Gene
Crohns Disease	CARD15	NOD2	• Encodes a receptor for detection of peptidoglycan bacterial cell walls[113] • Required for autophagosome formation[114,115]
	ATG16L1 Autophagy-related 16-like-1	ATG16L1	• Implicated in autophagy pathway[114,115] • Prevents necroptosis of intestinal cells[116]
	LRRK2 Leucine-rich repeat kinase-2	LRRK2	• Important for autophagy and regulation of NFAT[117,118] • Also found as a risk factor for Parkinsons[117]
	IRGM Immunity-related GTPase family M	IRGM	• Assists in the initiation and clearance of microbes by autophagy[119] • Participates in necroptosis pathway[120]
Ulcerative Colitis	CDH1	E-cadherin	• Important in intercellular adhesion of epithelial cells[121]
	HNFα Hepatocyte nuclear factor 4 alpha	HNFα	• Required for mammalian gastrointestinal development[122] • Important in maintaining intercellular junctions and mucosal architetchture[123]

Table 2.2: Genetic risk factors for IBD associated with autophagy and intestinal barrier function.

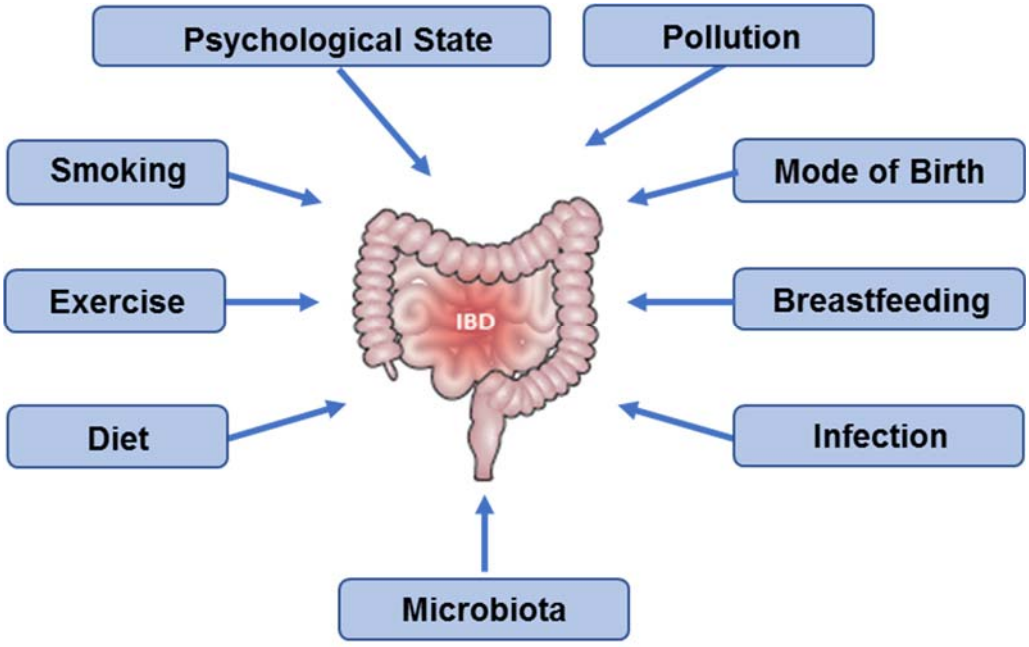

Figure 2.7: Environmental risk factors related to IBD development. Adapted from Ananthakrishnan et al. (2017). *Nature Reviews Gastroenterology Hepatology*[128].

2.3.3. Animal Models of Colitis

Research into IBD has relied heavily on chemically induced colitis models, that attempt to replicate key aspects of the disease's presentation. One of the most commonly utilized chemically induced colitis models; DSS, is inexpensive and highly reproducible, exhibiting similar clinical and histological characteristics to UC[129-131]. DSS is a sulfated polysaccharide with a highly variable molecular weight that has been shown to cause colitis in guinea pigs, hamsters, rats and mice with oral consumption[129]. It is important to note that only the 5 kDa and 40 kDa DSS particles induce colitis, with 500 kDa particles not consistently producing colitis[130]. Administration of DSS typically occurs through the drinking water, allowing the choice of chronic or acute colitis models by modifying DSS concentration and dosage timing[131]. While the exact mechanism is unknown, it is generally accepted that DSS exhibits cytotoxic effects on the epithelium, leading to disruption in the epithelial barrier and migration of luminal microbes and antigens[132]. Evidence has also shown that DSS specifically, not dextran associated molecules, combines with medium chain fatty acids to form nanopores and fuse with colonocyte membranes[133]. The inflammation with acute DSS models often is confined to the colon and affects the tissue superficially, leading to ulceration, edema, goblet cell depletion, and crypt abscesses[129]. While DSS does not appropriately replicate all aspects of human IBD (i.e.: spontaneous and episodic presentation), certain characteristics, like histopathology, share similarities with human UC, making it a somewhat representative model[130,131]. To explore the other subtype of IBD; CD, the DNBS colitis model may be employed.

DNBS is a hapten that binds to colonic or microbial derived products, forming immunogenic antigens that can be recognized by the immune system and elicit a strong immune response[134]. The DNBS model manifests with rapid and severe colitis that shows some similarities to UC and CD[134-136]. Animals often exhibit dramatic weight loss and severe inflammation within

the colon, cecum, and rectum[134-136]. Histopathological analysis of DNBS treated animals typically shows transmural inflammation, edema and cellular infiltration extending below the mucosal layer to the submucosa[135]. DNBS treated mice also exhibit increased neutrophil migration, indicated by higher myeloperoxidase (MPO) activity in colon tissues isolated from animals[135,136]. Effects of DNBS associated inflammation have also been shown to be far-reaching, affecting hippocampal brain regions and correlating with increased anxiety and depressive-like behaviors[136]. The use of both DNBS and DSS animal colitis models, while not exactly representative of human IBD, help researchers identify key points of intervention and possible therapeutic options. An emerging observational trend is being noted of mitochondrial dysfunction within both animal colitis models and IBD patients[20].

2.3.4. Mitochondrial Dysfunction in IBD

Early investigations into UC identified that alterations in substrate metabolism and energy deficiency could play a role in the disease's pathogenesis[101]. Since then, observations of mitochondrial bioenergetic impairment have been noted in both IBD patients and mouse colitis models[101,137,138]. In 1980, Roediger et al. found that isolated UC patient colonocytes from active and quiescent disease states exhibited reduced rates of butyrate metabolism by beta oxidation, requiring increased metabolism of both glutamine and glucose to compensate for the bioenergetic disparity[101]. These observations have since been replicated in biopsies isolated from UC and CD patients with quiescent and active disease[137,138]. In mice, beta oxidation has been shown to be critical for intestinal homeostasis, since genetic or pharmacological inhibition of beta oxidation leads to colitis development[139,140]. Given the importance of mitochondria in facilitating beta oxidation, mitochondrial dysfunction could be linked to the observed beta oxidation defects in IBD

patients. In support of this, mitochondrial dysfunction has been reported in UC patients at CII and both CII and CIV for the colitis mouse model of DSS[141]. Impaired mitochondrial function within mitochondrial disease patients, is also frequently associated with GI symptoms and complications suggesting that, to some degree, sufficient mitochondrial function is required for intestinal homeostasis[142-144]. Therefore, alterations in mitochondrial function could affect energy availability for colonocytes and potentially contribute to functional consequences within the intestine. Dysfunctional mitochondria may also play a role in triggering inflammation through the release of mitochondrial-derived DAMPs.

The shared characteristics of eukaryotic mitochondria with their prokaryotic ancestors make mitochondria and their derived components strongly immunogenic[145]. This evolutionary association makes the release of mitochondrial derived DAMPs a potential source of inflammation, thereby implicating mitochondrial dysfunction in inflammatory diseases. Under conditions of mitochondrial dysfunction or cellular stress, mitochondrial DAMP release can serve as a method of communicating with the innate immune system through PRR activation[145,146]. The release of mtROS, mtDNA and the mitochondrial phospholipid: cardiolipin, all activate the NLR pyrin containing domain-3 (NLRP3) inflammasome, allowing it to cleave immature forms of IL-18 and IL-1β into their mature active forms[145,146]. Increased release of IL-1β from NLRP3 hyperactivation has been shown to directly mediate CD in a previous case study[147]. Similar to their prokaryotic counterparts, mitochondria also contain N-formylated peptides, and their release has been shown to be a potent activator of neutrophils[148]. Increases in both N-formylated peptides and mtDNA have been identified in plasma samples from active IBD patients[149]. Colon biopsies isolated from these patients also contained structurally dysfunctional mitochondria, suggesting that these systemically circulating mitochondrial DAMPs could be of intestinal origin[149]. Clearance of

dysfunctional mitochondria relies on autophagic machinery, but genetic studies have often identified mutations in autophagic pathways for individuals with IBD (Table 2.2)[113-119]. An alternative solution could be inhibiting upstream mitochondrial fission in response to inflammation, thereby preserving mitochondrial morphology and function.

2.4. Molecular Inhibition of Excessive Mitochondrial Fission

2.4.1. P110

P110 is a systemically administered peptide that competitively inhibits the binding of Drp1 and Fis1, in order to reduce pathologically associated mitochondrial fission[150]. P110 was designed with several other peptides to mimic the potential binding sites on either DRP1 or Fis1 and inhibit this interaction (Figure 2.8)[150]. To increase cellular access of these peptides, the 47^{th} – 57^{th} amino acid sequence from the cell-penetrating peptide: HIV-1 transactivator of transcription (TAT^{47-57}) was attached[150]. In comparison to the other developed peptides, P110 corresponded to the greatest reduction in DRP1 GTPase activity and Fis1/DRP1 binding (Figure 2.9)[150]. In a test model of MPP^+ and $CCCP^+$ induced toxicity in neuronal cells, Qi et al. identified that inhibition of DRP1/Fis1 attenuated mitochondrial $\Delta\psi_m$ loss, reduced superoxide production and mitochondrial fragmentation (Figure 2.10A)[150]. Importantly, P110 also did not affect basal levels of fission, since non-specific inhibition of fission prevents quality control of mitochondrial networks by mitophagy (Figure 2.10B)[150]. This study also provided insight into the process by which mitochondria undergo pathological fission through the specific binding of Fis1 and DRP1, rather than Mff, which occurs in basal fission[150]. Further application of P110 in several other disease models has also proven effective, reducing pathological mitochondrial fission related to physiologically inflammatory events like myocardial infarction and chronic neurodegenerative diseases like Parkinson's, Huntington's and multiple sclerosis[64,65,158,159]. Inhibition of excessive DRP1 and Fis1 associated fission presents a novel method of reducing mitochondrial dysfunction in inflammatory diseases. The therapeutic benefits reported with P110 administration in previously examined disease models (reduced ROS production, improved mitochondrial function) may help resolve common features of mitochondrial dysfunction identified in IBD.

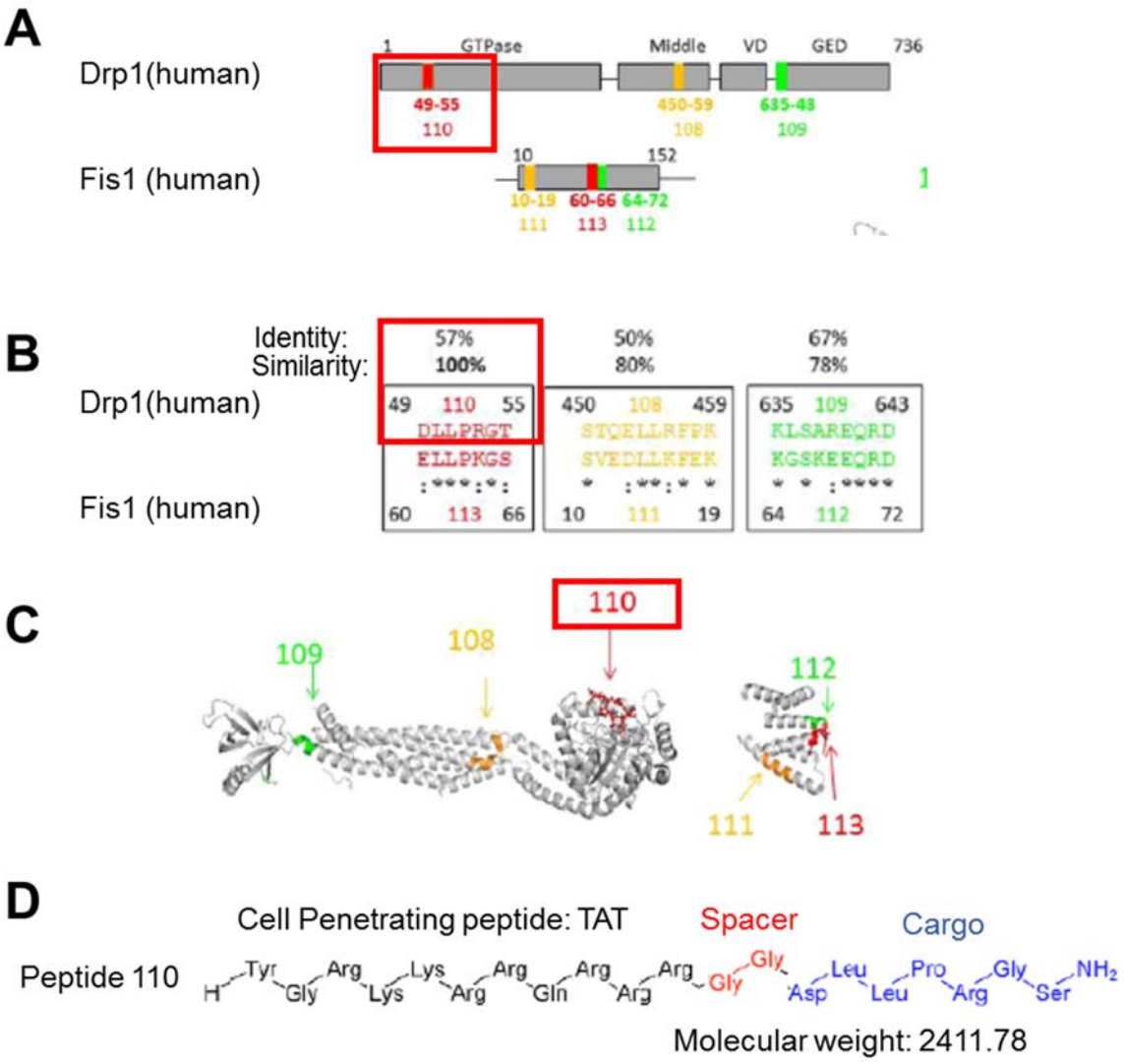

Figure 2.8: Genomic and proteomic data used to develop P110's structure. A) Regional domains of human DRP1 and Fis1 used for peptide development B) Sequence similarity between the identified regions C) 3D representations of DRP1 and Fis1 with the binding area of P110 highlighted D) Amino acid sequence of P110. Figures sourced and adapted from Qi et al. (2013). *Journal of Cell Science*[150] .

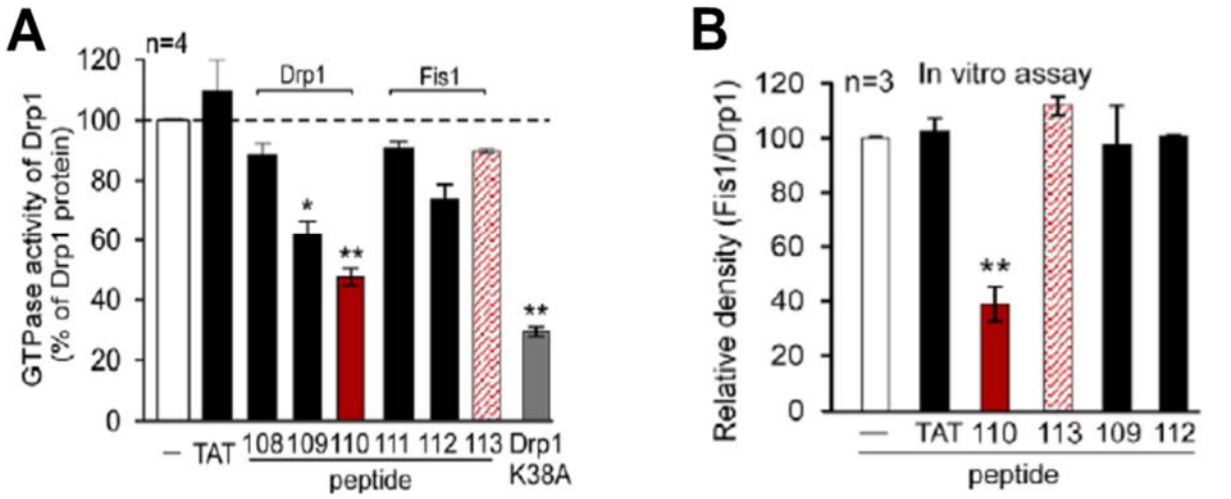

Figure 2.9: Evidence of P110's inhibitory action on DRP1. A) Comparison of human recombinant DRP1 GTPase inhibition using peptides with identical sequences to both DRP1 and Fis1 binding sites. K38A was used as a positive control for DRP1 GTPase inhibition. B) Immunoprecipitation of both recombinant DRP1 and Fis1 after incubation with peptides; 109, 110, 112 & 113. Figures sourced and adapted from Qi et al. (2013). *Journal of Cell Science*[150].

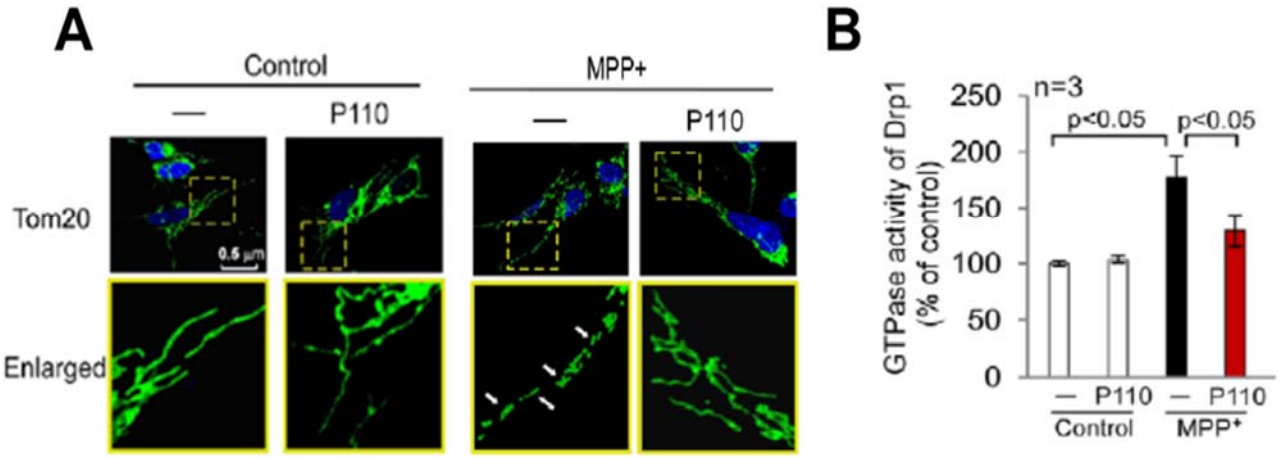

Figure 2.10: *In-vitro* testing of P110's inhibitory action within an MPP+ neurotoxicity model. A) Neuronal cells ± MPP and ± P110 treatments stained with Tom 20 for mitochondrial network morphology. B) DRP1 GTPase activity in neuronal cells ± MPP and ± P110 treatments. Figures sourced and adapted from Qi et al. (2013). *Journal of Cell Science*[150].

Chapter 3

Assessment of mitochondrial function in intestinal epithelial cells: a novel tool to explore mitochondrial involvement in inflammatory bowel disease

3.1. Introduction

IBD describes several chronic, inflammatory conditions of the gastrointestinal tract, that bear a significant burden to patients and healthcare systems. Despite the idiopathic etiology of IBD, deterioration of intestinal barrier function and increased intestinal permeability have consistently emerged as key factors in the disease's progression. Studies examining IBD patients have shown that increased intestinal barrier dysfunction can serve as a predictor for poorer outcomes, disease relapse, and mucosal healing[151-153]. Breakdown in intestinal barrier function has also been reviewed as an important component for how immunological, microbial and environmental risk factors confer IBD susceptibility[154-159]. Its relevance to IBD is also emphasized in studies examining IBD treatments, since improvements in intestinal permeability and barrier function are highlighted as markers of therapeutic efficacy[160-164]. Furthermore, investigation into factors pertaining to intestinal barrier function could yield novel disease targets and therapeutics for IBD. At the cellular level, IECs play a vital role in regulating both intestinal barrier function and permeability.

Like all cellular functions, the barrier maintained by IECs is reliant on adequate energy generation[101]. Dysfunction within the energy processes of mitochondrial OXPHOS and beta oxidation has been shown to affect IEC barrier function and is often a feature of animal colitis models and human IBD. IECs derive most of their energy through the complete oxidation of

butyrate by beta oxidation and OXPHOS within the mitochondria[101,159]. Dysfunction within the beta oxidation pathway has previously been identified in human IBD patients and causally tied to certain models of murine colitis[101,139,140]. Reduced mitochondrial activity has also been noted in IBD colon patient biopsies and the DSS murine colitis model[141]. A closer examination by *in-vitro* studies highlighted that chemical uncoupling of mitochondrial OXPHOS by 2-4 dinitrophenol or CCCP, negatively alters intestinal permeability and barrier function[102,103]. A separate study similarly showed that inhibition of OXPHOS led to ATP depletion, reduced intestinal barrier function and increased intestinal permeability[165]. Evidence connecting mitochondrial bioenergetic processes to intestinal barrier function highlight potential points of intervention for IBD treatments and provide support for further investigation.

Examination of these metabolic pathways can be performed through the use of respirometric machines like the Oxygraph-2k (O2k). This instrument allows measurements of oxygen consumption (O_2 flow or O_2 flux) based on titrations of various substrates, inhibitors or uncouplers. Substrates and inhibitors are typically used to identify the activity of mitochondrial complexes: CI, CII, CIV and ATP synthase (Table 3.1 & Figure 3.1). Uncouplers are proton shuttling chemicals used to determine the theoretical maximum for OXPHOS activity[166-168]. Other titrations like ADP, shift mitochondrial activity from ADP-limited respiration (state 2) to ADP-stimulated respiration (state 3), thereby allowing mitochondrial complex capacities to be identified[166-168]. By carefully administering these titrations, details on metabolic pathways and specific mitochondrial complex activity can be determined under a variety of treatments (Table 3.1). Within this paper, we outline detailed protocols on how to measure OXPHOS and beta oxidation activity within permeabilized cells using the O2k Respirometer.

Chemical	Substrate/ Inhibitor/ Uncoupler	Relevance to Mitochondrial OXPHOS
Adenosine diphosphate (ADP)	Substrate	• Required as a reactant in the production of ATP by ATP synthase • When titrated with other substrates, it allows State 3 substrate linked respiration to be examined
Pyruvate	Substrate	• NADH linked substrate, produced from the oxidation of glucose after glycolysis
Malate	Substrate	• NADH linked substrate, produced during the TCA cycle
Palmitoyl Carnitine	Substrate	• Substrate used in the examination of long chain fatty acid beta oxidation. Must be titrated with malate to ensure no feedforward inhibition
Cytochrome c	Substrate	• Electron carrier for CIII to CIV. Increased OCR in response to exogenous cytochrome c titrations indicate OMM damage
Glutamate	Substrate	• NADH linked substrate produced during glutaminolysis that feeds into the TCA cycle
Succinate	Substrate	• $FADH_2$ linked substrate, produced during the TCA cycle
TMPD	Substrate	• Substrate for determining CIV activity. Must be paired with ascorbate titrations to prevent auto-oxidation
Ascorbate	Substrate	• Donates electrons to TMPD and limits auto-oxidation of TMPD by oxygen
FCCP / CCCP	Uncoupler(s)	• Proton ionophore that uncouples mitochondrial OXPHOS. Rates of OCR under sufficient FCCP concentration indicate maximal OXPHOS
Rotenone	Inhibitor	• Inhibitor of mitochondrial complex I
Antimycin A	Inhibitor	• Inhibitor of mitochondrial complex III. Completely inhibits mitochondrial respiration when paired with rotenone
Azide	Inhibitor	• Inhibitor of CIV
Oligomycin	Inhibitor	• Inhibitor of ATP synthase

Table 3.1: Titrations and their corresponding links to mitochondrial complexes or metabolic pathways.

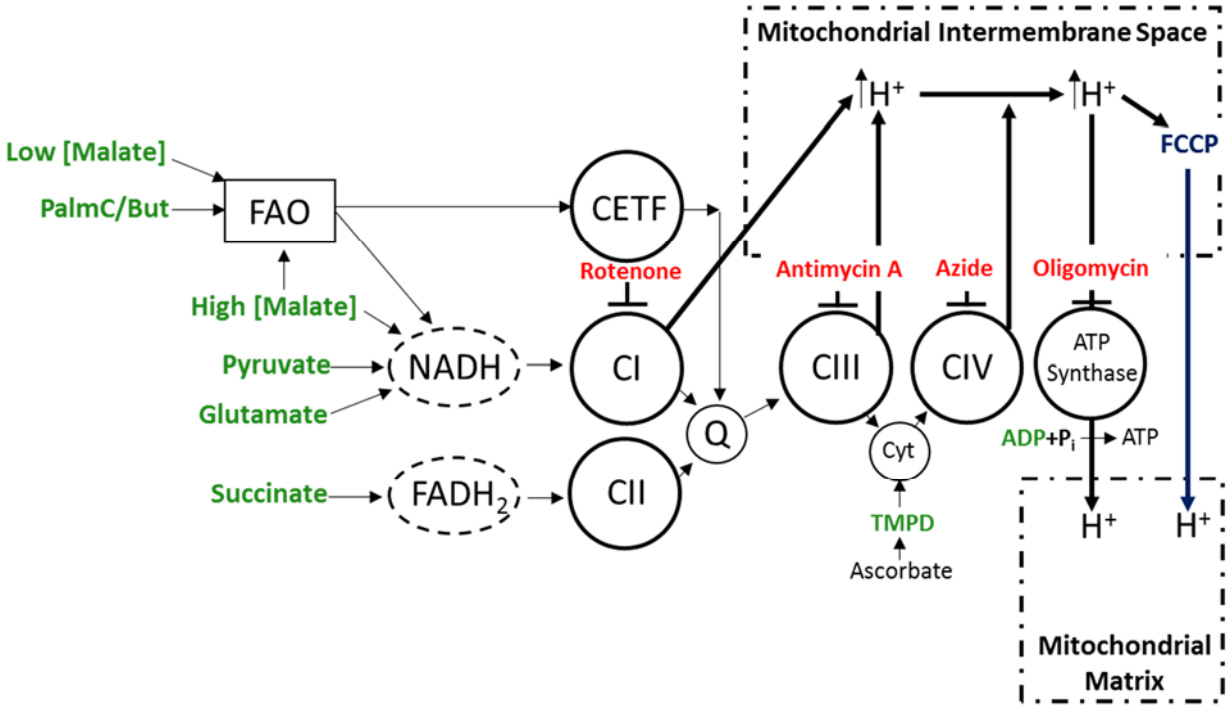

Figure 3.1: Flow diagram of substrate (green), inhibitor (red) and uncoupler (blue) interactions with their relevant mitochondrial pathways and complexes. PalmC: palmitoylcarnitine, But: butyrate, FAO: fatty acid oxidation, ETF: electron transferring flavoprotein complex, Q: coenzyme Q_{10}, Cyt: cytochrome C. Boxes indicate mitochondrial compartments

3.2. Material and Methods

3.2.1. Cell culture conditions

$IEC^{4.1}$ cells were cultured in high glucose Dulbecco's Modified Eagle Medium (DMEM, 500mL, Gibco, U.S) supplemented with 50mL of heat-denatured fetal bovine serum (Gibco, U.S), 3mL of L-glutamine (Gibco, U.S), 5mL of HEPES solution (Gibco, U.S) and 3mL of penicillin-streptomycin solution (Gibco, U.S). Subculturing of cells occurred every 2-3 days when cells were 80 - 90% confluent with trypsin containing 0.5% EDTA (Gibco, U.S). Trypsinized cells were then diluted with culture media at a 1:2 ratio of trypsin to media. The cell solution was then gently pipetted, collected and centrifuged at 1100RPM for 10mins. After centrifugation, the trypsin/media supernatant was siphoned off and the cell pellet was resuspended in 3mL of culture media. Cells were counted and seeded at approximately 1 x 10^6 cells in 100x20mm culture dishes (Falcon, U.S). Changes in cell viability and cell growth were monitored by counts using trypan blue (Gibco, U.S) during passages. Experiments were conducted on $IEC^{4.1}$ cells between the passages of 50 and 65.

3.2.2. MiR05 preparation

The mitochondrial respiratory solution (MiR05) is required for calibration and analysis with the O2k. MiR05 is prepared using 0.5mM EGTA, 3mM $MgCl_2*6H_2O$, 20mM taurine, 10mM KH_2PO_4, 20mM HEPES, 1g/L bovine serum albumin, 60mM potassium-lactobionate, 110mM sucrose, pH 7.1, adjusted at 30°C. Once made, MiR05 should be filter sterilized using 0.45µm filters and aliquoted into 50mL tubes for storage at -20°C until needed.

3.2.3. Calibration of O2k

Proper analysis of respirometry using the O2k requires several calibrations and corrections in order to ensure validity and reproducibility of results. Routine calibrations of oxygen concentrations at both air saturation and anoxic conditions within the chambers must be performed to define the highest and lowest concentrations of oxygen for the system and corresponding voltage measurements. Correction for instrumental background must also be experimentally determined as outlined by OROBOROS and input into the DatLab software prior to experiments. During calibration, stir tests and MiR05 contamination checks should also be performed. We recommend reviewing the instrumental background and calibration protocols outlined by the manufacturer[169].

3.2.4. O2k detailed protocols

3.2.4A. Cell preparation for O2k analysis

1) Aspirate off culture media, rinse plates with 2mL of pre-warmed PBS and aspirate
2) Add 2mL of trypsin containing 0.5% EDTA and incubate at 37°C for 6 - 8mins. Ensure cells are detached by viewing them under a microscope
3) Add 4mL of culture media to stop the trypsin reaction and gently pipette the cell suspension to minimize cell clumps
4) Centrifuge the cell suspension at 1100RPM for 10mins
5) Aspirate out the trypsin-media solution, leaving the cell pellet intact
6) Resuspend the cell pellet in 6mL of pre-warmed MiR05 and pipette gently to minimize cell clumps

7) Count live cells using trypan blue or another method and add MiR05 to make the final cell concentration: 1 x 10^6 cells/mL. During this step examine the cells to see if large clumps have formed, and if so, pipette the solution gently to separate the cells
8) Gently add 2.3mL of the 1 x 10^6 cell/mL cell suspension to the pre-calibrated O2k chambers. Slowly shift the stoppers downward into the "closed" position. This should be previously determined during liquid calibration of the O2k[168]
9) Open DatLab and observe the cells for 10mins or until respiration stabilizes

   NOTE: Avoid leaving the cells in the MiR05 for prolonged periods (≥1h) as they will become unresponsive to titrations once they are added to the chamber

3.2.4B. Optimization of permeabilizing agent

In order to ensure mitochondrial access to cell-impermeable substrates like succinate or ADP, the cell membrane must be permeabilized using detergents like saponin or digitonin[168,170,171]. The exact amount required for permeabilization must be determined experimentally, since over titrating these detergents leads to OMM damage. Here we outline the following steps to experimentally determine the correct concentration of digitonin for cell permeabilization

1) Prepare a 1 x 10^6 cell/mL suspension according to the steps previously outlined
2) Wait for 10 - 15mins or until respiration stabilizes
3) Titrate 1µL of 1M rotenone (0.5µM) into the O2k chambers and wait 5mins
4) Titrate 20µL of 1M succinate (10mM) into the O2k chambers and wait 5 - 10mins or until respiration stabilizes
5) Titrate 10µL of 0.5M ADP (2.5mM) into the O2k chambers and wait 5 - 10mins or until respiration stabilizes

6) Carefully titrate 0.2 - 0.4µL of 10mg/mL digitonin and wait 5mins or until respiration stabilizes
7) Repeat these titrations until respiration no longer increases with additional digitonin titrations. Over titration of digitonin is also possible and leads to a continuous decline in cell respiration
8) Record the concentration of digitonin required for permeabilization of cells and use that in future experiments

   NOTE: Both succinate and ADP titrations are not expected to elicit increases in respiration since they are cell impermeable, but with the addition of digitonin, should lead to increases in respiration

3.2.4C. Maximal complex specific activity in permeabilized cells

1) Prepare a 1 x 10^6 cell/mL cell suspension according to the steps previously outlined
2) Wait for 10 -15mins or until respiration stabilizes
3) Titrate sufficient volumes of digitonin in order to permeabilize cells based on experimentally determined results. Based on our findings: 0.8µL of 10mg/mL (4µg/mL) was enough for permeabilization

   NOTE: Addition of digitonin will lead to decreases in respiration due to cellular substrates leaving the cytoplasm after permeabilization
4) Titrate 10µL of 0.5M ADP (2.5mM) into the O2k chambers and wait 5-10mins or until respiration stabilizes

   OPTIONAL: For beta oxidation analysis titrate: 4µL of 50mM malate (0.1mM) and 10µL of 10mM palmitoylcarnitine (0.05mM) for LCFA beta oxidation or 4µL of 1M sodium

butyrate (2mM) for SCFA beta oxidation. An additional titration of 9.5µL of 400mM malate (2mM) ensures saturation of malate concentrations for beta oxidation and 400mM (2mM) malate for butyrate beta oxidation. If these titrations are performed, exclude the malate titration from the step below

5) Titrate 5µL of 2M pyruvate (5mM), 10µL of 2M glutamate (10mM) and 10µL of 400mM malate (2mM) and wait 10 - 15mins or until respiration stabilizes
6) Titrate 5µL of 4mM cytochrome c (10µM) into the O2k chambers and wait until respiration stabilizes

   NOTE: Dramatic increases in respiration with cytochrome c indicate OMM damage and should be taken into account when interpreting results
7) Titrate 1µL of 1M rotenone (0.5µM) into the O2k chambers and wait 5 - 10mins or until respiration stabilizes
8) Titrate 20µL of 1M succinate (10mM) into the O2k chambers and wait 5 - 10mins or until respiration stabilizes
9) Titrate 1µL of 5mM antimycin A (2.5µM) into the O2k chambers and wait 5 - 10mins or until respiration stabilizes
10) Titrate 5µL of 5mM ascorbate (2mM) followed immediately by a 5µL titration of 200mM *N,N,N′,N′*-tetramethyl-*p*-phenylenediamine (TMPD, 0.5mM). Open the chambers and record respiration for 20mins
11) Close the chambers and record respiration for an additional 5mins
12) Titrate 50µL of 4M sodium azide (≥100mM) and record respiration for the next 10mins

3.2.4D. Respiratory control ratio protocol in intact cells

1) Prepare a 1 x 10^6 cell/mL cell suspension according to the steps previously outlined
2) Wait for 10 - 15mins or until respiration stabilizes
3) Titrate 1µL of 5mM oligomycin (2.5µM) into the O2k chambers and wait for 5 - 10 mins or until respiration stabilizes
4) Carefully titrate 0.3µL of 1mM FCCP (0.15µM) and wait until respiration stabilizes
5) Repeatedly titrate 0.1 - 0.3µL of 1mM FCCP (0.05 - 0.15µM) until respiration shows no further increases. Over titration of FCCP is possible and leads to a continuous decline in respiration
6) Titrate 1µL of 1M rotenone (0.5µM) and 1µL of 5mM antimycin A (2.5µM) into the O2k chambers and record respiration for the next 5 - 10mins

3.3. Representative results

Utilizing protocols outlined in this paper, representative results were obtained and will be discussed in detail. Optimization of permeabilizing agents is critical for determining mitochondrial function of permeabilized cells without compromising the OMM. Rotenone is first titrated to ensure no reverse electron flow and limit oxaloacetate formation[173]. Oxaloacetate is a potent inhibitor of CII and could potentially diminish or ablate the expected response of succinate during cell permeabilization by digitonin[174]. Addition of succinate should not immediately elicit an increase in respiration since it is cell impermeable, but upon the introduction of digitonin, should lead to increased respiration as the cell becomes permeabilized (Figure 3.2)[175]. With continuous titrations of digitonin, respiration will eventually peak and level off, indicating the cell is fully permeabilized and exogenous succinate is being oxidized by CII (Figure 3.2). The amount of

digitonin required to reach this peak, whether it be final concentration or volume, should be recorded and used for future experiments. Importantly, over-titrating digitonin can lead to a continual decline in respiration due to OMM damage (Figure 3.2). The titration of ADP is important to shift succinate respiration from state 2 to state 3, thereby making the identification of succinate-linked responses to digitonin titrations more pronounced. Based on our results, we found that 4μg/mL was sufficient for IEC$^{4.1}$ cell permeabilization (Figure 3.2).

By applying the optimized digitonin concentrations, maximal activity of specific mitochondrial complexes could be determined. Beta oxidation of LCFA or SCFA members can be assessed by either titrating palmitoylcarnitine or butyrate with malate prior to the titrations of additional NADH linked substrates. Palmitoylcarnitine is utilized instead of palmitic acid to ensure that the substrate can freely enter the mitochondria without the otherwise needed modifications by CPT1[27]. While our titrations for palmitoylcarnitine follow previously established protocols, the final concentration for butyrate was selected to ensure it behaved as a substrate, rather than as a potential signaling molecule[175,176]. The addition of malate titrations during beta oxidation assessments is also necessary to prevent feedforward inhibition of beta oxidation by the accumulation of short chain acyl-CoAs and reduction in the acetyl-CoA pool[168,175]. As this protocol may be performed optionally, it is important to note that if included, beta oxidation activity must be factored into the activity of CI during analysis.

The specific activity of CI is examined by taking the respiration of cells in the presence of CI linked substrates (pyruvate, glutamate, malate) and subtracting the respiration obtained during CI inhibition by rotenone (Figure 3.3A). This inhibition of CI by rotenone also allows CII activity to be identified without any influence of CI respiration. Prior to rotenone titrations, cytochrome c is added to test for OMM damage (Figure 3.3A). If damage has occurred, exogenous

cytochrome c enters the mitochondrial ETC and participates in mitochondrial OXPHOS, leading to dramatic increases in respiration [168,175]. Identification of CII activity follows a similar methodology to identifying CI activity, with the subtraction of respiration in the presence of a substrate (succinate) by the respiration signal after titration of an inhibitor like antimycin A (Figure 3.3A). While antimycin A does not directly inhibit CII, its inhibition of CIII leads to the inability of CII to release electrons, thereby inhibiting it[168,175].

For CIV activity, TMPD is used to reduce cytochrome c, thereby acting as an indirect substrate for CIV[168,175]. TMPD rapidly undergoes autoxidation with oxygen, so ascorbate is titrated prior to TMPD in order to maintain TMPD in a reduced state[168,175]. Due to the autoxidation of ascorbate and respiration of CIV, respiration dramatically increases and therefore requires the opening of the O2k chambers in order to prevent cell hypoxia (Figure 3.3B). Upon closure of the chambers, respiration will dramatically increase, eventually peak and begin to linearly decline (Figure 3.3B). To examine CIV exclusively, the respiration measurement after this peak must be subtracted by the respiration measurement after CIV inhibition by sodium azide under similar time constraints (Figure 3.3B).

Gross mitochondrial function can be estimated by the identification of the respiratory control ratio (RCR) in intact cells. RCR is an important indicator of mitochondrial health and dysfunction, taking into account both maximal and minimal respiratory activity[168,175]. The protocol starts with a titration of oligomycin to inhibit ATP synthase and identify respiration linked to proton leak across the IMM (Figure 3.4). Following this, careful titrations of FCCP uncouple mitochondrial OXPHOS and allow protons to move freely across the IMM (Figure 3.4). These protons react with molecular oxygen, leading to dramatic increases in respiration and the theoretical maximum for mitochondrial OXPHOS to be identified (Figure 3.4). The last titrations

of rotenone and antimycin A allow non-mitochondrial related respiration to be determined and subtracted from all other values so that only mitochondrial related respiration is measured (Figure 3.4). RCR is identified by dividing the highest respiration measured in the presence of FCCP by the respiration measured in the presence of oligomycin. Larger RCR values typically indicate greater mitochondrial function, but a closer examination of changes in both the FCCP and oligomycin measurements must be made before making these conclusions.

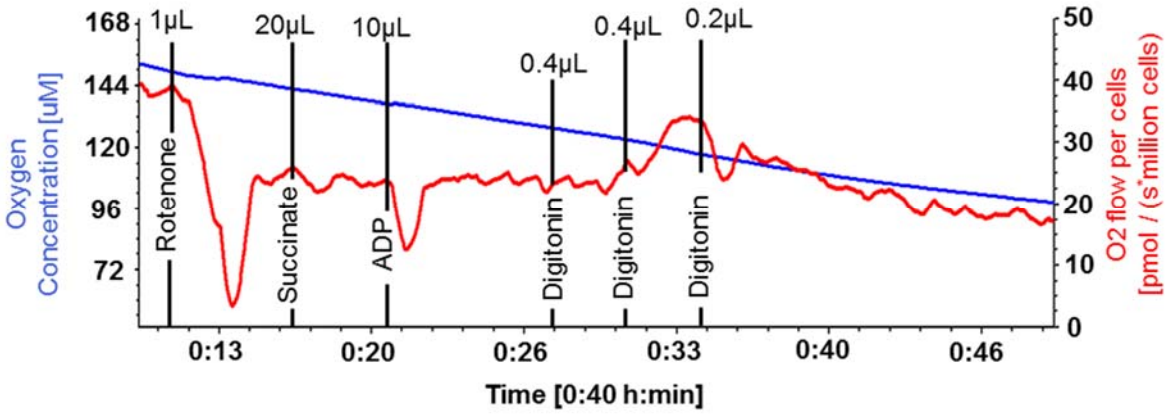

Figure 3.2: O2k representative tracing for digitonin optimization protocol in IEC$^{4.1}$ cells. Black vertical lines indicate titrations of substrates/inhibitors/uncouplers with volumes (µL) indicated at the top of the lines (Table 3.1). ADP: adenosine diphosphate.

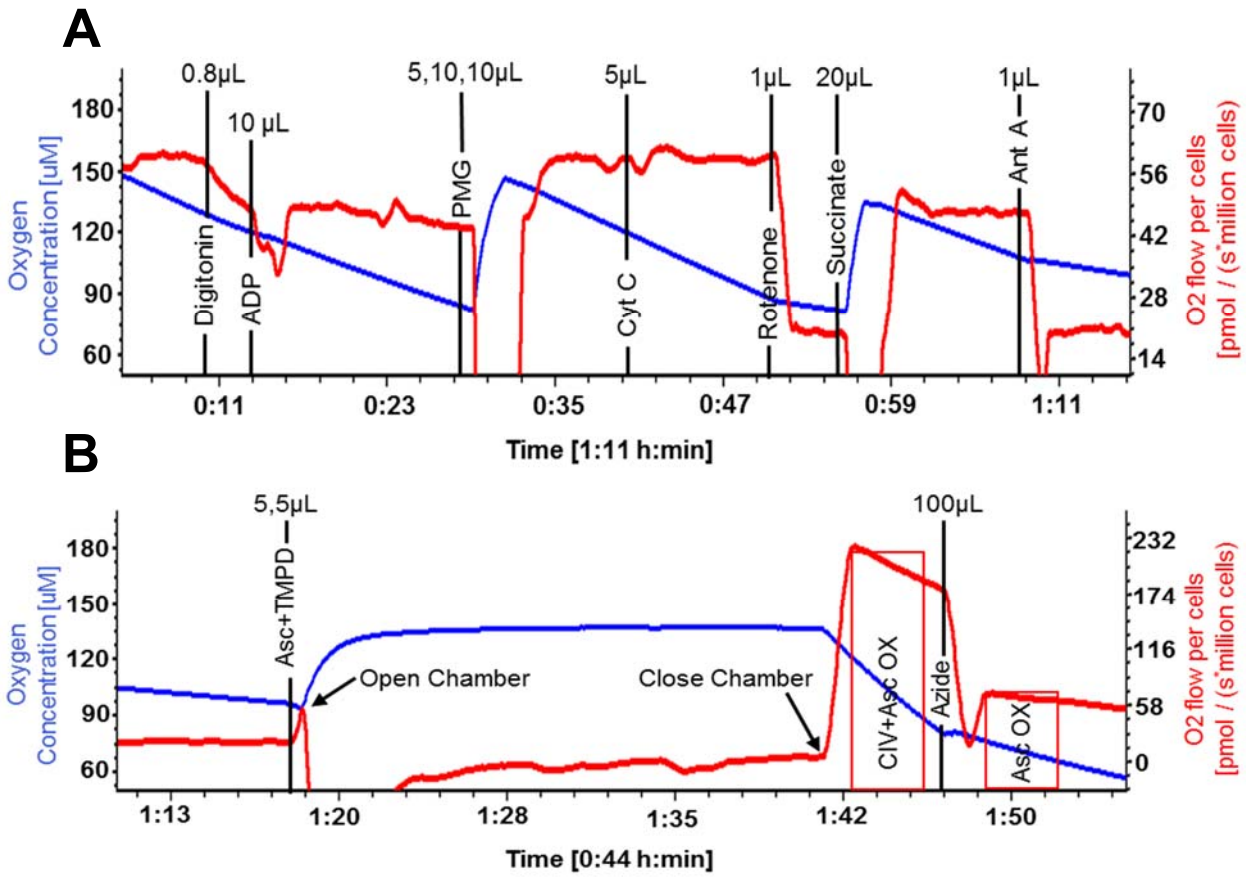

Figure 3.3: O2k representative tracing during analysis of mitochondrial complex specific function in permeabilized IEC$^{4.1}$ cells. A) Complex I and Complex II related titrations B) CIV related titrations. Black vertical lines indicate titrations of substrates/inhibitors/uncouplers with volumes (µL) indicated at the top of the lines (Table 3.1). ADP: adenosine diphosphate, PMG: pyruvate + malate + glutamate, Cyt c: cytochrome c, Ant A: antimycin A, Asc+TMPD: ascorbate+TMPD, CIV+Asc OX: CIV oxidation + ascorbate oxidation, Asc OX: ascorbate oxidation.

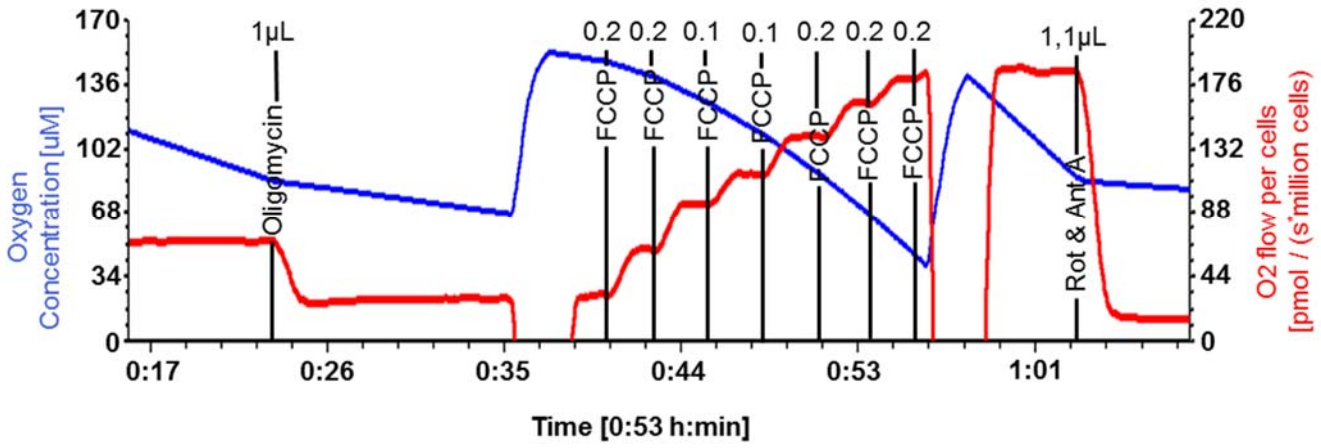

Figure 3.4: O2k representative tracing of intact IEC[4.1] cells during an RCR protocol. Black vertical lines indicate titrations of substrates/inhibitors/uncouplers with volumes (µL) indicated at the top of the lines (Table 3.1). Rot & Ant A: rotenone + antimycin A.

3.4. Discussion

Application of the O2k in measuring mitochondrial function has been performed in isolated tissues, (fat, genital, heart, kidney, liver, lung, skeletal muscle) cells, (blood, endothelial, fibroblast, lymphocytes, platelet and stem cells) and isolated mitochondria[177]. Despite its implementation in numerous tissue and cellular models, specific and detailed protocols for conducting O2k analysis in IECs is not available. This is particularly surprising since the O2k could allow for a comprehensive examination of mitochondrial pathways pertinent to IEC bioenergetic processes (beta oxidation, mitochondrial complex activity) under a variety of treatments and conditions. Indeed, given the importance of IEC bioenergetics in regulating the intestinal barrier and subsequent host exposure to microbes or noxious stimuli, further investigation into IECs may prove beneficial in identifying disease targets and therapeutics for

intestinal diseases like IBD[102,103,165]. This study therefore sought to develop and discuss, step-by-step instructions for the application of O2k protocols within IECs.

Measurement of mitochondrial function with the O2k respirometer allows careful and systematic evaluation of numerous pathways that may be pertinent to the disease process. When appropriately calibrated and serviced, this instrument also allows highly precise and consistent measurements, limiting possible variability in data. Application of potentially damaging titrations (digitonin, FCCP, CCCP) or mitochondrial inhibitors (rotenone, antimycin A, azide) can also be modified based on real-time responses, thereby ensuring that changes in O_2 flux reflect the applied titration and not mitochondrial damage or lack of uncoupling/inhibition. Despite these advantages, there are also several disadvantages to the analysis of mitochondrial function using the O2k. While the instrument is appropriate for cells that prefer being in a suspension, adherent cell types, in particular, will be stressed when removed from their culture environment and added to chambers with spinning stir rods. Protocol design and timing can also become an issue if measuring precious samples or samples that are not viable for long periods of time. The instrument also requires constant monitoring by trained personnel between and during experiments to ensure consistency in the operation of the machine and measurement of data. These factors should be considered by investigators when determining if the measurement of mitochondrial function using the O2k is appropriate.

3.5. Conclusion

Previous studies have described IBD as an "energy deficiency" disease, with impairments in both beta oxidation and mitochondrial OXPHOS being observed in human IBD and animal colitis models[101,139.141]. Within previous *in-vitro* studies, mitochondrial dysfunction has been shown to negatively affect both intestinal barrier function and intestinal permeability, thereby tying earlier observations regarding cellular bioenergetics to a well-recognized feature of colitis and IBD[102,103,165]. However, elaborating and building on these discoveries has remained difficult due to the gap in established protocols and techniques for mitochondrial bioenergetic analysis. Attempting to bridge this gap, this study outlines detailed protocols for conducting mitochondrial functional analysis using the O2k respirometer. Utilizing these techniques, novel therapies exploiting the evidence of mitochondrial function and the intestinal barrier can be further investigated as treatment options for IBD.

Chapter 4

Inhibiting DRP1-Fis1 mediated mitochondrial fission reduces DSS associated bioenergetic impairments in intestinal epithelial cells

4.1. Introduction

In understanding the complex pathogenesis of IBD, numerous molecular targets and pathways have been investigated. While no single causal factor has consistently been linked to IBD onset, previous evidence has shown support for beta oxidation and mitochondrial dysfunction in IBD patients. Novel findings by Roediger in the 1980s identified that intestinal epithelial biopsies from actively inflamed IBD patients showed an inability to metabolize the SCFA: butyrate, a key substrate required to meet approximately 70% of the intestinal epithelium's energy demands[101]. More recent evidence has also identified that mutations in genes encoding for key carnitine-sodium transporters (OCTN1, OCTN2) required for beta oxidation, are also genetic risk factors for IBD[178]. The importance of fatty acid metabolism in intestinal homeostasis is further emphasized since either pharmacological inhibition of beta oxidation or genetic deletion of OCTN2, leads to spontaneous colitis in mice[139,140]. Since beta oxidation occurs within the mitochondria, it can be hypothesized that mitochondrial dysfunction plays a role in beta oxidation defects and possibly IBD development. In support of this, reports of reduced mitochondrial complex function, disrupted mitochondrial ultrastructure and significantly higher production of ROS have been identified in IBD patient biopsies[101,141,145,179]. The association of beta oxidation with IBD and colitis could be tied to mitochondrial dysfunction, with further investigation being

warranted. Observations of mitochondrial dysfunction have also been noted in the IBD representative model of DSS colitis.

The DSS model of colitis has proven invaluable in elucidating potential disease mechanisms relevant to human IBD[131,180]. In addition to its similar histological presentation to human UC, the DSS colitis model also shows signs of mitochondrial dysfunction that reflect human IBD. The DSS molecule is a negatively charged polysaccharide that exists in a highly variable molecular size, with only the 40-50 kDa and 5 kDa sized particles creating colitis[129-131,180]. Despite its wide use, the exact mechanism for how DSS leads to colitis is currently unknown. It is generally agreed that DSS targets IECs and disrupts the epithelial barrier, thereby allowing the migration of intestinal microbes and corresponding inflammatory responses[133,180,181]. DSS colitis also leads to significant increases in ROS production, reduced mitochondrial complex function and alterations in beta oxidation metabolism, reflecting similar observations seen in human IBD[141,182,183]. Interestingly, targeting and treating consequences related to mitochondrial dysfunction, like excessive ROS has shown therapeutic potential in numerous studies that utilize DSS to induce colitis[102,184]. The presence of mitochondrial dysfunction in DSS colitis mirrors reported observations in human IBD, with treatment of these mitochondrial specific consequences being efficacious and potentially highlighting mitochondria as a therapeutic target for human IBD. One particularly novel and promising point of mitochondrial intervention could be the inhibition of excessive mitochondrial fission.

Mitochondria and the networks they form are constantly remodeling through the mitochondrial dynamic processes of fusion and fission. While basal levels of fusion and fission are beneficial, evidence suggests that excessive mitochondrial fission, mediated by the binding of DRP1 and Fis1, is associated with disease. Mitochondrial fusion is important in reducing

unnecessary mitochondrial degradation, promoting the transfer of mitochondrial contents between mitochondria and protecting cells during conditions of nutrient starvation[66,80,185]. The opposing process, mitochondrial fission, is necessary for cellular replication, degradation of mitochondria by mitophagy and initiating programmed cell death by apoptosis[66,80,186]. Under homeostatic conditions, mitochondrial fission is mediated by interactions between DRP1 and its receptors: Fis1, Mff, MiD49, and MiD51[66,80]. However, studies have noted that increased binding of DRP1 and Fis1 is associated with excessive mitochondrial fission, and the formation of "fragmented", dysfunctional mitochondrial networks[15,18,19,187]. These fragmented mitochondrial networks have been identified in numerous cellular and animal disease models and are related to increased ROS production, reduced mitochondrial function and increased cell death[13-19,150,187-189]. Evidence of DRP1 and Fis1 associated mitochondrial fission with mitochondrial dysfunction and disease, suggests that targeting this interaction could yield therapeutic benefit. Indeed, previous work using the DRP1 and Fis1 inhibitor, P110, has shown therapeutic benefit in neurodegenerative and cardiovascular disease models, but still has yet to be tested within a relevant colitis context[13-19,150,187-189]. Therefore, this study sought to examine if DSS treated IEC$^{4.1}$ cells exhibit change in mitochondrial dynamics and function, and if these changes could be mitigated with P110.

4.2. Materials and Methods

4.2.1. Cell culture conditions

The murine intestinal epithelial cell line, IEC$^{4.1}$, was originally isolated from Balb/c mice and immortalized through SV-40 large gene transfer[190]. After isolation, these cells were found to exhibit similar characteristics to normal enterocytes[190]. Cells were cultured in IEC$^{4.1}$ media consisting of high glucose DMEM (Gibco, ThermoFisher Scientific) supplemented with 50mL of heat denatured fetal bovine serum (Gibco, U.S), 3mL of L-glutamine (Gibco, ThermoFisher Scientific), 5mL of HEPES solution (Gibco, U.S) and 3mL of penicillin-streptomycin solution (Gibco, ThermoFisher Scientific). Subculturing of cells occurred every 2 - 3 days when cells were 80 - 90% confluent with trypsin containing 0.5% EDTA (Gibco, U.S). Trypsinized cells were then diluted with culture media at a 1:2 ratio of trypsin to media. The cell solution was then gently pipetted, collected and centrifuged at 1100RPM for 10mins. After centrifugation, the trypsin/media supernatant was siphoned off and the cell pellet was resuspended in 3mL of culture media. Cells were counted and approximately 1 x 10^6 cells were seeded in 100x20mm culture dishes (Falcon, Corning). Changes in cell viability and cell growth were monitored by counts using trypan blue (Gibco, ThermoFisher Scientific) during passaging. Experiments were conducted on IEC$^{4.1}$ cells between the passages of 50 and 65.

4.2.2. Optimization of DSS and P110 dosage using the AlamarBlue assay

Alamar blue, also known as resazurin, is a dye that is commonly used to determine the cytotoxicity of chemicals and to optimize the dosage of therapeutic agents[191-193]. In its oxidized form, it exhibits a strong dark blue color, but changes to a light pink, highly fluorescent compound called resorufin when reduced by NADH in the presence of mitochondrial diaphorases[193]. The color difference in resazurin and resorufin can be read by fluorescence plate readers and provide

information on the concentration of NADH[193]. IEC$^{4.1}$ cells were seeded at 2 x 10^4/well in 96 well plates (Nunc Delta, ThermoFisher Scientific) and allowed to incubate for 24h before treatments. A pre-treatment of culture media containing P110 (2.5µM) was applied to P110 groups for 45mins. This P110 containing media was then diluted to either 0.5µM, 1µM or 1.5µM with untreated IEC$^{4.1}$ culture media or DSS culture media, such that the final concentration of DSS (40 kDa, Affymetrix) was either 1%, 1.5% or 2% (w/v). Cells were then incubated with the treatments for either 18h or 24h to assess optimal exposure times. AlamarBlue (Gibco, ThermoFisher Scientific) was added to the culture media at a 1:10 ratio and allowed to incubate with the cells for 5.5h prior to measurement. After 5.5h, plates were read at 550nm and 590nm for excitation and emission spectra respectively (SpectraMax I3, Molecular Devices). Plate and group blanks were subtracted from the raw data to get the final values. Based on results obtained, 2% DSS and 1.5µM P110 applied in the manner described above, was sufficient for use in further experimentation (Figure A.1)

4.2.3. Measurement of cell viability and normalization of data

Cells were seeded into 12 well plates (Nunc Delta, ThermoFisher Scientific) at 2.4 x 10^5 cells per well and treated according to the optimized DSS and P110 treatments (Figure A.1). After the P110 and DSS treatments, culture media, PBS rinses and trypsinized cells were collected in tubes and centrifuged at 1100RPM for 10mins. The solution was suctioned out and cells were resuspended in 100µL IEC$^{4.1}$ culture media. After resuspending, 10µL of this cell suspension was aliquoted and diluted at a 1:1 ratio with trypan blue, then counted on a hemocytometer. Normalization of cells for several *in-vitro* experiments followed a similar manner, with exceptions to the volume cells were resuspended in.

4.2.4. O2k mitochondrial OXPHOS analysis

Real-time mitochondrial functional analysis was performed with the Oxygraph-2k C-series (OROBOROS Instruments, Austria). Titration of mitochondrial relevant chemicals was modeled after the "substrate uncoupler inhibitor titration protocol-002" (SUIT-002, OROBOROS Instruments, Austria), with modifications to digitonin and FCCP titrations (Figure A.2)[195]. A total of 1.5 x 10^6 cells were seeded into 100x20mm culture dishes and incubated for 24h. DSS and DSS+P110 treated culture media was then applied in the manner previously described (Figure A.1). After the DSS±P110 treatments, cells were trypsinized, counted and resuspended at the concentration of 1 x 10^6 cells/mL in MiR05 containing 0.5mM EGTA, 3mM $MgCl_2.6H_2O$, 20mM taurine, 10mM KH_2P0_4, 20mM HEPES, 1 g/L bovine serum albumin, 60mM potassium-lactobionate and 110mM sucrose, pH 7.1.

Two separate protocols were performed to separately examine SCFA and LCFA metabolism in $IEC^{4.1}$ cells. Examination of LCFA metabolism was performed as a component of the modified SUIT-002 protocol. Both protocols started out with the permeabilization of cells using digitonin (4µg/mL) and followed by a titration of excess ADP (5µM) to ensure state 3 respiration for future substrates. SCFA and LCFA metabolism was then assessed by titrations of malate (0.1mM) and sodium butyrate (NaBut, 2mM) for SCFA or malate (0.1mM) and palmitoylcarnitine (PalmC, 0.05mM) for LCFA. After the NaBut and PalmC titrations for the SCFA and LCFA protocols respectively, an additional malate (2mM) titration was performed. Inclusion of malate titrations is necessary to reduce feedforward inhibition of beta oxidation by short chain acyl-CoA accumulation and reduction in the acetyl-CoA pool[168,175,196]. By titrating different concentrations of malate (0.1mM, 2mM), beta oxidation can also be examined under different degrees of NADH substrate saturation[195]. During these titrations, exogenous cytochrome

c (10μM) was added to determine OMM integrity after digitonin permeabilization[168,195]. Participation of exogenous cytochrome c in the ETC promotes a rapid increase in O_2 flux and indicates damage to the OMM from permeabilizing agents[168,195].

At this point, the SCFA protocol ended, while the modified SUIT-002 protocol continued. Further titrations of substrates linked to CI (pyruvate, glutamate) and CII (succinate) were used to examine specific changes in substrate oxidation by there respective mitochondrial complexes[168,195]. After these titrations, the theoretical maximum capacity for oxidative phosphorylation (MAX_{OX}) was identified with careful titrations of FCCP[168,195]. FCCP is a chemical uncoupler that dissipates the proton gradient between the IMS and mitochondrial matrix. The dramatic influx of protons into the mitochondrial matrix then react with molecular oxygen, resulting in significant O_2 flux increases and a theoretical measure of MAX_{OX}. During the protocol, MAX_{OX} was identified as the point at which respiration no longer responds to additional FCCP titrations. To eliminate non-mitochondrial contributions to oxygen consumption measures, O_2 flux during complete mitochondrial inhibition by rotenone (0.5μM) and antimycin A (2.5μM) was isolated[168,175]. This O_2 flux was then subtracted from all other values to ensure only mitochondrial-related respiration was examined[168,175].

Activity of CIV was determined through titrations of ascorbate (2mM) and TMPD (0.5mM). TMPD reduces cytochrome c, thereby allowing it to serve as a substrate for CIV and allow changes in respiration to be related to CIV function. Since TMPD undergoes auto-oxidation with oxygen, ascorbate must be added to maintain TMPD in a reduced state[168,195]. Additions of both ascorbate and TMPD lead to dramatic increases in O_2 flux due to the combination of increased CIV activity and auto-oxidation of ascorbate by oxygen. In order to isolate O_2 flux related only to CIV, sodium azide (100mM) is titrated to inhibit CIV activity, thereby leaving only the O_2 flux

related to ascorbate auto-oxidation. Once determined this can be isolated and subtracted from the O_2 flux of CIV and ascorbate oxidation, leaving only O_2 flux related to CIV.

Upon completion of the analysis, 1mL of cells was collected from the chambers and 10µL of the cell suspension was mixed with trypan blue at a 1:1 ratio for counting on a hemocytometer and normalization of data. Absolute O_2 flux values from these Oxygraph-2k experiments can also be found in the Appendix (Figure A.3-A.5). Respirometric tracings and data was recorded with DatLab 4 and analyzed using DatLab 7 (OROBOROS Instruments, Austria).

4.2.5. Mitochondrial staining, imaging and morphology quantification

IEC$^{4.1}$ cells were seeded into 8-well glass bottom chamber slides (Nunc LabTek II, ThermoFisher Scientific) at 5 x 10^4 cells per well and allowed to incubate for 24h. Prior to P110 and DSS treatments, mitochondrial networks were stained with MitoTracker Red CMXRos dye (50nM) (ThermoFisher Scientific) for 30mins and rinsed three times with PBS. Nuclear staining was then performed with Hoescht dye (1µg/mL) (ThermoFisher Scientific) for 10mins and followed by two PBS washes. After DSS and P110 treatments, cells were imaged using the Leica DMI6000B Diskovery Flex spinning disk microscope (Leica Microsystems). Quantification of mitochondrial networks was performed blinded and consisted of counting 20 cells from different fields of view per well. Cells were then categorized as either fragmented, intermediate or fused mitochondrial morphologies based on visual criteria (Figure A.6)[197,198]. Cells exhibiting >80% spherical mitochondria were categorized as “fragmented”. If the majority of mitochondria present in the cell existed as interconnected networks spanning across >50% of the cell, they were categorized as “fused”. If cells displayed characteristics of both fragmented and fused

mitochondria morphologies or short, separate, mitochondrial tubules, they were categorized as "intermediate".

4.2.6. Cellular ATP content

Cellular ATP was measured using the Cell-Glo Titer ATP Luciferase kit (Promega, U.S). This assay uses firefly luciferase to catalyze the reaction of beetle luciferin, ATP and molecular oxygen into a high energy intermediate, oxyluciferin[199]. The return of oxyluciferin to its ground state yields a colorimetric change, which can be measured by a plate reader to determine intracellular ATP content[199]. Cells were seeded at 2.4 x 10^5 cell/mL into 12 well plates (Cellstar, Greiner Bio-One) and treated based on the previously described DSS±P110 protocol (A.1.1). DSS±P110 media was then aspirated off and 200µL of ATP luciferase reagent was added to each well. Plates were then placed on a shaker for 5min. After shaking, plate wells were pipetted vigorously to ensure complete lysis of cells. The lysed cell suspension was collected and plates were rinsed with 100µL of luciferase reagent to ensure collection of remaining lysed cells. Samples were then added in duplicates (100µL each) to white opaque 96 well plates (Greiner Bio-One). Standard curves of known ATP concentrations (500k nM - 5nM) and blanks containing ATP luciferase reagent without cells were used to determine ATP concentration of samples in nmol units. Plates were equilibrated for 10mins prior to reading at changes in luminescence by the plate reader (Victor 3v, Perkin Elmer). ATP concentration was then normalized to protein concentration by a Bradford assay. ATP Luciferase samples were diluted 10x in dH_2O and 10µL was added in duplicates to 96 well plates. Standard curves with bovine serum albumin at known concentrations and blanks containing dH_2O were generated and used to normalize ATP content to nmol of ATP/pg protein. Each sample then received 200µL of 1:5 diluted Bradford reagent (BioRad Laboratories,

USA) and plate absorbance were read at 595nM (Victor 3v, Perkin Elmer). Results were analyzed using the Workout 2 Software package (Perkin Elmer).

4.2.7. Mitochondrial membrane potential analysis

Mitochondrial $\Delta\psi_m$ was determined using the red-orange fluorescent probe tetramethylrhodamine ethyl ester (TMRE). TMRE is a positively charged dye that migrates to the negatively charged mitochondrial matrix, where its accumulation shifts both the absorption and emission spectra towards infra-red wavelengths[200]. Upon IMM damage or chemical uncoupling, protons may freely migrate from the IMS to the negatively charged mitochondrial matrix.[49,200]. As the mitochondrial matrix becomes increasingly more positively charged, the localization of the cationic TMRE dye is reduced due to electrochemical repulsion, resulting in a lower fluorescence[49,200]. The opposite also holds true, that if the mitochondrial matrix becomes more negatively charged, TMRE will accumulate more readily and fluorescence will increase[49]. Inhibition of ATP synthase by oligomycin illustrates this phenomenon since protons cannot be transferred into the mitochondrial matrix, leading to increased polarization between the IMS and mitochondrial matrix[49].

TMRE dye concentration must be optimized to limit the non-specific binding of the dye to mitochondrial proteins[49]. This can be determined by comparing the fluorescence of TMRE dyes under varying concentrations to groups exposed to a positive control for mitochondrial depolarization, like FCCP, under similar TMRE dye concentrations. Optimization of TMRE dye concentrations identified that concentrations ranging from 0 - 90nM did not show non-specific binding (Figure A.7). The concentration of 45nM TMRE was selected for future experiments

because it maintained the highest ratio of fluorescence when compared to its depolarized control (45nM + FCCP) (Figure A.7).

To examine the effects of DSS±P110 on mitochondrial polarization, 2 x 10^4 $IEC^{4.1}$ cells were seeded in 96 well plates, incubated for 24h and treated with DSS±P110 for either 1h or 24h. Positive controls for mitochondrial depolarization (FCCP) and mitochondrial hyperpolarization (oligomycin) were included to confirm the extent of polarization in DSS±P110 treated cells[49]. FCCP+P110 and oligomycin+P110 groups were also included to determine P110's potential effect during mitochondrial depolarization and hyperpolarization. FCCP and oligomycin treated groups had their untreated culture media aspirated off and replaced with culture media containing FCCP (10µM) (Sigma) and oligomycin (4µg/mL) (Sigma) and incubated for 30mins. After the 30min incubation, treated culture media was siphoned off from the experimental groups and all groups then received TMRE dye (45nM) (ThermoFisher Scientific) suspended in cell culture media. Cells were then allowed to incubate for 30mins with the dye. Immediately prior to measurement, cells were washed twice with PBS containing 0.2% (w/v) bovine serum albumin. Plates were then loaded with 100µL of the 0.2% bovine serum albumin+PBS solution. After loading the plate was read at 530nM and 580nM for excitation and emission spectra respectively (Spectra Max I3, Molecular Devices). Blanks for each group were also generated, measured and subtracted from their respective group.

4.2.8. Statistical analysis

Data is presented as mean ± standard error of the mean (SEM). Analysis and statistical tests were performed using GraphPad Prism 6 and the significance level was set at $p<0.05$. Parametric data was analyzed using either One-Way ANOVA, ordinary Two-Way ANOVA or

repeated measures Two-Way ANOVA tests. Non-parametric data was analyzed using a Kruskal-Wallis test. If $p<0.05$, then either a Tukey's, Dunn's or Sidak's multiple comparison test was applied.

4.3. Results

4.3.1. DSS associated reductions in NADH concentration are prevented with P110

Prior to examining DSS's or P110's effect on IEC^{4,1} cells, these treatments were optimized to ensure appropriate exposure, dosage, and timing for future experiments. Utilizing the colorimetric alamarBlue assay, both DSS (1 - 2%) and P110 (0.5 - 1.5µM) concentrations and exposure times (18h & 24h) were optimized. At 18h of DSS exposure, there was no significant change in alamarBlue metabolism between control and DSS treated cells (data not shown). With 24h exposure at 2% DSS (85.83 ± 3.44), alamarBlue metabolism was significantly reduced compared to control (Control: 100 ± 0) ($p<0.05$) (Figure 4.1). In contrast, DSS cells given 0.5µM P110 showed no difference in alamarBlue metabolism compared to control cells (DSS+P110 0.5 µM: 88.99 ± 2.53; $p>0.05$). Furthermore, increasing concentrations of P110 incrementally by 0.5µM, reduced impairments in AlamarBlue metabolism by DSS, peaking at 1.5µM P110 (95.95 ± 2.23) ($p<0.05$). As a potential indicator of NADH concentration, reductions in alamarBlue metabolism with 2% DSS for 24h, and recovery of this change by the addition of 1.5µM P110 for 24h, suggested that these doses and concentrations would be appropriate for further mitochondrial experiments**.** Therefore, 2% DSS and 1.5µM P110 for 24h were used in future experiments and applied in the same manner described for the alamarBlue assay (Figure A.1.1)

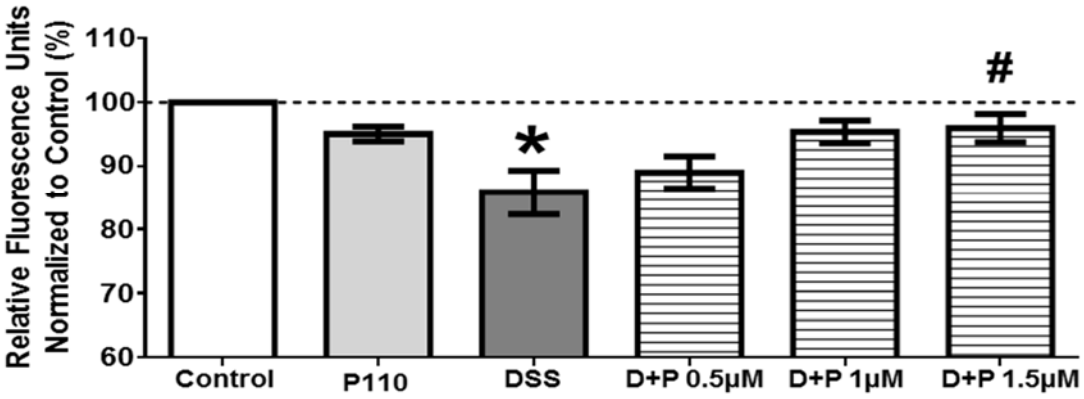

Figure 4.1: Dose optimization of 24h DSS±P110 treatments for IEC$^{4.1}$ cells using alamarBlue. D (DSS) + P (P110) represents cells treated with 2% DSS and 0.5µM, 1µM, 1.5µM P110. Data is represented as mean ± SEM, n = 8 replicates from 2 independent experiments. *Represents significant differences between the control group, #Represents significant differences between the 2% DSS group, $p<0.05$, One-Way ANOVA, Tukey's multiple comparison test.

4.3.2. Optimized dosage and exposure of DSS exerts similar cytotoxicity in DSS and DSS+P110 IEC$^{4.1}$ cells

To determine if 2% DSS exerted any cytotoxic effects on IEC$^{4.1}$ cells, and if 1.5μM P110 affected potential DSS cytotoxicity, cell survival was measured through a trypan blue exclusion test. The trypan blue dye is permeable to dead cells, thereby marking them easily for separation from healthy cells and the determination of cell survival rates. In both DSS (36.88 ± 1.57) and DSS+P110 (35.84 ± 1.91) groups a significant increase in cell death was observed when compared to control cells (2.28 ± 0.47; $p<0.05$) (Figure 4.2). When compared to DSS cells, DSS+P110 cells were found to have similar rates of cell death ($p>0.05$) (Figure 4.2). P110 control cells (1.40 ± 0.19) did not show any changes in cell death when compared to the control group ($p>0.05$) (Figure 4.2).

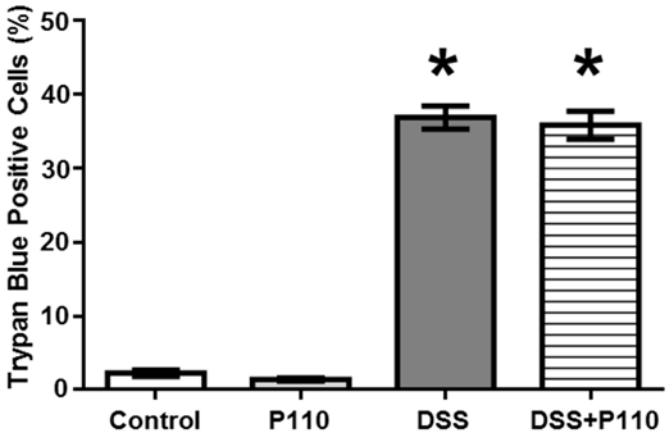

Figure 4.2: Cytotoxicity of 24h DSS±P110 treatments to IEC$^{4.1}$ cells based on a trypan blue exclusion test. Data is represented as mean ± SEM, n = 8-9 replicates from 3 independent experiments. *Represents significant differences between the control group, $p<0.05$, One-Way ANOVA, Tukey's multiple comparison test.

4.3.3. DSS impairments to mitochondrial function can be partially mitigated with P110

4.3.3.A Basal and non-mitochondrial respiration

In order to comprehensively examine if mitochondrial function was affected by DSS±P110 exposure, O2k respirometric techniques and protocols were employed. After permeabilization of cells during both the modified SUIT-002 and SCFA protocols, measurements were taken to determine "basal" mitochondria respiration. No differences were observed between basal respiration of control and P110 cells during both the modified SUIT-002 protocol (Control: 65.0 ± 5.21; P110: 68.2 ± 4.41) and the SCFA protocol (Control: 45.9 ± 1.9; P110: 39.4 ± 3.44) ($p>0.05$) (Figure 4.3A & 4.3B). DSS treated cells showed significant reductions in O_2 flux during basal respiration of both the modified SUIT-002 (43.6 ± 3.75) and SCFA protocols in comparison to control cells (32.6 ± 2.36) ($p<0.05$) (Figure 4.3A & 4.3B). These reductions in basal O_2 flux were not observed in DSS+P110 cells during the modified SUIT-002 protocol (51.0 ± 3.83; $p>0.05$) and were actually significantly higher than DSS cells (42.4 ± 2.64; $p<0.05$) during the SCFA protocol (Figure 4.3A & 4.3B).

Non-mitochondrial respiration was examined by inhibiting CI with rotenone and CIII with antimycin A, thereby inhibiting mitochondrial OXPHOS[168,175]. For the modified SUIT-002 protocol, no significant changes in O_2 flux were observed during non-mitochondrial respiration in control (12.5 ± 2.36) P110 (14.9 ± 1.56), DSS (6.4 ± 1.36) and DSS+P110 (7.8 ± 1.7) groups ($p>0.05$) (Figure 4.3C). However, with the SCFA protocol, both DSS (3.2 ± 0.51) and DSS+P110 (3.4 ± 0.48) treated cells showed significantly lower O_2 flux in comparison to control cells (24.2 ± 1.32) ($p<0.05$) (Figure 4.3D).

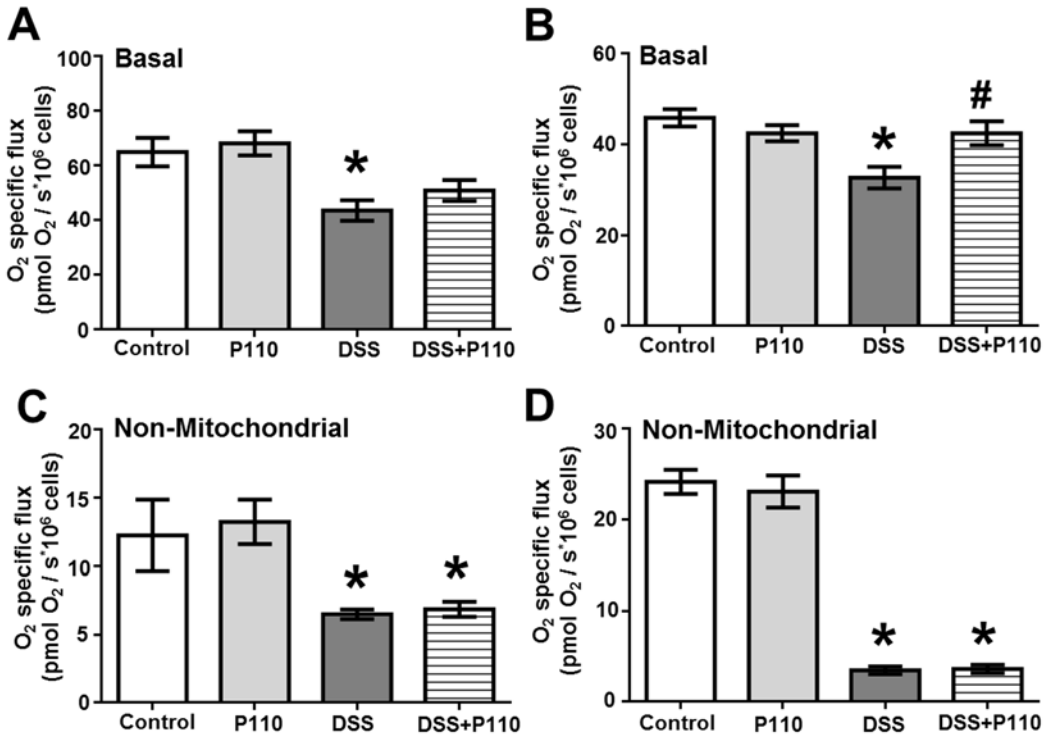

Figure 4.3: O_2 specific flux of IEC$^{4.1}$ cells during basal and non-mitochondrial respiration after 24h DSS±P110 treatments. Graphs A & B represent O_2 flux of cells after digitonin permeabilization (basal) for the modified SUIT-002 and SCFA protocols respectively. Graph C & D show O_2 flux of cells after rotenone and antimycin A titrations (Non-mitochondrial) for the modified SUIT-002 and SCFA protocols respectively. Data is represented as mean ± SEM, Graphs A & C, n = 6-8 replicates from 3 independent experiments; Graphs B & D, n = 6-8 replicates from 2-3 independent experiments. *Represents significant differences between the control group, #Represents significant differences between the DSS groups, $p<0.05$, One-Way ANOVA, Tukey's multiple comparison test.

4.3.3B. Beta oxidation and OMM quality control test

The titration of PalmC in the presence of different concentrations of malate allowed for both stimulated (PalmC) and maximal beta oxidation (2mM malate) activity to be determined. O_2 specific flux of control (PalmC: 52.7 ± 4.12; malate 2mM: 64.2 ± 4.04) and P110 (PalmC: 55.5 ± 4.00; malate 2mM: 68.7 ± 1.99) treated cells did not show any differences between the groups ($p>0.05$). DSS treated cells did not show any changes in O_2 flux during stimulated LCFA beta oxidation (PalmC = 43.5 ± 5.97; $p>0.05$) but at maximal beta oxidation, significant reductions in O_2 flux were observed in comparison to control cells (malate 2mM = 58.8 ± 2.11; $p<0.05$) (Figure 4.4A & 4.4B). Similarly, DSS+P110 cells showed no changes in stimulated beta oxidation (PalmC = 49.7 ± 6.12; $p>0.05$), but during maximal beta oxidation DSS+P110 cells showed significantly higher O_2 flux compared to cells with DSS alone (malate 2mM = 68.3 ± 3.12; $p<0.05$) (Figure 4.4A & 4.4B). Quality control checks of the OMM with cytochrome c showed no significant changes in O_2 flux after these titrations ($p>0.05$) (Figure 4.4E).

Similar to the LCFA component previously described, butyrate beta oxidation can be measured during stimulated (NaBut) and maximal beta oxidation (2mM malate). O_2 flux of control (NaBut: 42.1 ± 1.53; 2mM malate: 49.1 ± 0.85) and P110 (NaBut: 31.8 ± 3.05; 2mM malate: 42.3 ± 4.37) cells did not significantly differ during stimulated or maximal beta oxidation conditions ($p>0.05$) (Figure 4.4C & 4.4D). DSS treated cells showed significant O_2 flux reductions during stimulated (NaBut: 31.7 ± 2.00) and maximal beta oxidation (2mM malate: 40.5 ± 2.62) when compared to control cells ($p<0.05$) (Figure 4.4C & 4.4D). These same O_2 flux reductions were not seen in DSS+P110 treated cells when compared to control (NaBut: 37.0 ± 1.87; 2mM malate: 44.5 ± 2.57; $p>0.05$) (Figure 4.4C & 4.4D). OMM quality control checks with cytochrome c showed no significant differences between groups ($p>0.05$) (Figure 4.4F).

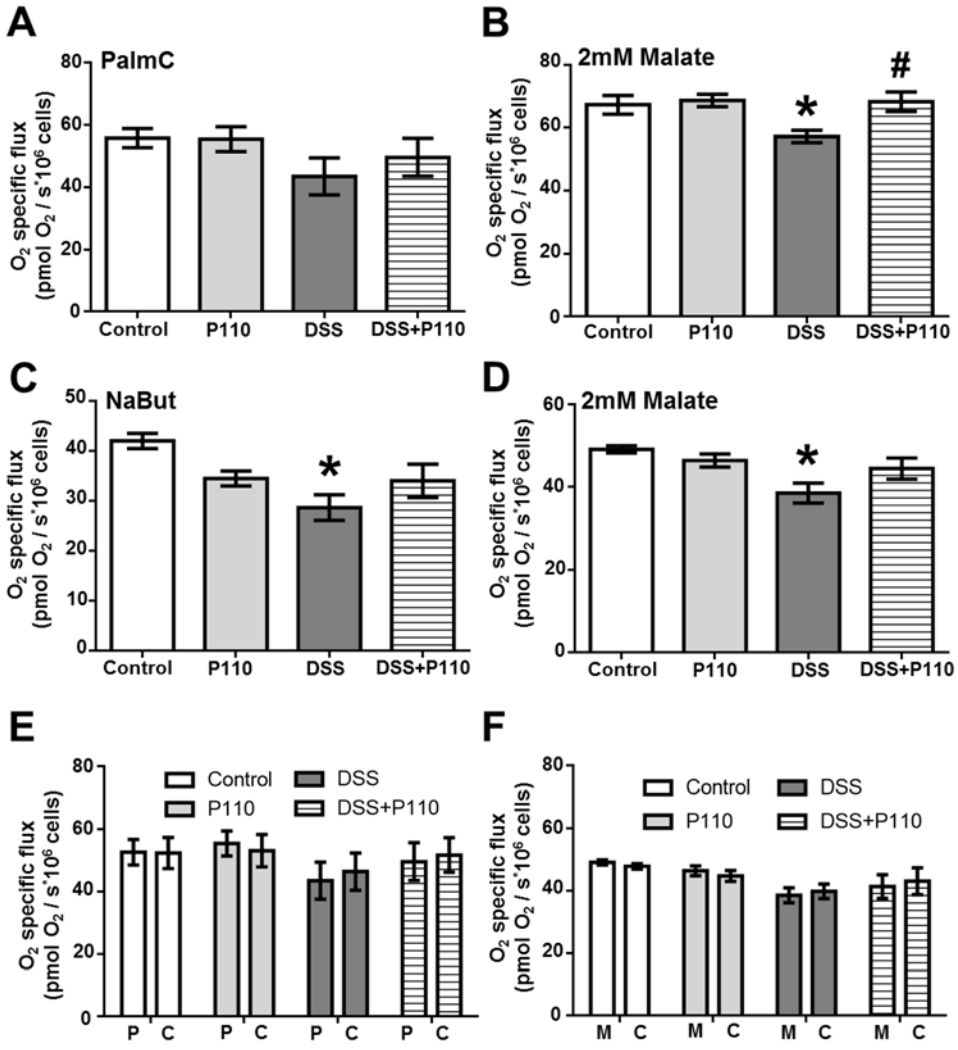

Figure 4.4: O_2 specific flux of IEC$^{4,.1}$ cells during LCFA/SCFA beta oxidation after 24h DSS±P110 treatments. Graphs A, B & E represents O_2 flux of cells during the LCFA component of the SUIT-002 protocol: A) 0.05mM PalmC B) 2mM malate E) cytochrome C test. Graphs C, D & F represents the O_2 flux of cells during a separate SCFA protocol C) 2mM sodium butyrate (NaBut) D) 2mM malate F) cytochrome C test. Graphs E & F present O_2 flux of cells after titrations of (P) PalmC and (C) cytochrome c or (M) malate and (C) cytochrome c. Data is represented as mean ± SEM, Graphs A, B & E, n = 6-8 replicates from 3 independent experiments; Graphs C, D, F, n = 6-8 replicates from 2-3 independent experiments. *Represents significant differences between the control group, #Represents significant differences between the DSS groups, $p<0.05$, A-D) One-Way ANOVA, Tukey's multiple comparison test, E & F) Repeated measures Two-Way ANOVA, Sidak's multiple comparison test.

4.3.3C. Mitochondrial complexes and MAX_{OX}

Following the LCFA component of the SUIT-002 protocol, substrates linked to complex I (pyruvate, glutamate) and complex II (succinate) were titrated in excess to identify complex specific function of $IEC^{4.1}$ cells under DSS±P110 treatments. Pyruvate, glutamate and succinate titrations elicited no changes in O_2 flux between control (pyruvate: 63.3 ± 3.2; glutamate: 70.5 ± 4.20; succinate: 96.3 ± 3.34) and P110 (pyruvate: 66.1 ± 1.43; glutamate: 72.0 ± 1.63; succinate: 91.2 ± 3.41) treated cells ($p>0.05$) (Figure 4.5A-C). Comparisons of DSS treated cells to control cells showed no significant changes in O_2 flux during pyruvate (59.7 ± 2.57; $p<0.05$), glutamate (65.9 ± 3.40) or succinate (86.1 ± 6.53) titrations ($p>0.05$) (Figure 4.5A-C). DSS+P110 cells exhibited increased pyruvate O_2 flux over DSS cells (70.1 ± 2.93) ($p<0.05$) but no improvements in O_2 flux during glutamate (76.4 ± 4.35) and succinate (104.6 ± 7.66) titrations ($p>0.05$) (Figure 4.5A-C).

Measurement of cells during MAX_{OX} was determined afterward. Both control (156.4 ± 6.52) and P110 (170.5 ± 12.47) displayed the lowest O_2 flux during MAX_{OX} ($p>0.05$) (Figure 4.5D). A higher trend in O_2 flux was observed with DSS cells at MAX_{OX} (200.7 ± 23.49) but this was not significant ($p>0.05$) (Figure 4.5D). With DSS+P110 cells (238.0 ± 18.17) however, O_2 flux was significantly higher than control cells ($p<0.05$) (Figure 4.5D). At the end of the protocol, mitochondrial CIV activity was identified. Control (214.7 ± 4.15) P110 (215.1 ± 6.82) and DSS (210.4 ± 17.12) treated cells exhibited similar CIV O_2 flux ($p>0.05$) (Figure 4.5E). CIV O_2 flux in DSS+P110 cells (285.8 ± 24.59) was not only significantly higher than DSS treated cells, but also significantly higher than control and P110 cells ($p<0.05$) (Figure 4.5E).

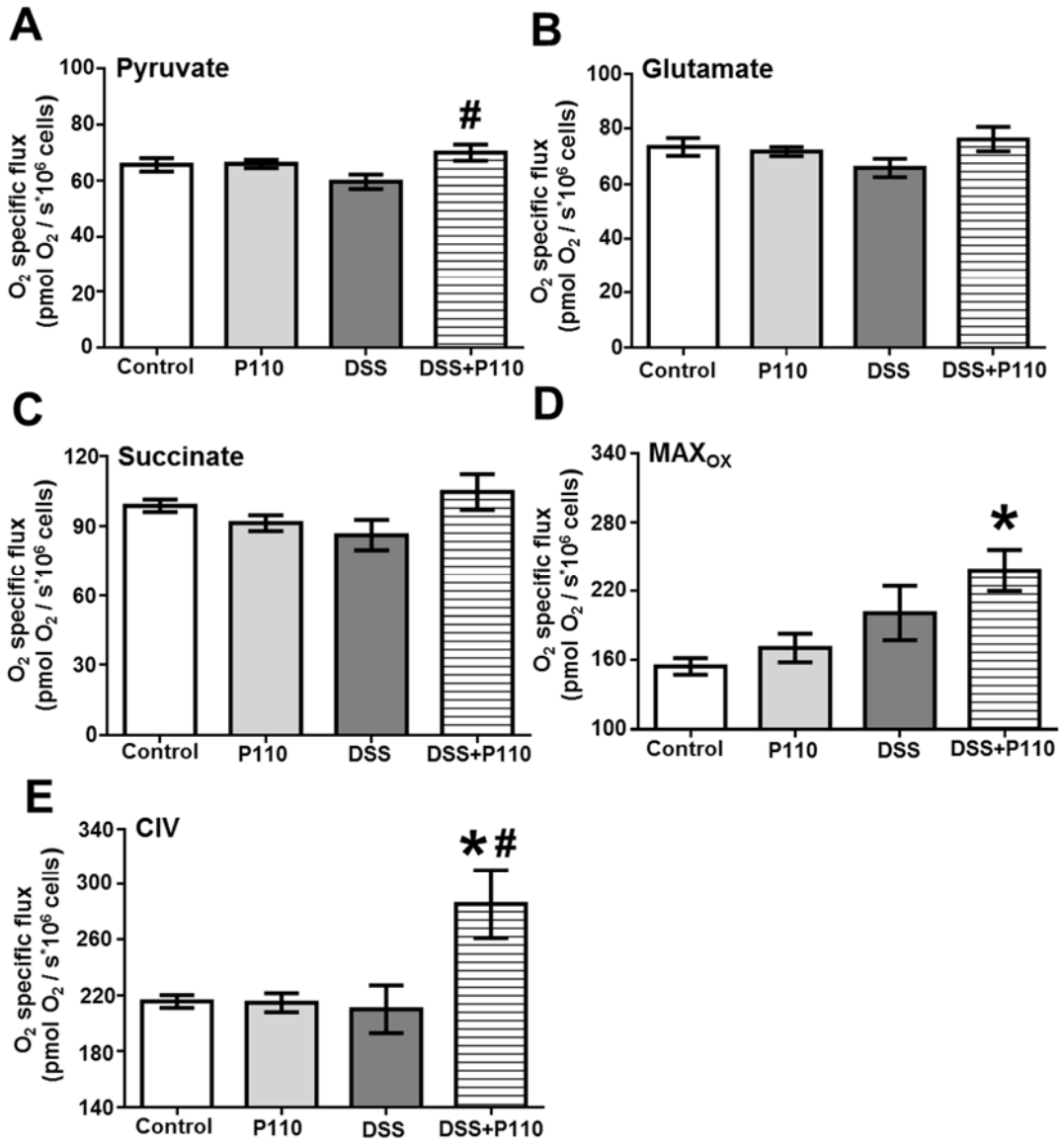

Figure 4.5: O_2 specific flux of 24h DSS±P110 treated IEC$^{4.1}$ cells in the presence of chemicals linked to CI, CII, MAX_{OX} & CIV during the modified SUIT-002 protocol. Graphs represent O_2 flux of cells after the following titrations: A) 5mM pyruvate B) 10mM glutamate C) 10mM succinate D) 0.3-0.6µM FCCP. Graph E) represents O_2 flux in the presence of 2mM ascorbate & 0.5mM TMPD subtracted by the O_2 flux after CIV inhibition with 100mM sodium azide. Data is represented as mean ± SEM, n = 6-8 replicates from 3 independent experiments. *Represents significant differences between the control group, #Represents significant differences between the DSS groups, $p<0.05$, One-Way ANOVA, Tukey's multiple comparison test.

4.3.4. Intracellular ATP content is reduced with DSS and not affected by P110 administration

Previously identified changes in alamarBlue metabolism and beta oxidation suggested that DSS may exert some effect on IEC[4.1] bioenergetics. Furthermore, improvements to these DSS related impairments with P110 warranted further investigation. Therefore, changes in cellular ATP content were examined to see if they reflected the observed metabolic O_2 flux with DSS±P110. Control (24.1 ± 0.85) and P110 (23.8 ± 1.28) groups exhibited no change from each other and both contained the highest concentration of intracellular ATP ($p>0.05$) (Figure 4.6). DSS (16.6 ± 1.53) and DSS+P110 (18.2 ± 1.5) were both significantly lower than control and did not significantly differ from each other ($p>0.05$) (Figure 4.6).

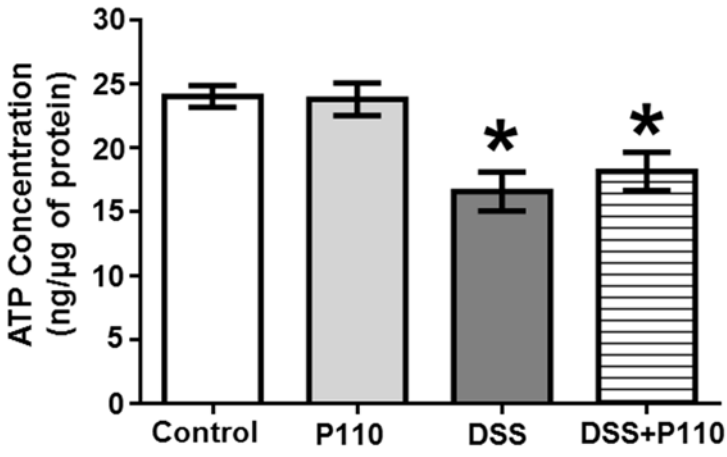

Figure 4.6: Normalized intracellular ATP concentrations in IEC[4.1] cells exposed to DSS±P110 for 24h. Data is represented as mean ± SEM, n = 10-11 replicates from 3 independent experiments. *Represents significant differences between the control group, $p<0.05$, One-Way ANOVA, Tukey's multiple comparison test.

4.3.5. Inhibition of DSS related mitochondrial fission by P110 promotes an intermediate mitochondrial morphology

To understand how mitochondrial dynamics may be perturbed by DSS and if P110 could rescue these changes, mitochondrial morphology was examined. Control and P110 treated cells exhibited predominantly fused (Control: 45.83 ± 4.55; P110: 49.17 ± 2.39) and intermediate networks (Control: 49.17 ± 3.75; P110: 46.67 ± 2.11) ($p>0.05$) (Figure 4.7). Treatment of cells with DSS led to a decreased presence of fused networks (22.00 ± 5.15) and an increased presence of fragmented networks (24.00 ± 6.00) ($p<0.05$) (Figure 4.7). DSS+P110 cells also displayed less fused networks (25.00 ± 5.92) when compared to control ($p<0.05$) (Figure 4.7). Unlike cells treated with DSS alone, DSS+P110 displayed no change in fragmented networks (10.00 ± 2.89) when compared to control (5.00 ± 1.83) ($p>0.05$) (Figure 4.7). Interestingly, DSS+P110 also showed a significant increase in intermediate mitochondrial networks (65.00 ± 3.87) compared to control cells (49.17 ± 3.75) ($p<0.05$) (Figure 4.7).

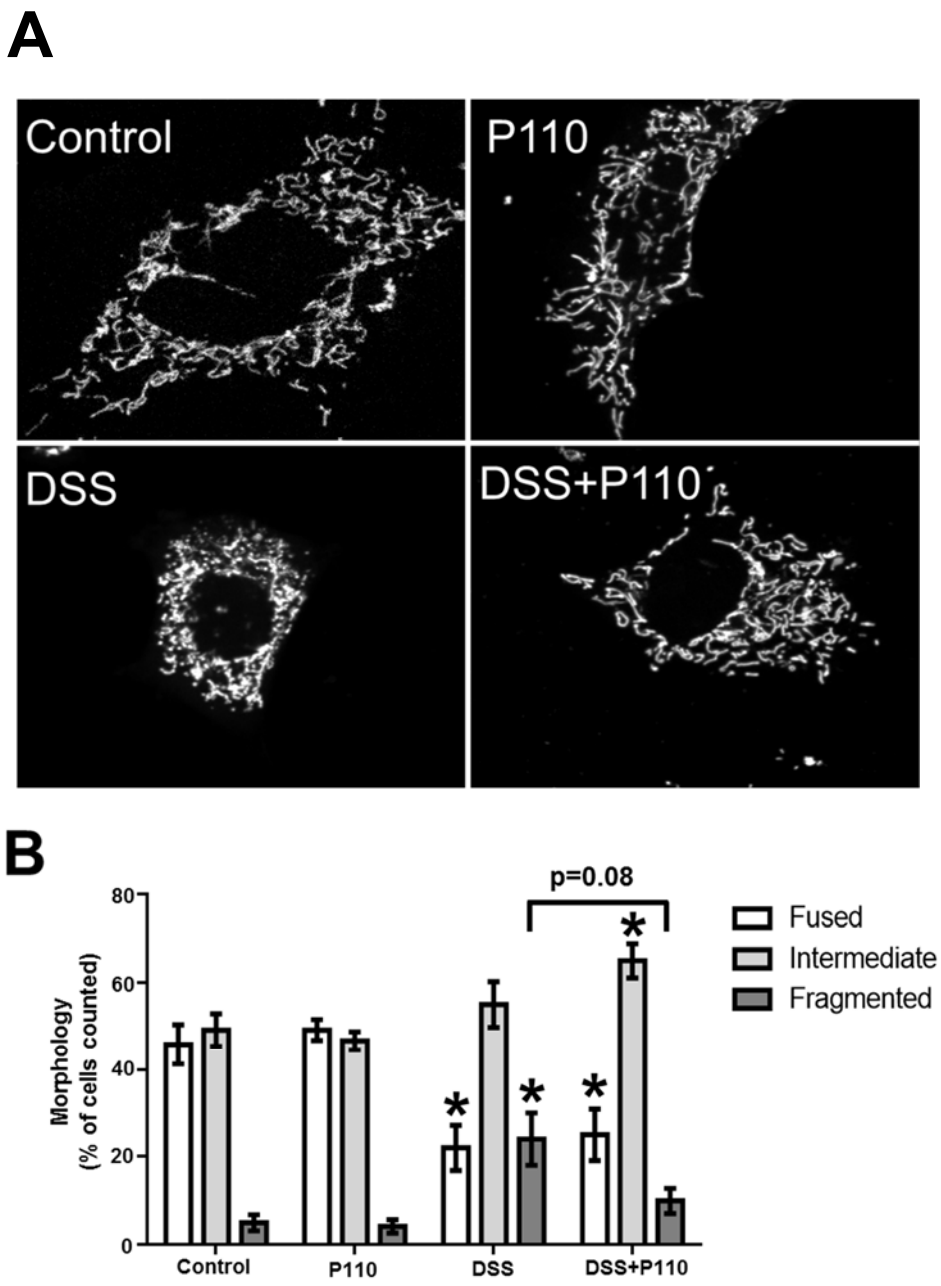

Figure 4.7: Mitochondrial network morphology of IEC$^{4.1}$ cells after 24h DSS±P110 treatments. A) Representative images were taken for each treated group based on the predominant morphology identified B) Mitochondrial network quantification based on group treatments. The predominant morphology was determined by counting 20 cells from each well and identifying the networks as either fused, intermediate or fragmented (total cells = 100-120 cells from 5-6 wells in 3 independent experiments). Data is represented as mean ± SEM. *Represents significant differences between the control group, $p<0.05$, Ordinary Two-Way ANOVA, Tukey's multiple comparison test. Quantification of mitochondrial networks was performed by Nicole Mancini.

4.3.6 IEC$^{4.1}$ exhibit different mitochondrial polarization states based on exposure to DSS

Since mitochondrial polarization events can precede signs of mitochondrial dysfunction, changes in mitochondrial polarization were examined at both 1h and 24h DSS exposure times. Readings taken after DSS±P110 treatments showed that absolute fluorescence obtained from control (4.1 ± 0.03) and P110 cells (4.3 ± 0.14) did not significantly differ from each other ($p>0.05$) (Figure 4.8A). Treatments of cells with either DSS (4.5 ± 0.29) or DSS+P110 (4.7 ± 0.43) for 1h led to no changes in fluorescence when compared to control cells at 0min ($p>0.05$) (Figure 4.8A). However, measurements taken at both 40min and 80min showed a large increase in TMRE fluorescence for both DSS (40min: 7.7 ± 0.73; 80min: 7.2 ± 0.68) and DSS+P110 (40min: 7.1 ± 0.55; 80min: 6.6 ± 0.71) groups ($p<0.05$) (Figure 4.8B). This increase in TMRE fluorescence at 40min and 80min with 1h DSS was comparable to increases in TMRE fluorescence observed with oligomycin treated cells (40min: 7.9 ± 0.41; 80min: 8.0 ± 0.42) ($p>0.05$) (Figure 4.8B). As expected both positive controls for hyperpolarization (oligomycin) and depolarization (FCCP) were found to be significantly higher (oligomycin: 6.1 ± 0.34) and lower (FCCP: 1.9 ± 0.13) with respect to control cells at 0min ($p<0.05$) (Figure 4.8A). Unexpectedly, the use of P110 in FCCP treated cells (3.7 ± 0.41) led to greater TMRE fluorescence when compared to those given FCCP alone at 0min measurements ($p>0.05$) (Figure 4.8A). Cells exposed to DSS for 24h (0min: 2.5 ± 0.10; 40min: 3.2 ± 0.22; 80min: 3.0 ± 0.18) had a lower fluorescence when compared to control cells (0min: 4.1 ± 0.03; 40min: 4.5 ± 0.21; 80min: 4.2 ± 0.11) during all assessed time points ($p<0.05$) (Figure 4.8C). At 0min readings (3.0 ± 0.18; $p<0.05$) DSS+P110 cells showed similar reductions in fluorescence to DSS treated cells, but not at both 40min (4.2 ± 0.22) and 80min (3.6 ± 0.21) post-treatment ($p>0.05$) (Figure 4.8C). In fact, measurements taken at 40min showed that

24h DSS+P110 cells had significantly higher fluorescence compared to cells exposed to just DSS for 24h ($p<0.05$).

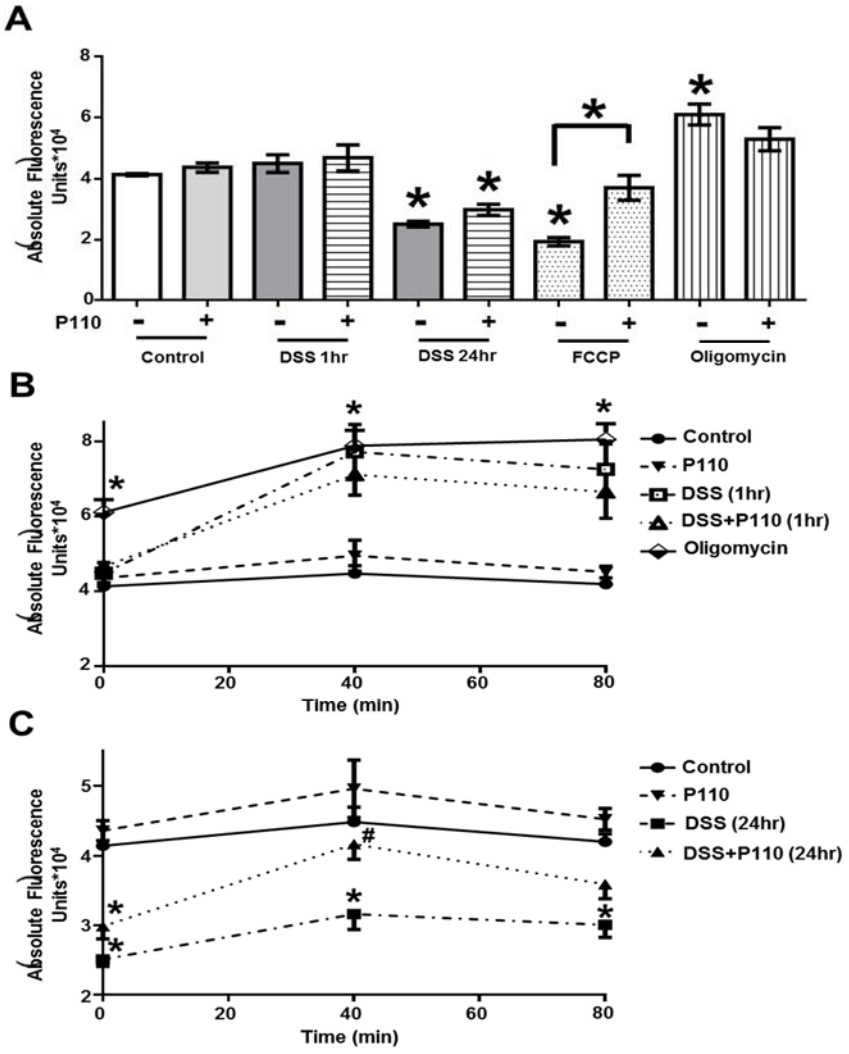

Figure 4.8: TMRE fluorescence of IEC$^{4.1}$ cells under DSS±P110 treatments for either 1h or 24h. A) TMRE fluorescence measured at 0min B) TMRE fluorescence of 1h DSS±P110 treated cells at 0, 40 and 80min C) TMRE fluorescence of 24h DSS±P110 treated cells for at 0, 40 and 80min. Data is represented as mean ± SEM, n = 8 replicates from 2 independent experiments. *Represents significant differences between the control group, #Represents significant differences between the DSS groups; bars indicate significant differences between indicated groups, $p<0.05$, A) One-Way ANOVA, Tukey's multiple comparison test, B & C) Repeated measures Two-Way ANOVA, Tukey's multiple comparison test.

4.4. Discussion

Evidence regarding DSS's effect on IEC mitochondrial dynamics and function could offer interesting insights into not only the animal models of DSS colitis, but also potentially human IBD. To that end, we sought to examine the effect that DSS±P110 had on IEC$^{4.1}$ mitochondrial dynamics and function. In support of the studies hypothesis that DSS perturbs mitochondrial function, we identified reduced resorufin fluorescence with 2% DSS after 24h exposure (Figure 4.1). Furthermore, administration of 1.5μM P110 mitigated these DSS associated impairments in the reduction of alamarBlue to its fluorescent product: resorufin (Figure 4.1). Since alamarBlue can react with NADH in the presence of mitochondrial diaphorases, differences in the reaction of alamarBlue may serve as an indicator for mitochondrial NADH concentrations and potentially metabolic processes tied to NADH production[193]. However, since DSS has been shown to have cytotoxic effects, differences in cell death could affect the number of functioning mitochondria and subsequent NADH production, thereby accounting for our observed differences in alamarBlue reaction rates between control, DSS and DSS+P110 cells[132]. While we did find that 2% DSS led to significant cell death in both DSS and DSS+P110 groups, the similar rates of cell death between DSS and DSS+P110 treated cells could not account for the fluorescent differences in resorufin observed with DSS and DSS+P110 cells (Figure 4.1 & 4.2). Therefore, differences in the conversion of alamarBlue to resorufin between DSS and DSS+P110 cells could be tied to changes in NADH concentration or mitochondrial diaphorase activity. In order to identify if there were any alterations in NADH linked pathways, we employed mitochondrial respirometric analysis.

Using O2k respirometric analysis we identified that cells exposed to 2% DSS for 24h exhibited lower respiratory activity during basal and beta oxidation conditions (Figure 4.3 & 4.4). Given the bioenergetic importance of fatty acids to IECs, reduced beta oxidation could indicate a

significant disparity in energy availability between DSS treated and control cells[101]. P110 not only prevented most of these DSS associated metabolic impairments but also led to significant increases in pyruvate, MAXOX and CIV linked respiration (Figure 4.5). Since both pyruvate and beta oxidation are linked to NADH production, respiratory differences in these pathways between DSS and DSS+P110 treated cells could also tie into the previously observed fluorescence differences between DSS and DSS+P110 cells during the alamarBlue assay (Figure 4.4 & 4.5). Building on this metabolic data, we also identified that 2% DSS for 24h led to decreased intracellular ATP content (Figure 4.6). In summarizing this data, our results suggest that continued metabolic deficits (basal, beta oxidation) accrued with DSS exposure, ultimately leads to a significant disparity in ATP cellular content. While P110 did not improve intracellular ATP concentrations in DSS treated cells, specific measures examining differences in beta oxidation, CI, CIV and MAXOX activity suggest that steady-state production of ATP from these pathways would be higher in DSS+P110 cells (Figure 4.4 & 4.5). In order to relate DSS±P110 metabolic changes to mitochondrial dynamics, we examined mitochondrial morphology changes after 24h DSS±P110 treatment.

Cells given DSS alone were found to contain fewer fused mitochondrial networks and more fragmented mitochondrial networks compared to control cells (Figure 4.7). Coadministration of P110 with DSS cells did not alleviate DSS associated reductions in fused mitochondrial networks, but it did appear to limit the fragmentation of mitochondrial networks by DSS (Figure 4.7). This change in mitochondrial morphology of DSS cells with P110, a known DRP1-Fis1 inhibitor, suggests that DRP1-Fis1 interactions occur and mediate, in part, excessive mitochondrial fission during DSS exposure in IEC[4.1]. In connecting these results to previous findings, Rambold et al. identified that a certain degree of mitochondrial fusion is required for fatty acid metabolism,

since Mfn-1 and OPA-1 KO mouse embryonic fibroblasts cells cannot import fatty acids[201]. Therefore, fragmentation of mitochondrial networks in DSS treated cells could affect fatty acid import and lead to our observations of reduced beta oxidation activity. Furthermore, preservation of mitochondrial network morphology by P110's inhibition of DRP1-Fis1 binding could limit these possible morphological consequences on fatty acid import and subsequent rates of beta oxidation. Building on the identified effects of DSS±P110 on mitochondrial networks and function, we next examined the degree of mitochondrial dysfunction with DSS treatment.

Since mitochondrial depolarization is closely tied to mitochondrial dynamic changes and often coincides with dysfunctional mitochondrial networks, mitochondrial polarization of DSS±P110 treated IEC$^{4.1}$ cells was examined at both 1h and 24h[23,202]. Unexpectedly, 1h treatment with 2% DSS led to significant increases in TMRE fluorescence at both 40min and 80min post-treatment (Figure 4.8A & B). Use of P110 was found to not affect these fluorescence changes with 1h DSS (Figure 4.8A & B). Given that these fluorescence changes with DSS and DSS+P110 were comparable to oligomycin, a positive control for mitochondrial hyperpolarization, 1h DSS exposure could be leading to mitochondrial hyperpolarization. While evidence on mitochondrial hyperpolarization and cellular consequences is relatively unexamined in IEC's, hyperpolarization in T-cells has been shown to precede dramatic depolarization events that lead to ATP depletion and increased sensitivity to necrosis[52,203]. Indeed, TMRE fluorescence of DSS cells after 24h was found to be significantly lower than control cells, suggesting that sustained DSS exposure led to eventual mitochondrial depolarization (Figure 4.8C). However, DSS cytotoxicity could have reduced viable cells and mitochondrial networks, resulting in lower mitochondrial TMRE dye uptake and consequently fluorescence output at 24h measurements (Figure 4.2 & 4.8C). In interpreting the effects of P110 on mitochondrial polarization within 24h DSS treated cells,

increased TMRE fluorescence at 40min would suggest potential benefit (Figure 4.8C). Unfortunately, the return of DSS+P110 TMRE fluorescence at 80min to comparably similar values to DSS alone, complicate potential conclusions that could be made.

4.5. Conclusion

Incredible progress has been made in the past few decades towards understanding the molecular, genetic and environmental factors that affect IBD pathogenesis. This progress, in part, has relied heavily on colitis models like DSS to examine molecular sources and consequences of colitis on intestinal homeostasis. Despite its wide implementation, the direct mechanism of how DSS leads to colitis is unknown. Here we report that murine IECs exposed to DSS undergo early mitochondrial hyperpolarization at 1h and possible mitochondrial depolarization at 24h. Addition of P110 did not appear to affect these DSS related consequences or DSS cellular cytotoxicity. Cells surviving DSS exposure exhibited lower respiration during both basal and beta oxidation conditions, which could potentially be attributed to DSS fragmentation of mitochondrial networks. P110 was found to limit DSS associated mitochondrial fragmentation, preserving mitochondrial networks in an "intermediate" morphology, that exhibited higher beta oxidation rates. These findings build upon the current understanding of how DSS may lead to colitis and provide a potential explanation for the previously reported findings of mitochondrial dysfunction in DSS colitis. More importantly, these results also reflect observed characteristics of mitochondrial dysfunction in IBD patients (reduced beta oxidation), with P110 improving several of these bioenergetic consequences in this DSS *in-vitro* model. This suggests that DRP1 and Fis1 mediated mitochondrial fission could be a feature in colitis and that targeting mitochondrial dynamic imbalances with P110 could exert therapeutic potential in IBD patients.

Chapter 5

Pharmacological inhibition of DRP1 and Fis1 mediated mitochondrial fission reduces murine DSS and DNBS colitis

5.1. Introduction

The heterogenic nature and presentation of IBD and its subtypes: UC and CD, makes treatment and pharmacological interventions particularly difficult in correcting the observed inflammatory imbalances. Disease maintenance has therefore focused on the use of immunosuppression in order to shift the aberrant inflammation into a state of remission and reduce further tissue damage[204]. Depending on patient responsiveness and progression, treatment may involve the individual or combined use of corticosteroids, thiopurines or biologic therapies[204]. Corticosteroids bind to cytoplasmic glucocorticoid receptors, which upon activation, lead to downstream alterations in pro-inflammatory gene transcription by direct binding or protein-protein interactions with inflammatory mediators[205,206]. Short-term use of corticosteroids can be effective at shifting IBD into remission, but long term use is not recommended due to the numerous side effects[207,208]. Thiopurines exert a more specific effect, directly targeting immunoregulatory elements to modify innate and adaptive immune cell activation, apoptosis, and cytokine release[209-213]. Biological therapies employ monoclonal antibodies to bind and inhibit strongly inflammatory cytokines like tissue tumor necrosis factor-α[214-217]. Despite their effectiveness, both thiopurines and biologics may show limited or no treatment response during initial administration, with some patients also becoming refractory to these medications over time[218,219]. While the advent of new immunotherapies in recent decades has provided a boon for IBD treatment and management, examining other targets implicated in IBD pathogenesis could also yield therapeutic benefit, with potentially fewer limitations to conventional therapies. One novel target could be attenuating the

intestinal epithelial barrier defects frequently reported in IBD patients and animal colitis models[151,180,220-224].

Given the plethora of potential inflammatory sources within the intestine, restoration of the epithelium could prove useful in limiting both the entry of inflammatory provocateurs to host tissues and the resulting inflammation. Since mitochondria have been shown to play a role in both epithelial barrier maintenance and breakdown, therapeutics targeting mitochondria may prove beneficial in restoring intestinal barrier defects[102,103,165]. For decades now, it has been understood that IECs derive most of their energy from mitochondrial processes like beta oxidation and OXPHOS[101]. Pharmacological disruption to mitochondrial OXPHOS has been shown to adversely affect intestinal barrier function and permeability within *in-vitro* cellular models[102,165]. When taking these findings into account with reports of mitochondrial dysfunction in UC patients and murine DSS colitis models, there is evidence that diminished mitochondrial function could contribute to the intestinal barrier defects observed in DSS colitis and human IBD[141,143,183]. Mitochondrial dysfunction has also been associated with other molecular consequences tied to intestinal barrier disruption and colitis[225-230]. Interestingly, improvements in mitochondrial function or the targeted removal of mitochondrial derived ROS by antioxidants has been shown to protect against chemically induced colitis[102,104,184,231]. Given the bioenergetic importance of mitochondria in intestinal barrier function and ultimately intestinal homeostasis, therapeutics aimed at maintaining or improving mitochondrial function may prove useful in limiting intestinal barrier defects associated with colitis and human IBD. One potential therapeutic, known as P110, has shown benefits in numerous cellular and animal disease models by limiting mitochondrial dysfunction associated with excessive mitochondrial fission[13-19,150,188,189].

The dynamic mitochondrial processes of fission and fusion, in coordination with mitophagy, facilitate regulation of mitochondrial quality and function[23,66,68]. While basal levels of mitochondrial fission and fusion are required to facilitate this process, excessive mitochondrial fission may prove maladaptive and potentially contribute to disease. Studies have demonstrated that the binding of DRP1 and Fis1 in particular, is associated with excessive mitochondrial fission and the fragmentation of mitochondrial networks[15,17-19,150,187,188]. These fragmented networks are often linked to pathologically associated consequences such as: reduced energy generation, elevated ROS, and increased cell death[15,17-19,150,187,188]. Inhibition of DRP1 and Fis1 binding has been shown to limit excessive mitochondrial fission and preserve both mitochondrial morphology and function[15,17-19,150,187,188]. Symptomatic outcomes associated with representative models of multiple sclerosis, Alzheimer's, Parkinson's, Huntington's, amyotrophic lateral sclerosis, ischemic-reperfusion injury, have also shown improvement with DRP1 and Fis1 inhibition[13,14,15,17,18,188]. Current evidence does support the notion that DRP1-Fis1 binding is maladaptive, with studies demonstrating a beneficial effect on mitochondrial function through inhibition. Given that intestinal barrier function relies on sufficient mitochondrial function and could be a novel target for new IBD therapeutics, this study wished to identify if DRP1 and Fis1 inhibition could reduce colitis in the murine DSS and DNBS models representative of human UC and CD.

5.2. Material and Methods

5.2.1. Animal maintenance

All experimental procedures were performed under the ethical guidelines and standards approved by the University of Calgary Animal Care and Use Committee (Calgary, AB, Canada). Experiments were conducted in male Balb/C mice (7-9 wk old; Charles River Laboratories, Senneville, QC, Canada). The animals were housed in standard micro-isolator cages with *ad libitum* access to standard chow pellets. Mice were assessed daily in the morning for changes in weight. If mice had undergone a >10% weight reduction, a subcutaneous injection of sterile saline was provided and if a >20% weight reduction was observed, the mice were immediately euthanized. During the daily weighing period, the intraperitoneal injection site was cleaned with rubbing alcohol and 0.5mL injections of P110 (3mg/kg/day) was administered using a 30-gauge needle in combination with the prepared 1mL syringes.

5.2.2. Murine model of DSS colitis

Mice were randomly selected into control, P110, DSS and DSS+P110 (n= 8-21 per group, 2-5 independent experiments). P110 and DSS+P110 treated mice received intraperitoneal saline (0.9% w/v) injections containing P110 (3mg/kg/day) for each day of the experiment (Figure 5.1A). A pretreatment of P110 injections was also given for the two days prior to DSS administration (Figure 5.1A). Day 0 of the experiment started with DSS and DSS+P110 mice receiving 5% w/v 40 kDa (Affymetrix, Santa Clara, California) orally through their drinking water for 5 days. This was followed by a 3-day recovery period with DSS free water (Figure 5.1A). Necropsy occurred on the morning of the 8th day (Figure 5.1A). Earlier experiments examined if either sham TAT$^{47-57}$ or saline injections provided any extraneous effects, with no significant changes being identified (data not shown).

5.2.3. Murine model of DNBS colitis

In addition to the murine DSS colitis model, we wished to identify if P110 exerted any therapeutic benefit in a DNBS murine colitis model. Treatment and prophylactic based protocols were used to identify if the timing of P110 administration affected DNBS±P110 outcomes. For the treatment protocol, mice were randomly selected into either control, DNBS or DNBS+P110 groups (n = 7-11 per group, 2 independent experiments). On Day 0, DNBS and DNBS+P110 mice groups received DNBS (3mg/kg in 50% EtOH solution, MP Biomedicals, Ohio, USA) intrarectally (Figure 5.3A). Afterwards, DNBS+P110 mice were given saline (0.9% w/v) injections containing P110 (3mg/kg/day) intraperitoneally, once daily on Days 1-3 (Figure 5.3A). The experiment continued for 5 days with necropsy occurring on the morning of the 5th Day (Figure 5.3A).

For the prophylactic protocol, mice were randomly selected into either control, DNBS or DNBS+P110 (n = 11-15 per group, 3 independent experiments). Similar to the treatment protocol, DNBS (3mg/kg in 50% EtOH solution, MP Biomedicals, Ohio, USA) was provided intrarectally on Day 0 (Figure 5.5A). However, during the prophylactic protocol, intraperitoneal saline (0.9% w/v) injections containing P110 (3mg/kg/day) were administered before the DNBS gavage on Day 0 (Figure 5.5A). These P110 injections were also given on Day 1 and 2 (Figure 5.5A) The experiment lasted for 3 days with necropsy occurring on the 3rd day (Figure 5.5A).

5.2.4. Bead extrusion test

Prior to tissue collection, mice were anesthetized using isofluorane. After being anesthetized, a blunted and smoothed 20-gauge needle was then used to push PBS lubricated beads 2cm into the colon[231]. Colonic motility time was started immediately after withdrawing the needle and stopped once the bead was visible at the anal verge[231]. Time constraints were put on the test at 10min.

5.2.5. Assessment of colitis

During necropsy, the entire colon was excised out from the caeco-colic junction to anus for disease activity scoring. Scoring of colonic inflammation included: severity of diarrhea (wet anus, fluid in the colon, soft stool, empty colon), tissue damage (bloody anus, fecal blood, ulceration) and colon shortening[102,232]. Maximum scores could not exceed 4, unless the animal did not reach experimental endpoints due to disease treatment, at which point, a score of 5 was automatically given[102,232].

.

5.2.6. Hematoxylin and eosin histology preparation

Once the colon was assessed for disease activity score, 20% of the colon was cut and reserved for cross-sectional histology. The tissue selected was cut 2cm above the distal end to ensure the bead extrusion test did not influence the histopathology analysis. To see how DSS±P110 treatments affected a larger portion of the colon, one experiment used the distal 2/3 of the colon in a "swiss roll" preparation, rolling from distal to proximal[233]. The tissues reserved for cross-sections and swiss rolls were then fixed in a 10% neutral buffered formalin fixing solution until they could be further processed. The tissues were then placed in histology cassettes and run through varying

concentrations of ethanol (70-85-90%), toluene (3 baths) and hot paraffin wax baths (60˚C) by a tissue processor (Leica TP1020). Processed samples were then embedded using the (Leica EG1160) into histology cassettes with paraffin wax and allowed to solidify before slicing. Histology slices were cut at 5-7µm by microtome (Leica RM2125) and placed into a lukewarm bath to minimize wrinkling of samples. Glass slides were used to collect the samples and dry overnight on a slide warmer. Hematoxylin and eosin (H&E) staining of histology slides involved immersion in neoclear (2-3min), decreasing concentrations (100-95-90-80-70) of ethanol (3-5min each), de-ionized water (3-5min), Gill 2 hematoxylin (5min), de-ionized water (20min) and eosin (2-3min). Slides were then rinsed with decreasing concentrations of ethanol (100-95-90-80-70) for 10 seconds each and finished with a 2-3min bath in neoclear. If adequate staining was observed, slides were given 2-3 drops of permount and a coverslip.

5.2.7. Histopathological scoring

Cross-sectional scoring was performed by individuals blinded to the treatments and scored based on: architecture destruction (0-3), cellular infiltration (0-3), smooth muscle thickening (0-2), presence of crypt abscesses (0-1), level of global cell depletion (0-1), ulceration (0-1) and severity of edema (0-2)[102,232]. Representative images were taken using the Olympus BX41 Confocal microscope with a 4X objective lens and processed using Q-Capture Pro 7 (QImaging, Canada).

5.2.8. Blood smear

During necropsy, a single drop of blood was extracted from the tail of mice samples and placed on glass slides. A clean slide was used to spread the blood droplet over the surface and then left to air dry for two days prior to staining. Staining was performed with a Wright-Giesma stain and allowed to air dry for 24h before applying a coverslip. Coverslips were mounted using permount and allowed to dry for 24h before viewing. Slides were viewed under 20X magnification with the Olympus BX41 Confocal microscope and white blood cells present were categorized as either monocytes, neutrophils or eosinophils until a total of 300 white blood cells were counted.

5.2.9. Myeloperoxidase activity

MPO activity serves as an indicator of neutrophil migration to tissues during inflammation and can be assessed using a colorimetric assay[234,235]. To determine the degree of neutrophil infiltration in DSS and DNBS mice, the distal 10-20% of colon tissue was homogenized in 50mM hexa-decyl-trimethyl ammonium bromide buffer[235]. Sample homogenate was then centrifuged (13,500RPM, 30min) and the pellet was discarded. The remaining supernatant was deposited into a 96-well plate along with o-dianisidine dihydrochloride buffer (0.167mg/ml, Sigma) and 1.2% H_2O_2. Absorbance was read immediately using a spectrophotometer (3 readings, 30-second intervals, 450nm) and the maximum slope was used to calculate the units of MPO activity/mg of tissue (1 unit MPO = 1μmol of H_2O_2 split)[235].

5.2.10. Statistical analysis

Data is presented as mean ± SEM. Analysis and statistical tests were performed using GraphPad Prism 6 and the significance level was set at $p<0.05$. Parametric data was analyzed using either One-Way ANOVA, ordinary Two-Way ANOVA or repeated measures Two-Way ANOVA tests. Non-parametric data was analyzed using a Kruskal-Wallis test. If $p<0.05$, then either a Tukey's or Dunn's multiple comparison test was applied.

5.3. Results

5.3.1. P110 reduces DSS colitis based on improvements in weight recovery, disease severity and motility

No differences were observed between control and P110 mice for percent weight change (control Day 8: 103.6 ± 0.67; P110 Day 8: 104.1 ± 0.76), colon length (control: 9.8 ± 0.23; P110: 9.5 ± 0.22), and macroscopic disease score (control: 0.0 ± 0.03; P110: 0.1 ± 0.06) ($p>0.05$) (Figure 5.1B-D). In contrast, DSS mice showed significant weight loss at Day 8 (99.3 ± 0.76), greater colon shortening (7.5 ± 0.25), higher disease score (3.1 ± 0.19) and dysmotility (251 ± 54.8) when compared to control animals ($p<0.05$) (Figure 5.1B-E). DSS associated weight loss and dysmotility was not observed in DSS+P110 mice ($p>0.05$) (Figure 5.1B & 1E). Additionally, DSS+P110 mice were found to have greater weight gain, when compared to DSS mice by Day 8 (DSS+P110: 101.8 ± 0.75), improved motility (120.0 ± 24.3), longer colon length (8.5 ± 0.29) and lower macroscopic disease score (1.5 ± 0.24) ($p<0.05$) (Figure 5.1B & E). Signs of colitis were still observed in DSS+P110 mice, since colon shortening and macroscopic disease score were significantly worse than control ($p<0.05$).

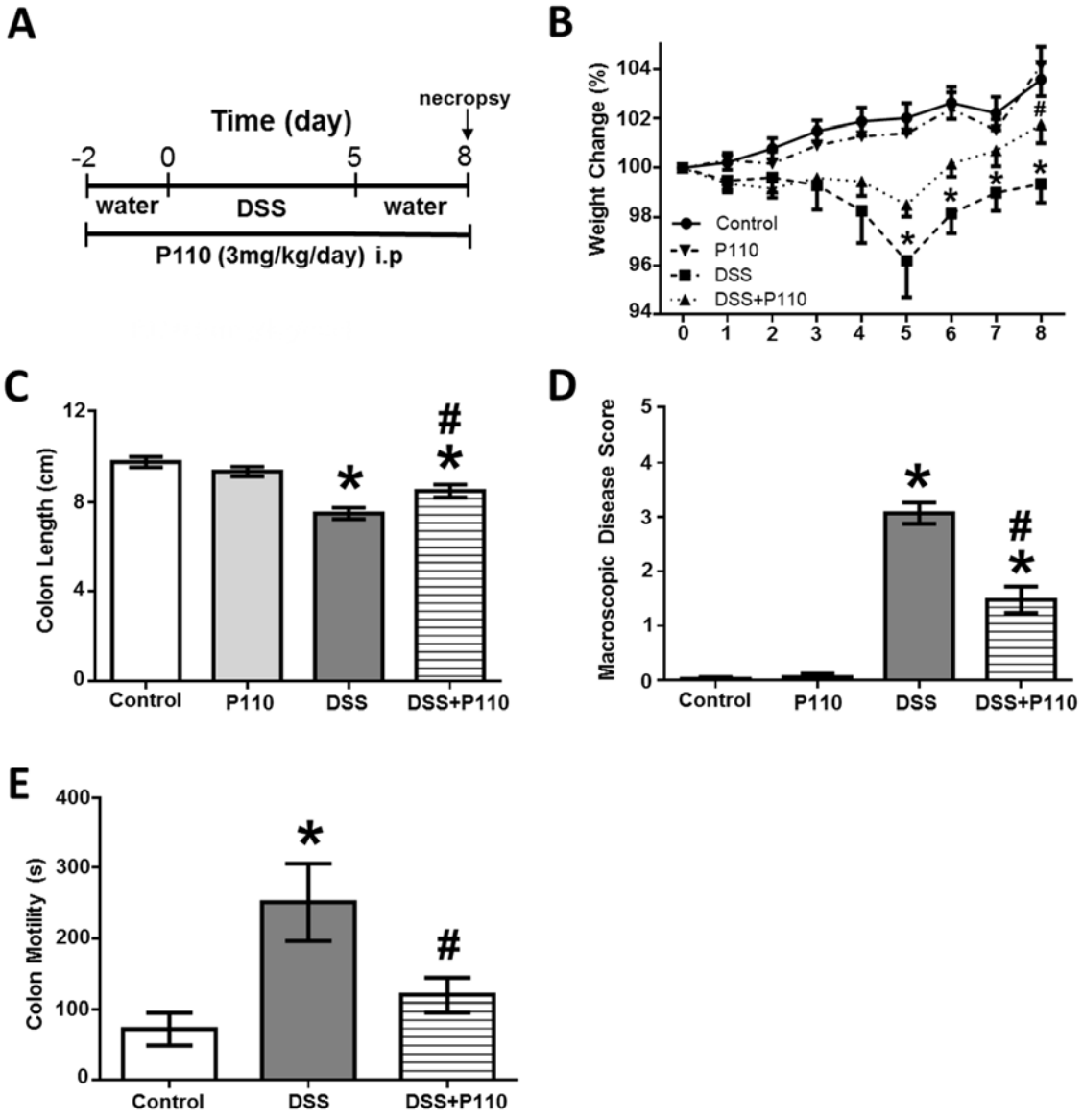

Figure 5.1: Macroscopic assessment of murine colitis after DSS±P110 trial. A) Experimental protocol B) Percent weight change during experiment C) Colon length D) Macroscopic disease score E) Colon motility. Data is represented as mean ± SEM, n = 8-21, 2-4 independent experiments. *Represents significant differences between the control group, #Represents significant differences between the DSS group, $p<0.05$, B) Repeated measures Two-Way ANOVA, Tukey's multiple comparison test, C & E) One-Way ANOVA, Tukey's multiple comparison test, D) Kruskal-Wallis, Dunn's multiple comparison test.

5.3.2. DSS associated changes in inflammatory markers are not mitigated with P110

Inflammatory changes associated with DSS colitis were determined through changes in circulating lymphocytes, MPO activity in colon tissues and histopathology of colon tissue. No changes in circulating lymphocytes or histopathology were observed between control and P110 animals ($p>0.05$) (Figure 5.2A & C). DSS and DSS+P110 mice had proportionally lower circulating monocytes (DSS: 181 ± 7.5; DSS+P110: 166 ± 10.0) and higher circulation of neutrophils (DSS: 112 ± 6.4; DSS+P110: 129 ± 10.3) compared to control mice (monocytes: 208 ± 6.6; neutrophils: 78 ± 6.0; $p<0.05$) (Figure 5.2A). A higher trend in MPO activity for both DSS and DSS+P110 groups (DSS: 2.5 ± 0.82; DSS+P110: 1.8 ± 1.16) suggested a greater presence of neutrophils within colon tissues compared to control (0.2 ± 0.24) ($p>0.05$) (Figure 5.2B). Trends in MPO activity were also mirrored by increases in histopathology for both DSS (7.7 ± 0.55) and DSS+P110 (7.4 ± 0.72) mice compared to control (0.2 ± 0.08) ($p<0.05$) (Figure 5.2Ci-iii). No changes were seen in blood smear counts, MPO activity or histopathology scoring between DSS and DSS+P110 mice ($p>0.05$).

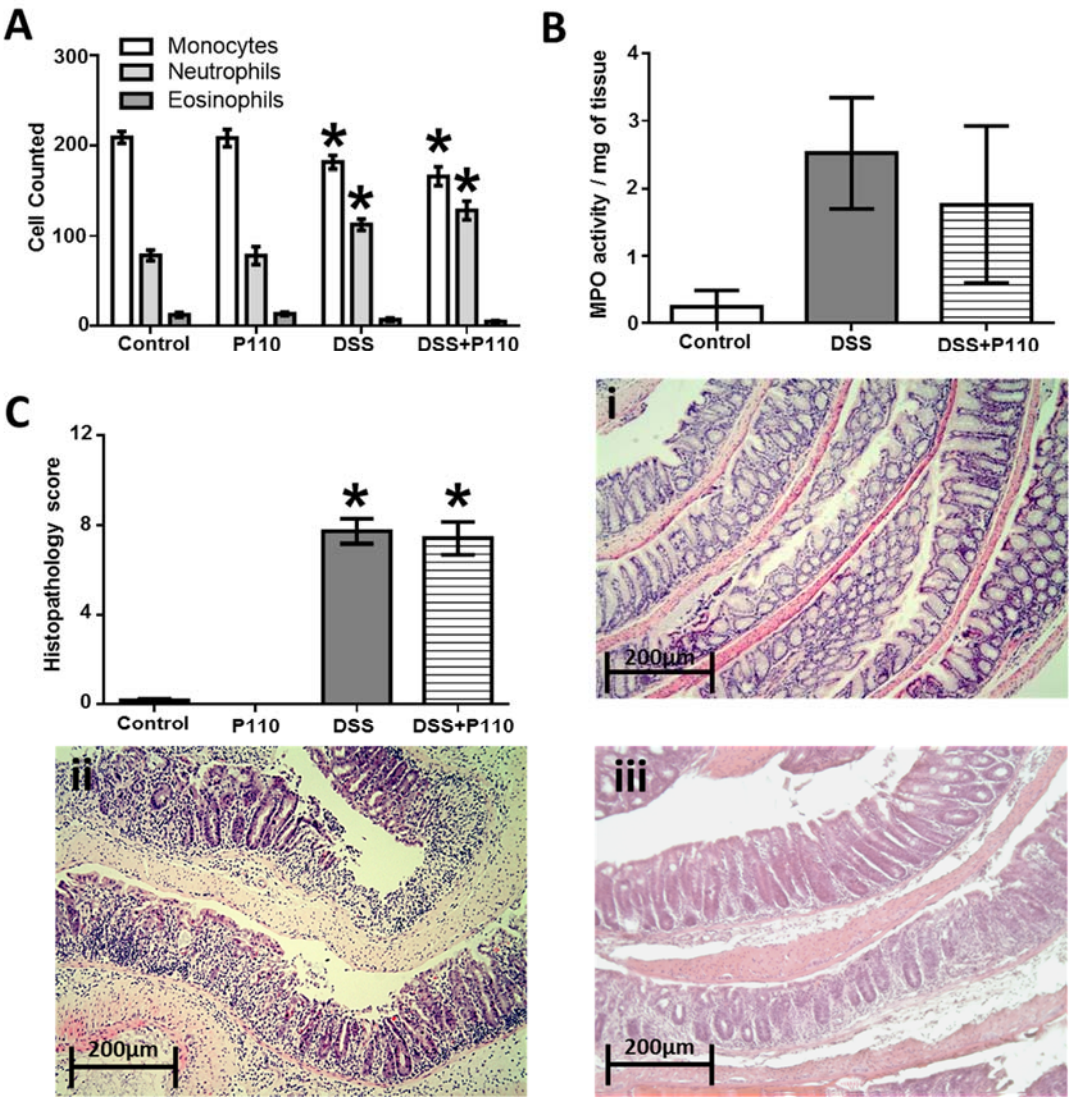

Figure 5.2: Immunological assessment of murine colitis after DSS±P110 trial. A) Blood smear cell counts, n = 8-12, 3 independent experiments B) MPO activity, n = 3-4, 1 independent experiment C) Histopathological score of H&E stained colon tissue with representative images of: i) Control, ii) DSS & iii) DSS+P110 groups. Data is represented as mean ± SEM, n = 8-21, 2-4 independent experiments. *Represents significant differences between the control group, $p<0.05$, A) Ordinary Two-Way ANOVA, Tukey's multiple comparison test, B) One-Way ANOVA, Tukey's multiple comparison test, C) Kruskal-Wallis, Dunn's multiple comparison test.

5.3.3. Administration of P110 after DNBS induction offers mild protection

Comparatively to DSS colitis, DNBS manifests quicker and more aggressively due to the inherent immunogenic response generated by DNBS's binding to intestinal proteins[134]. In support of this, DNBS mice showed significant weight loss by Day 3 (91.1 ± 1.38) compared to control (100.4 ± 0.68), which continued until Day 5 (control: 100.6 ± 1.03; DNBS: 90.8 ± 2.99) ($p<0.05$) (Figure 5.3B). Similarly, DNBS+P110 mice showed significant weight loss at Day 3 (92.7 ± 3.49; $p<0.05$) compared to control, but no differences on Days 4 (94.8 ± 2.43) & 5 (94.6 ± 2.50) ($p>0.05$) (Figure 5.3A). Looking at other indicators of colitis severity, DNBS mice were found to have significantly greater colon shortening (8.3 ± 0.43) and macroscopic disease scores (3.0 ± 0.49), which also related to a lower animal survival rate (73%) ($p<0.05$) (Figure 5.3C, 5.3D & 5.3F). DNBS mice given P110 did not show these significant changes and exhibited no premature death from DNBS colitis ($p>0.05$) (Figure 5.3C, 5.3D & 5.3F). Changes in colon motility were not identified between control, DNBS and DNBS+P110 treatment groups ($p>0.05$) (Figure 5.3E).

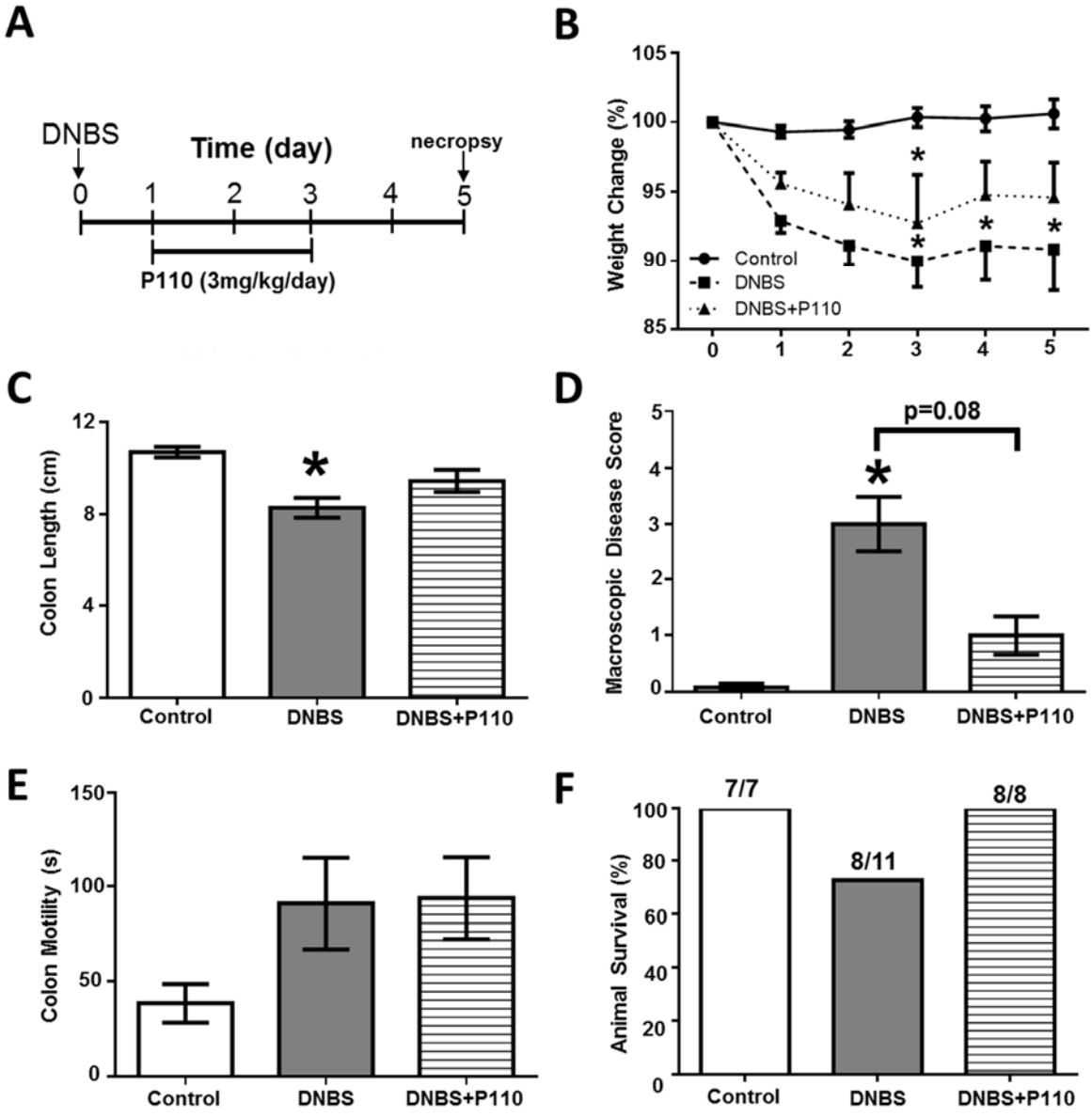

Figure 5.3: Macroscopic assessment of murine colitis after DNBS±P110 treatment protocol. A) Experimental protocol B) Percent weight change during experiment C) Colon length D) Macroscopic disease score E) Colon motility, n = 4-7, 2 independent experiments F) Animal survival rates. Data is represented as mean ± SEM, n = 7-11, 2 independent experiments. *Represents significant differences between the control group, $p<0.05$, B) Repeated measure Two-Way ANOVA, Tukey's multiple comparison test, C & E) One-Way ANOVA, Tukey's multiple comparison test, D) Kruskal-Wallis, Dunn's multiple comparison test.

5.3.4. Inflammatory markers associated with DNBS colitis are not prevented with P110 treatment

Control mice exhibited no colitis associated changes to circulating lymphocytes, MPO activity or histopathology (Figure 5.4A-C). Both DNBS and DNBS+P110 groups showed dramatic increases in circulating neutrophils (DNBS: 172 ± 20.1; DNBS+P110: 145 ± 13.9), and proportionally lower amounts of circulating monocytes (DNBS: 124 ± 19.6; DNBS+P110: 151 ± 13.7), when compared to control groups (neutrophils: 89 ± 15.0; monocytes: 206 ± 14.5) ($p<0.05$) (Figure 5.4A). This increase in circulating neutrophils was also identified at the tissue level based on increases in MPO activity for both DNBS (1.5 ± 0.44) and DNBS+P110 mice (1.4 ± 0.31) compared to control (0.2 ± 0.10) ($p<0.05$) (Figure 5.4B). Increased histopathology was also observed in DNBS (7.3 ± 0.80) but not DNBS+P110 mice (4.6 ± 0.43) compared to control (1.0 ± 0.53) ($p<0.05$) (Figure 5.4Ci-iii).

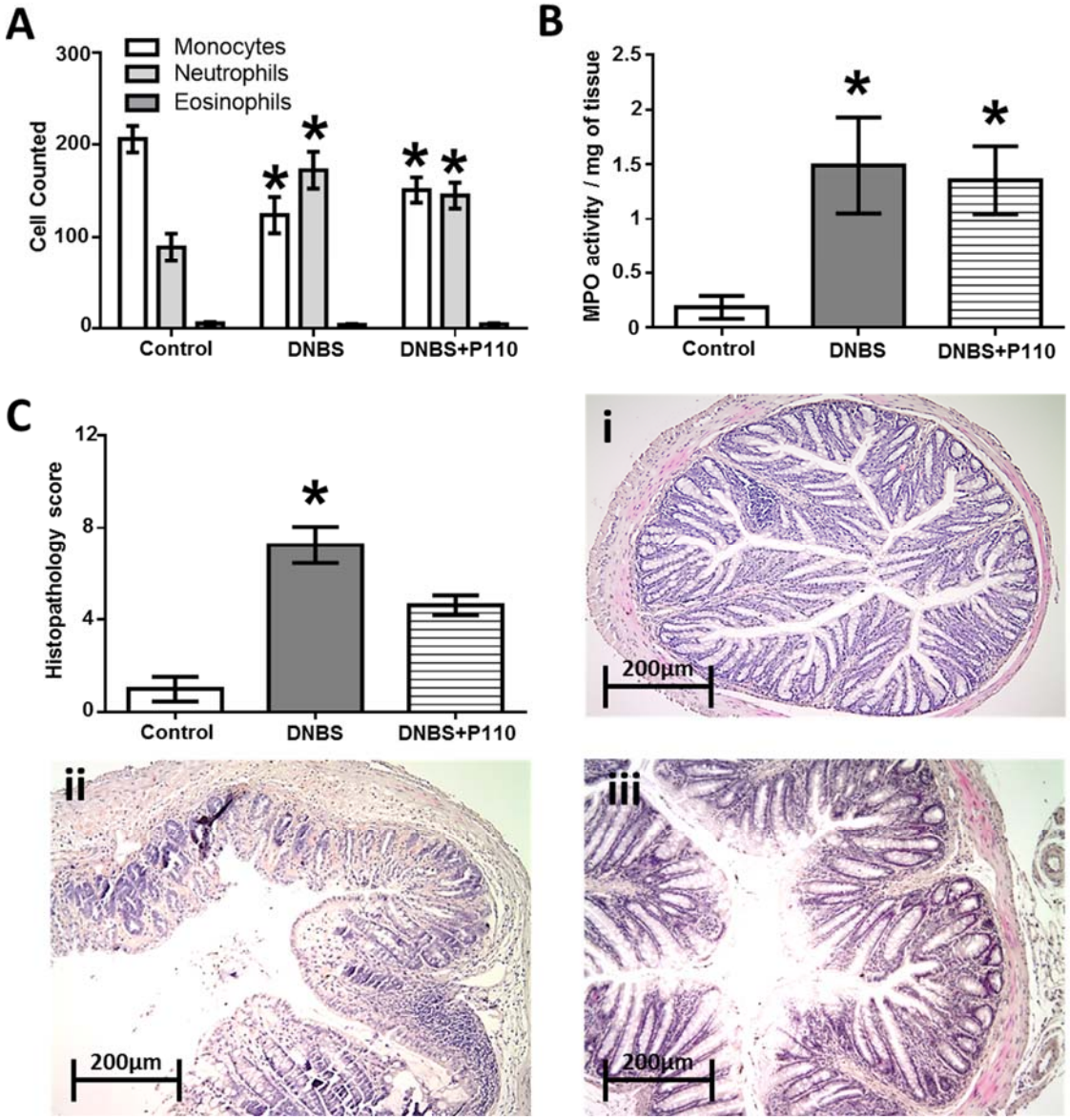

Figure 5.4: Immunological assessment of murine colitis after DNBS±P110 treatment protocol. A) Blood smear cell counts B) MPO activity C) Histopathological score of H&E stained colon tissue with representative images of: i) Control, ii) DNBS & iii) DNBS+P110 treatment groups. Data is represented as mean ± SEM, n = 7-11, 2 independent experiments. *Represents significant differences between the control group, $p<0.05$, A) Ordinary Two-Way ANOVA, Tukey's multiple comparison test, B) One-Way ANOVA, Tukey's multiple comparison test, C) Kruskal-Wallis, Dunn's multiple comparison test.

5.3.5. Prophylactic administration of P110 yields greater efficacy against DNBS colitis

Similar to the DNBS±P110 treatment protocols, DNBS mice showed significant weight loss in comparison to control mice, albeit at an earlier timepoint at Day 2 (control: 100.1 ± 0.25; DNBS: 86.6 ± 2.26; $p<0.05$) (Figure 5.5B). DNBS mice also presented with greater colon shortening (7.5 ± 0.46), macroscopic disease scores (4.0 ± 0.22) and reduced survival rates (73%) compared to control ($p<0.05$) (Figure 5.5C, 5.5D & 5.5F). In comparison to DNBS mice, DNBS+P110 mice also lost significant weight by Day 2 (92.5 ± 1.45; $p<0.05$), but this weight loss was not as severe as mice with DNBS alone ($p<0.05$) (Figure 5.5B). This same trend was also seen for colon length (8.7 ± 0.27) and macroscopic disease score (1.9 ± 0.35) showing a much milder presentation of colitis compared to mice provided DNBS alone ($p<0.05$) (Figure 5.5C & 5.5D). P110 use in DNBS mice also led to increased survival (93%) (Figure 5.5F). Although no significance was observed between any experimental groups for colon motility, DNBS mice showed a large trend towards dysmotility (261 ± 117.2) which was not seen in the DNBS+P110 group (76 ± 27.6) ($p>0.05$) (Figure 5.5E).

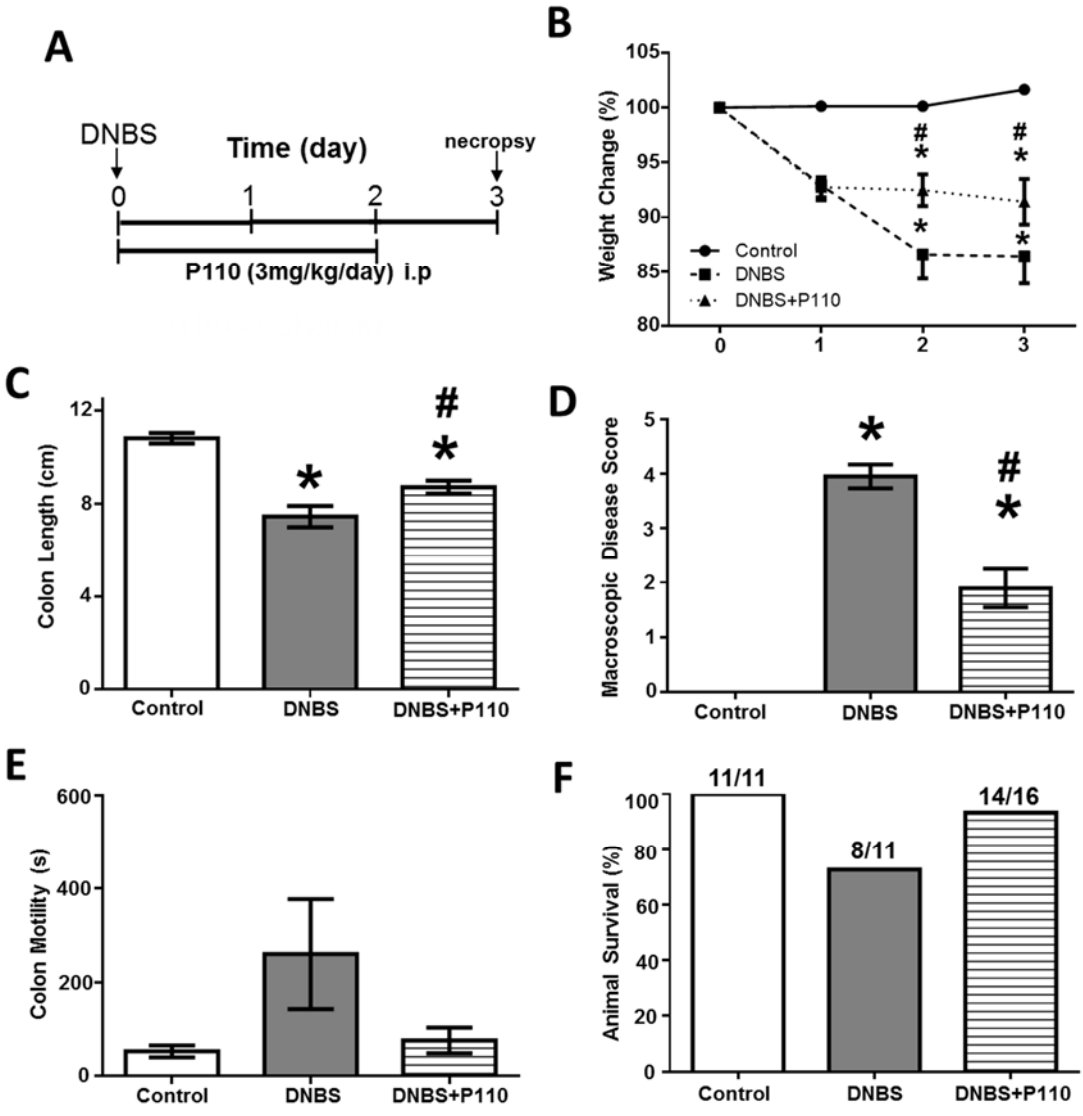

Figure 5.5: Macroscopic assessment of murine colitis after DNBS±P110 prophylactic protocol. A) Experimental protocol B) Percent weight change during experiment C) Colon length D) Macroscopic disease score E) Colon motility, n = 5-6, 2 independent experiments. Data is represented as mean ± SEM, n = 8-16, 3 independent experiments. *Represents significant differences between the control group, #Represents significant differences between the DNBS group, $p<0.05$, B) Repeated measures Two-Way ANOVA, Tukey's multiple comparison test, C & E) One-Way ANOVA, Tukey's multiple comparison test, D) Kruskal-Wallis, Dunn's multiple comparison test.

5.3.6. DNBS associated histopathology presents with less severity when P110 is applied prophylactically

Since no prior evidence suggested a change in circulating lymphocytes or MPO with P110 during the previous DSS and DNBS trials, these measures were omitted during the DNBS±P110 prophylactic protocol. Previous improvements in DNBS histology with P110 treatment, however, supported further histopathological investigation. DNBS mice exhibited significantly worse histological damage (10.8 ± 0.48) in comparison to control mice (0.3 ± 0.21), with DNBS+P110 mice showing much milder histological damage (4.8 ± 1.66) ($p<0.05$) (Figure 5.6).

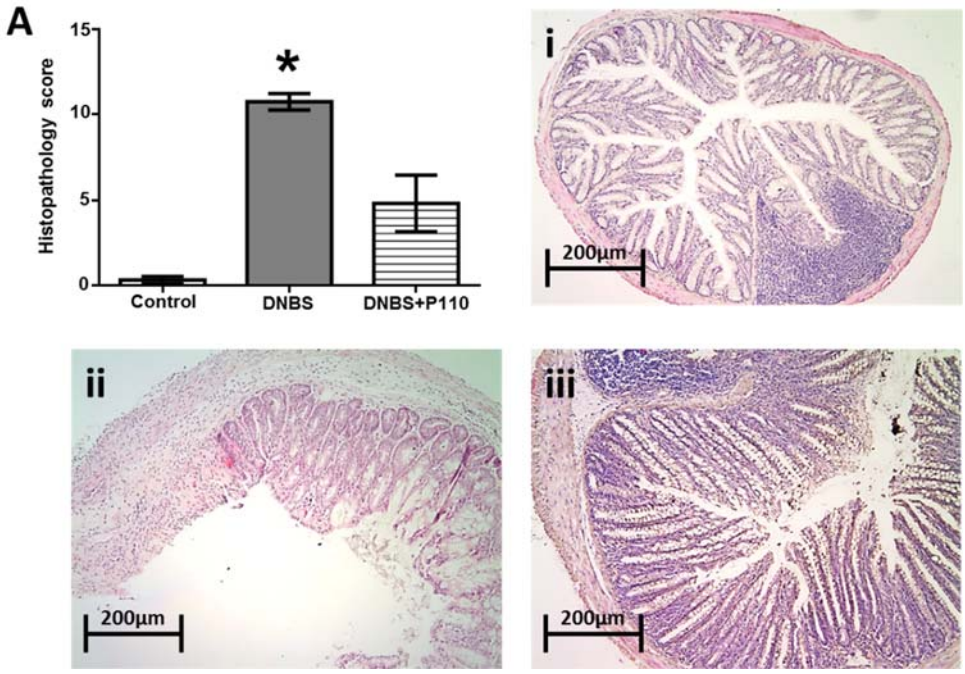

Figure 5.6: Histopathological assessment of murine colitis after DNBS±P110 prophylactic protocol. A) Histopathological score of H&E stained colon tissue with representative images of: i) Control, ii) DNBS & iii) DNBS+P110 prophylactic groups. Data is represented as mean ± SEM, n = 4-6, 2 independent experiments. *Represents significant differences between the control group, $p<0.05$, Kruskal-Wallis, Dunn's multiple comparison test.

5.4. Discussion

Through exploration and investigation of different therapeutic targets, the evolution of immunosuppressive treatments for IBD has allowed for a transition from systemic methods of immunosuppression (corticosteroids) to more specific methods (biologics)[236,237]. While resolving inflammation is important in limiting tissue damage and disease progression, there are still other targets for intervention that may elicit benefit for IBD patients in a manner independent of immunosuppression. Sufficient intestinal barrier function is critical to limiting inflammation by reducing the penetrance of luminal microbes and their products to the host's tissues. This functional property depends on energy contribution from mitochondrial processes, with impairments to mitochondrial function potentially leading to compromised barrier function[102,165]. Therefore, processes tied to mitochondrial function and dysfunction, could affect intestinal barrier function in disease and likewise be targeted for therapeutic benefit. Evidence has suggested that excessive fission mediated by DRP1 and Fis1, promotes mitochondrial dysfunction and contributes to disease, with additional evidence suggesting that inhibition may exert therapeutic potential. Based on this notion, we examined if inhibition of DRP1 and Fis1 binding by P110 could limit murine DSS and DNBS colitis.

Given the similarities in histopathological presentation of murine DSS and DNBS colitis to human UC and CD respectively, both of these models were used to examine P110's potential effect against murine colitis[131,136]. Since no adverse effects were identified in P110 control mice during the DSS trial, this group was omitted in DNBS treatment and prophylactic experiments. As expected, DSS and DNBS mice manifested with worse colitis than control mice based on macroscopic indicators (weight loss, colon shortening, disease score, and motility) and assessed inflammatory changes (blood smears, MPO, histopathology). DSS and DNBS mice receiving P110

prophylactically were found to have greater colitis protection than mice that had P110 applied as a treatment (Figure 5.1, 5.3 & 5.5). This suggests that P110 would be better applied as a prophylactic prior to colitis onset, rather than as a treatment option for colitis that has already manifested. Indeed, it makes sense that prophylactic use of P110 could limit excessive DRP1 and Fis1 mediated fission at inflammation onset, thereby preserving mitochondrial networks and function more effectively than if it was administered after the onset of inflammation. However, since IBD presents in an unpredictable, relapse-remission fashion, timing of P110 administration as a "prophylactic", would remain difficult.

Interestingly, the observed improvements in macroscopic parameters of DSS and DNBS prophylactic protocols occurred despite limited changes in inflammatory measures indicative of neutrophil recruitment to tissues (MPO) (Figure 5.2, 5.4 & 5.6). Since neutrophils are key mediators of intestinal inflammation during murine DSS/DNBS colitis, lack of differences between systemic recruitment (blood smear counts) and intestinal tissue localization (MPO) of neutrophils suggests a similar inflammatory burden in P110 treated animals and their disease positive counterparts[238,239]. Histopathological differences were found to be negligible with P110 in DSS trials, but some reductions were observed in DNBS mice independent of the timing of P110 administration (ie: prophylactic/treatment) (Figure 5.2, 5.4 & 5.6). Differences in the mechanism of how DSS and DNBS induce colitis could possibly account for why P110 exerted histopathological benefit in DNBS, but not DSS colitis trials. Because DSS has been shown to directly interact with one of the hypothesized targets of P110, the epithelium, DSS could be exerting additional effects to the epithelium that ablate potential histopathological benefit with P110[133,180,181]. In contrast, although DNBS colitis still exerts epithelial damage, its mechanism action for colitis induction occurs through a delayed hypersensitivity response, rather than direct

molecular interactions with the epithelium[240]. Indeed, observations of mitochondrial dysfunction within the epithelium of DSS and DNBS treated animals, and amelioration of similar consequences by P110, suggest that the epithelium would benefit if it was the recipient of P110's inhibitory action[13-15,18,150,183,241].

Previous studies utilizing P110 have shown beneficial effects including: improved mitochondrial function, reduced oxidative stress and lower cell apoptosis[13-15,18,150,187]. Selectively targeting and resolving some of these mitochondrial related consequences has previously shown benefit in both DSS and DNBS models, with P110 possibly exerting benefit by inhibiting DRP1 and Fis1 interactions and these associated downstream consequences[102,104,183,241-244]. Observations of mitochondrial dysfunction have been identified in colitis models based on structural abnormalities (DSS, DNBS), reduced mitochondrial function (DSS), increased mitochondrial-mediated apoptosis (DSS) and elevated mtROS production (DSS, DNBS)[102,104,183,241-244]. Numerous studies have demonstrated that targeting excessive mtROS in DSS and DNBS colitis with antioxidants is beneficial and while only examined in DSS colitis, evidence of enhancing or restoring mitochondrial function has similarly shown benefit[102,104,183,241-244]. Limiting mtROS through antioxidants has also been shown to reduce mitochondrial-mediated apoptosis after DSS exposure[183,245]. Based on previous studies demonstrating therapeutic outcomes with P110, inhibition of DRP1 and Fis1 could be mitigating DSS and DNBS associated characteristics of mitochondrial dysfunction (increase ROS, reduced function, disrupted structure), thereby assisting in the maintenance of the epithelium after chemical and inflammatory injury.

5.6. Conclusion

In this study, we show that prophylactic and systemic delivery of the DRP1-Fis1 inhibitor: P110, reduced colitis according to macroscopic indices in both DSS and DNBS murine colitis models. Importantly, these observations occurred despite there being limited changes in the assessed acute inflammatory markers, suggesting that P110 exerted anti-colitic benefit in animals, despite similar disease burden. Observations of anti-colitic benefit with P110 in two commonly employed colitis models (DSS & DNBS) lends support that further examination of mitochondrial dynamics, and more specifically DRP1-Fis1 binding, could yield new therapeutic targets for colitis. Ideally, this research could open new therapeutic options for the treatment and management of IBD, with potentially less risk of drug tolerance and resistance compared to current immunosuppressive treatments.

Chapter 6

General Discussion

6.1. Summary of Project Rationale

IBD consequences are numerous, exerting significant burden to patients (inherent inflammation, extraintestinal manifestations, personal costs) and healthcare systems (medications, surgeries, treatment of co-morbidities and extraintestinal manifestations)[1,6,8,9,246,247]. In treating the disease, research has extensively focused within the niche of immunosuppressive medications and has opened up numerous treatment options (biologics, corticosteroids, thiopurines) that assist in shifting active disease to remission[248,249]. However, subpopulations of IBD patients can show no response to biologics, thiopurines or become refractory to biologic and corticosteroid with prolonged use[248,250,251]. Therefore, other potential targets should be explored to either supplement or replace current pharmacological options.

Mounting evidence supports mitochondrial involvement and dysfunction in IBD. Direct consequences related to mitochondrial dysfunction (lower energy production, higher oxidative stress, and increased cell death) have been shown to exist in representative models of colitis and in human IBD[101,141,143,145,179,183]. Furthermore, improving mitochondrial energy production or reducing ROS production has proven beneficial in animal colitis models[102,104,184,241-245]. Regulation of mitochondrial function and quality occurs through the dynamic processes of fusion and fission, with evidence suggesting that excessive mitochondrial fission could be a maladaptive response to consistent cellular stress[66,68,150]. Inhibition of two mediators of this process: DRP1 and Fis1, by P110, was demonstrated to be beneficial by Qi et al.[150], with further studies in other disease models showing similar benefit[13-19].

Investigation of mitochondrial dynamics within the context of colitis is nearly non-existent and techniques to explore in depth functional characteristics of mitochondria are minimal. Therefore, this project sought to i) develop a protocol for highly specific measurements of mitochondrial function to supplement current investigative techniques in IBD research ii) examine *in-vitro* effects of DSS on $IEC^{4.1}$ mitochondria and if use of a DRP1 and Fis1 inhibitor could ameliorate potentially adverse DSS consequences iii) identify if DRP1 and Fis1 inhibition exerted any anti-colitic benefit in DSS and DNBS murine colitis. In testing these aims, we wished to identify if excessive mitochondrial fission mediated by DRP1 and Fis1 binding is an inherent feature of colitis and if this could act as a novel target for the treatment of IBD.

6.2. Assessment of mitochondrial function in intestinal epithelial cells: a novel tool to explore mitochondrial involvement in inflammatory bowel disease

The Oxygraph-2k was an ideal platform to examine mitochondrial function within IECs, owing to its measurement sensitivity and flexibility in both protocol design and titration application. While established protocols are readily available for other cell types, to the best of our knowledge, this is the first O2k protocol for murine IECs[177]. Specific to the $IEC^{4.1}$ cell population, it was determined that the concentration of digitonin required for permeabilization (4µg/mL) was lower than the recommended amount of 5µg/mL, with further titrations leading to respiratory decline in cells[252]. This emphasizes the importance of optimizing digitonin titrations prior to experiments, to ensure cells are both sufficiently permeabilized and the OMM is not damaged. Future experiments utilizing this digitonin concentration confirmed it was appropriate since the exogenous addition of cell-impermeable substrates (succinate, ADP) were able to stimulate respiration. Additionally, at this digitonin concentration, observations of OMM damage (as

indicated by a cytochrome c test) remained infrequent if cell suspensions were between 7 x 10^5 cells /mL and 1 x 10^6 cells/mL.

Another particularly important and relevant pathway for intestinal homeostasis is the mitochondrial process of beta oxidation. Protocols detailing how to perform beta oxidation analysis with the O2k are available for medium and LCFA, but there are currently no protocols detailing how to examine beta oxidation of SCFA metabolites like butyrate[167,168,175]. Since butyrate represents a far more physiologically relevant substrate to IECs, we developed an optional protocol for the analysis of butyrate beta oxidation through the titration of 4µL of 1M NaBut (2mM)[101]. This substrate concentration was specifically selected since a previous colon cancer cell line: HT-29, reached saturation of butyrate beta oxidation at 2mM based on the conversion of ^{14}C-butyrate to ^{14}C-CO_2[176]. Additionally, since butyrate can affect gene transcription by its action on histone deacetylase, concentrations exceeding mitochondrial oxidative capacities could lead to variable cellular responses during measurement[253,254]. This presents a particular concern since cells are permeabilized and butyrate has increased cellular access, even if cellular exposure to butyrate is relatively transient. Optional tailoring of the complex specific protocol to include beta oxidation analysis, highlights the flexibility of O2k protocol design and allows tremendous amounts of mitochondrial bioenergetic data to be garnered from experiments. Such a wealth of information could be useful in understanding if/how mitochondrial bioenergetic decrements affect epithelial cellular and functional outcomes during intestinal inflammation.

By pairing the developed O2k protocols with measures of barrier function (transepithelial resistance), the relationship of intestinal barrier function and mitochondrial energetics could be more thoroughly examined and potentially elucidate molecular targets for pharmacological development[106,165]. Mitochondrial bioenergetics is also important in regulating cell death, since

inflammatory quiescent modes of cell death, like apoptosis, require ATP to proceed[255,256]. Given that the epithelium exhibits a high turnover with cells constantly undergoing apoptosis and being replaced, reduced mitochondrial function and energy availability could shift apoptosis to the much more inflammatory provocative cell death pathway of necrosis[84]. Therefore, in-depth analysis of mitochondrial function could prove useful in studies examining apoptosis or necrosis cell fate decision, by providing a bioenergetic justification for shifts from apoptosis to necrosis. Indeed, development and utilization of these protocols could prove to be a particularly novel tool in the study of IBD.

6.3. Inhibiting DRP1-Fis1 mediated mitochondrial fission reduces DSS associated bioenergetic impairments in intestinal epithelial cells

Within the DSS animal model, signs of epithelial barrier deterioration and increased intestinal permeability have been shown to precede inflammation and tissue damage[257,258]. As demonstrated by *in-vitro* studies, intestinal barrier function and permeability are tied to sufficient mitochondrial function, with pharmacological disruption leading to adverse outcomes in these parameters[102,104,165]. Therefore, early features of DSS colitis (intestinal barrier defects, increased intestinal permeability) could be a consequence of mitochondrial dysfunction within epithelial cells. In exploring the effects of DSS in an *in-vitro* IEC[4.1] model, we wished to identify if DSS induced mitochondrial dysfunction and if this dysfunction could be ameliorated by DRP1 and Fis1 inhibition through P110.

Indeed, signs that DSS could affect mitochondrial function, were identified with the alamarBlue assay during the optimization of DSS and P110 dosage and exposure. Reduced fluorescence with 2% DSS for 24h suggests that NADH concentration was lower within cells.

Furthermore, the addition of 1.5μM P110 prevented this fluorescence decrease, thereby providing evidence that P110 could mitigate DSS's effect on NADH concentration and potentially metabolic processes tied to NADH production. However, further experiments were required to determine whether the differences in NADH concentration were due to DSS cytotoxicity or actual production of NADH. Interestingly, significant cell death for DSS treated cells provided a reason for lower alamarBlue fluorescence changes, but under similar rates of cell death, DSS+P110 treated cells showed no comparable reductions in alamarBlue fluorescence. This showed that in spite of significant cell death, DSS+P110 cells were able to produce sufficient amounts of NADH, such that the concentrations of NADH rivaled control cell populations. Since NADH may be produced through different mitochondrial pathways (beta oxidation, oxidation of malate/pyruvate/glutamate), we investigated which pathway could account for reduced NADH production in DSS cells.

Using the developed O2k protocols we were able to assess which NADH pathways could be affected with DSS administration. Rates of O_2 flux were found to be significantly lower in DSS treated cells after the titration of beta oxidation linked substrates. Coadministration of P110 with DSS cells lead to higher O_2 flux during measurement of these same beta oxidation substrates. However, changes in O_2 flux based on DSS and P110 treatments cannot indicate if this is due to actual functional defects in CI, or just a lack of NADH available for oxidation by CI. A study by Ahmad et al., showed that DSS impairs butyrate beta oxidation in mice, but that this change occurred within the beta oxidation pathway[259]. If DSS is behaving similarly in our *in-vitro* model, then alterations within beta oxidation could lead to reduced production of NADH and therefore lower O_2 flux related to CI. In agreement, our alamarBlue results also support that differences in

NADH concentrations could be tied to the observed oxygen flux decreases in DSS cells and improvements in oxygen flux for DSS+P110 cells.

In order to identify if DSS induced mitochondrial fragmentation and if P110 exerted its purported benefit of limiting mitochondrial fragmentation, by DRP1-Fis1 inhibition, we needed to look at mitochondrial morphology under DSS±P110 treatments. As predicted, DSS led to significant fragmentation of mitochondrial networks, with co-treatment of P110 resulting in a shift from fragmented morphology to a more intermediate morphology. Importantly, these results support that P110 does not completely inhibit fission, since some level of fission was required to shift mitochondrial networks from a fused morphology to an intermediate morphology in response to DSS treatment. Additionally, the differences in fragmented networks between DSS and DSS+P110 cells, demonstrates that P110 can limit the excessive fission related to DRP1-Fis1 binding, thereby supporting its inhibitory effect. Interestingly, beta oxidation requires a certain degree of fused mitochondrial networks, and preservation of mitochondrial networks in an intermediate state by P110 could be related to our observed increases in beta oxidation with P110 in DSS treated cells[201]. Lack of fusion in Mfn1 KO cells leads to fragmentation of mitochondrial networks and lack of fatty acid uptake by mitochondria[201]. These findings could explain why DSS cells containing fragmented mitochondrial networks also exhibit reduced beta oxidation, resulting from a lack of fatty acid import rather than dysfunction within the beta oxidation pathway[201]. In order to examine additional characteristics of mitochondrial dysfunction, mitochondrial polarization was examined.

Unexpectedly, DSS promoted dramatic increases in fluorescence after 1h DSS incubation, and decreased fluorescence at 24h. Coadministration of P110 did not prevent the DSS associated changes in TMRE fluorescence. Considering previous observations of cell death in both

DSS and DSS+P110 groups after 24h, reductions in viable cells and by extension mitochondrial networks, would be associated with less TMRE mitochondrial uptake and fluorescence. Therefore, the presumption that "depolarization" occurred with DSS exposures could be incorrect and rather be a consequence of DSS induced cell death. However, the increased fluorescence with 1h DSS exposure would not be affected by DSS associated cell death and suggests that mitochondrial hyperpolarization could be occurring early on with DSS application. Mitochondrial hyperpolarization could be related to inhibition of ATP synthase or changes in mitochondrial ion concentrations[39,49,260,261]. In examining the literature, no published observations have identified an inhibitory effect by DSS on ATP synthase. However, there is some evidence that DSS could lead to changes in mitochondrial ion concentrations, through its influence on cytosolic Ca^{2+} concentrations[262,263].

The presence of a $\Delta\psi_m$ within mitochondria allows them to absorb or release various ions in response to cytosolic changes, allowing them to buffer against fluctuations that may otherwise lead to cell death[261,264]. In response to numerous stimuli, mitochondrial hyperpolarization has been reported to coincide with Ca^{2+} mitochondrial uptake[265-269]. With neurons, in particular, hyperpolarization after oxygen-glucose deprivation allows mitochondria to buffer against dramatic changes in cytosolic Ca^{2+} that would otherwise lead to cell death[270,271]. Specific to our model, Samak et al.[262] and Gangwar et al.[263] have shown that 3% DSS led to increased cytosolic Ca^{2+} as early as 10-30min and that this process was associated with dramatic ROS production, alterations in tight junction and reduced barrier function. Therefore, mitochondria could be altering their $\Delta\psi_m$, prior to, or as a consequence of, cytosolic Ca^{2+} changes in order to increase their uptake. However, in the case of prolonged and sustained Ca^{2+} uptake, mitochondrial Ca^{2+} overload can lead to numerous consequences including ROS production, the formation of the mitochondrial

permeability transition pore (mPTP) and initiation of the intrinsic apoptotic pathway by cytochrome c release[272,273]. In the study by Gangwar et al. depletion of Ca^{2+} by BAPTA-AM or inhibition of mPTP by cyclosporin A, ameliorated DSS consequences of ROS production and barrier deterioration, suggesting that these processes are linked[263]. Interestingly, Ca^{2+} overload and hyperpolarization have also been shown to increase DRP1-Fis1 binding in prostate and hepatic cancer cells, as well as human T-cells[274-276]. Therefore, our observations of DSS induced fragmentation could also result from mitochondrial Ca^{2+} overload and hyperpolarization, with P110 limiting the DRP1-Fis1 binding. In summary, hyperpolarization of mitochondria may be indicative of an adaptive response to high cytosolic Ca^{2+} changes with DSS, allowing increased mitochondrial Ca^{2+} uptake that over longer periods of time could lead to Ca^{2+} overload and initiation of mitochondrial-mediated apoptosis and DRP1-Fis1 mitochondrial fission.

6.4. Pharmacological inhibition of DRP1 and Fis1 mediated mitochondrial fission reduces murine DSS and DNBS colitis

While no animal colitis model appropriately replicates the complexity of human IBD presentation and progression (ie: spontaneous, relapse-remitting), the establishment of certain models, allow key aspects of the disease to be examined[277,278]. The acute DSS colitis model is typically utilized to examine treatment effectiveness after epithelial damage, barrier disruption and subsequent inflammation[278-280]. In contrast, the DNBS model is useful for identifying treatment responses to acute and aggressive inflammation, instigated after recognition of either colon or microbial antigens within the colon[134]. These models are also frequently utilized as representative models for UC (DSS) and CD (DNBS), given their similar histopathological presentation[136,280]. Therefore, these models seemed appropriate for examining the possible anti-colitic benefit of

DRP1 and Fis1 inhibition by P110, and potentially additional inferences regarding its use in human IBD.

Signs of colitis were observed in both DSS and DNBS models based on macroscopic characteristics (weight loss, colon shortening, disease score, and motility) and immunological changes (MPO, blood smears). Administration of P110 in a prophylactic manner showed macroscopic benefit in DSS and DNBS mice, while the use of P110 as a treatment in DNBS mice showed much milder changes in macroscopic indices. While macroscopic benefit was observed with P110, DSS and DNBS associated inflammatory changes remained unchanged with P110. DSS histopathology remained nearly identical between DSS and DSS+P110 groups, but some benefit was identified in DNBS mice with treatment and prophylactic administered P110. Based on our original hypothesis that P110 exerts benefit on the IECs within the epithelium, changes in histopathology could be tied to characteristics of the disease models. Since DSS has shown to be directly cytotoxic to IECs in our *in-vitro* model, remaining unaffected by DRP1-Fis1 inhibition, breaches in the epithelium by DSS *in-vivo* and lack of prevention by P110, could have led to our histopathological observations. In contrast, while DNBS colitis manifests in an acute and severe manner, it may not exhibit the same degree of targeted epithelial damage as DSS, thereby allowing P110 to exhibit its potential benefit on preserving mitochondrial morphology and beta oxidation. Despite these findings, since the localization of P110 was not determined *in-vivo* we cannot conclusively state that these changes were due to DRP1-Fis1 inhibition at the epithelium.

In administering P110 intraperitoneally, P110 would most likely be absorbed across the visceral peritoneum and enter portal circulation[281,282]. Therefore, P110 would encounter several tissues prior to its hypothesized target of the colon epithelium, including the liver, heart, lungs, brain and numerous abdominal organs. The conjugation of P110 to the cell-penetrating peptide

TAT[47-57], also mires which specific cell/tissue could be the recipient of DRP1-Fis1 inhibition due to its ability to pass through normally inaccessible areas like the blood-brain barrier[283,284]. In treatment naïve mice, fluorescein isothiocyanate (FITC) labeled P110 given through subcutaneous osmotic pumps (3mg/kg/day) was shown to localize within brain striatum tissues, demonstrating P110's reach following systemic administration[18].

Multiple studies have shown that intraperitoneal P110 administration leads to beneficial effects in multiple sclerosis, stroke and myocardial infarction rodent models[13,14,18]. However, localization of P110 was not confirmed in these studies, and rather the presence of P110 at afflicted tissues was only inferred based on beneficial outcomes and decreased DRP1 protein expression in mitochondrial isolates[13,14,18]. While our study similarly demonstrates beneficial outcomes with P110 against DSS and DNBS colitis, it is difficult for us to determine exactly the tissue and or cellular recipient(s) without labeling of P110 and tracing its migration *in-vivo*. Because P110 was shown to localize in brain tissues with subcutaneous osmotic pump administration, and given its beneficial findings in numerous neurodegenerative models, inhibition of DRP1 and Fis1 could be occurring in neuronal cells[13,14,17,19,188,189].

Due to the intimate and bidirectional interactions of the gut and brain, experimental colitis could also lead to neuronal changes[285,286]. Studies have observed neurological consequences after DSS and DNBS colitis, including increases in anxiety and depressive-like behaviors[136,287-290]. Interestingly, Haj et al. showed that DNBS related anxiety and depressive-like behaviors were tied to dysfunctional hippocampal mitochondria that produced less energy and greater ROS[136]. Therefore, intraperitoneally administered P110 could also be limiting mitochondrial dysfunction within brain mitochondria and possibly mediating some of our DNBS and/or DSS findings. Several papers utilizing P110 *in-vivo* have demonstrated neurological benefit within Parkinson's,

multiple sclerosis, amyotrophic lateral sclerosis, and Huntington's animal models[13,14,17,19,188,189]. Our findings of reduced DSS and DNBS colon dysmotility by P110 could also support this notion, however, it cannot be conclusively said if this benefit is from limiting DRP1-Fis1 binding in neurons of the central, enteric or peripheral nervous system, smooth muscle or potentially another cell type.

Chapter 7
Conclusions

7.1. Summary

The overall goal of this thesis was to examine the relevance of DRP1-Fis1 mediated mitochondrial fission to disease in both an *in-vitro* DSS epithelial cell model and *in-vivo* through DSS and DNBS murine colitis models. Key findings of this thesis were as follows:

1) O2k respirometric analysis can be utilized to examine in-depth mitochondrial functional changes in IECs and could prove useful in supplementing current investigative techniques for epithelial cells.

2) Exposure of IECs to 2% DSS for 1h led to mitochondrial hyperpolarization, which was unaffected by P110 (1.5μM). At 24h, 2% DSS exposure increased cell death and reduced mitochondrial NADH concentrations, beta oxidation linked respiration and cellular ATP content. Morphological changes were also observed with 2% DSS leading to increased mitochondrial network fragmentation. Of these DSS related consequences, inhibition of DRP1-Fis1 binding by P110 ameliorated reductions in cellular NADH and beta oxidation respiration, in addition to limiting mitochondrial fragmentation.

3) Inhibition of DRP1-Fis1 *in-vivo* with prophylactic and systemic administration of P110, led to macroscopic improvement in both DSS and DNBS murine colitis models. These benefits occurred despite a lack of change in markers associated with neutrophil recruitment and tissue migration.

A schematic illustrating these conclusions may be found in Figure 7.1. In summary, these results provide important insight into the role of DRP1 and Fis1 mediated mitochondrial fission and the functional implications of their interaction within a colitis framework.

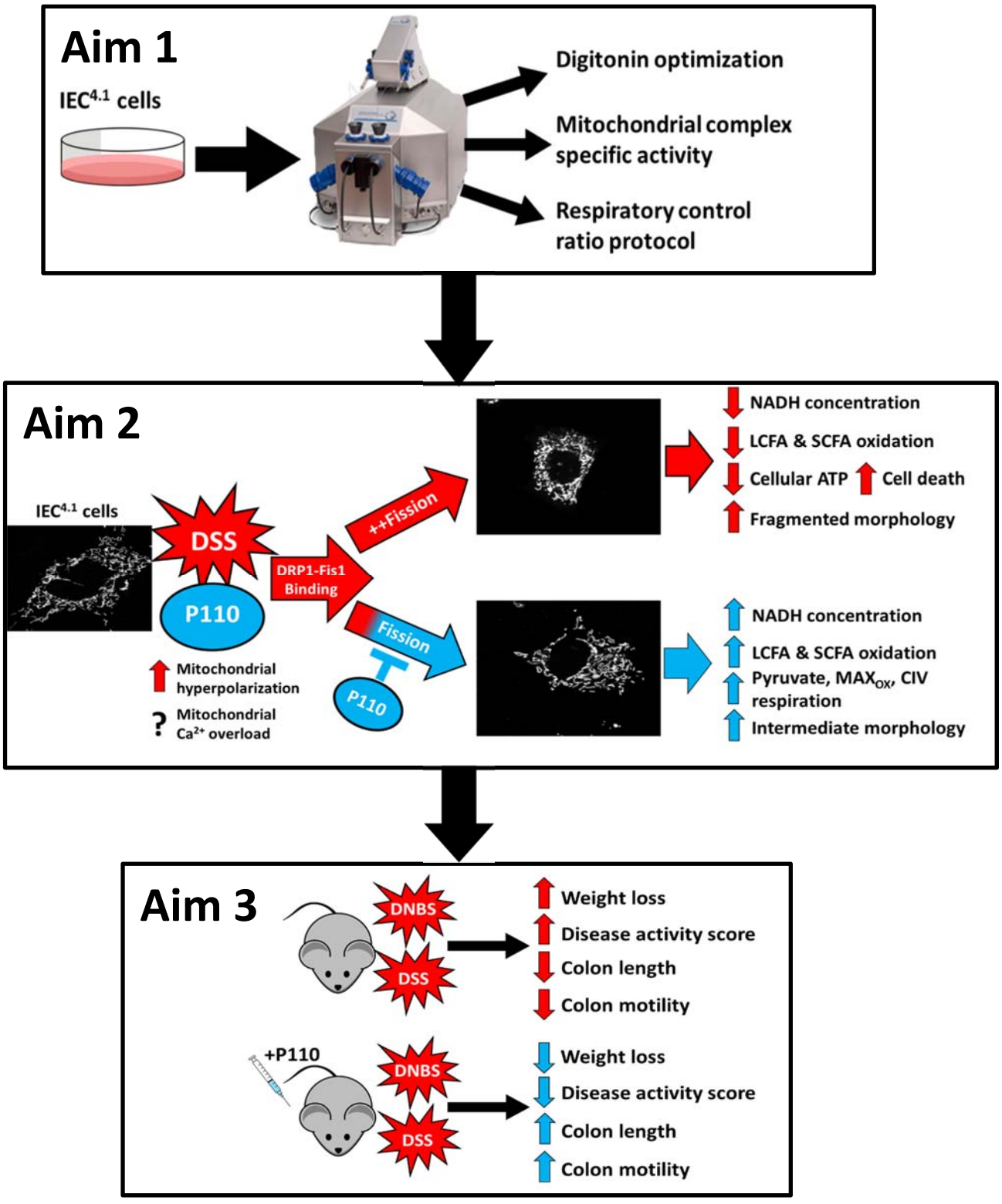

Figure 7.1: Schematic summary of key findings with regard to the thesis aims

7.2. Study Limitations

In translating results obtained from the DSS *in-vitro* model to *in-vivo* DSS colitis and subsequently to human IBD, there are several limitations that must be highlighted.

7.2.1. Relevance of in-vitro DSS epithelial cell model to in-vivo DSS colitis model

As a frequent consequence of using cellular models, translatability to *in-vivo* findings can be difficult. By optimizing the dosage of DSS and P110 with alamarBlue prior to further experimentation, the effects of DSS±P110 on IECs could be more appropriately examined and tested i*n-vitro*. However, whether these concentrations are truly representative of *in-vivo* conditions is not known, thereby limiting translatability of our results. The *in-vitro* model also lacks numerous factors pertaining to the extremely complex colon microenvironment including gut microbiota, presence of other cell types, microarchitecture of the mucosa and microbial/cellular secreted factors. Specific to the epithelial cell line we used, its isolation and immortalization could have also changed its original phenotype and introduced malignancy. Since cancer cells exhibit dramatically different metabolic characteristics, particularly in regard to mitochondrial metabolism, the metabolic results obtained may not be truly representative of a non-transformed epithelial cell population[291,292].

7.2.2. Quantification of mitochondrial networks

In categorizing mitochondrial network morphology, specific criteria were set to ensure a degree of objectivity in measures. Unfortunately, these criteria do not account for the numerous other characteristics of mitochondrial morphology (aspect ratio, mitochondrial branching, mitochondrial area, mitochondrial number) that could be pertinent to this study[293]. Additionally,

in characterizing differences of mitochondrial networks by nominal data (ie: “fused”, “intermediate” or “fragmented”), specific numerical differences between treatment groups are lost. In performing mitochondrial morphological quantification with recently developed software programs like Mitograph, these limitations could have been accounted for[294].

7.2.3. Translation of murine colitis model findings to human IBD

Ease in experimental reproducibility and cost-effectiveness make murine chemically induced colitis models an ideal choice for the testing of a therapeutics anti-colitic potential. Despite these benefits, chemically induced animal colitis models do not properly recapitulate the key aspects of human IBD (spontaneous, relapse-remitting). Specific to the DSS model used, inflammation within the acute DSS protocol has been shown to be mediated predominantly by neutrophils and eosinophils, lacking the immunological complexity observed during the chronic inflammation of human IBD (macrophages, T-cells, B-cells)[295]. In contrast, DNBS colitis occurs largely due to a delayed hypersensitivity reaction from the recognition of self-antigens, showing greater immunological complexity, but still no spontaneous or relapse remission symptom presentation[240]. Sex differences to P110 treatments were also not examined, since females tend to not survive DNBS colitis. Lastly, these models also lack the input of genetic and environmental variables often associated with human IBD. Regardless of these limitations, both DSS and DNBS models are appropriate for identifying if inhibition of DRP1-Fis1 could yield any anti-colitic benefit.

7.2.4. P110 localization in-vivo

By employing cell-penetrating peptides like TAT^{47-57}, the effectiveness of compound delivery and bioavailability can be dramatically increased[296,297]. However, because TAT^{47-57} can initiate endocytosis mediated uptake of the cargo P110 molecule with numerous cellular types, identifying cellular recipients for P110's beneficial effect remains difficult[296,297]. Indeed, several cellular targets could be the recipients of P110's inhibitory effect, long before it reaches its hypothesized target of the colonic epithelium (liver, brain, heart, lungs). Additionally, while we did not see changes in markers of neutrophil recruitment and tissue migration with P110, other immunological cells could still be affected by P110 and mediate our anti-colitic observations. Degradation of P110 prior to, or after cell entry could also be a likely outcome, since "escape" of molecules from the endosome after entry requires specific design elements to be incorporated into the original molecule. It has been suggested that the half-life of P110 could be as short as 1h, but these claims have not been substantiated with evidence[15]. Therefore, tracing P110's migration and localization *in-vivo* is paramount to identifying the fate of P110-TAT^{47-57} molecules *in-vivo* and relating the observed anti-colitic effects by P110 to possible cellular and tissue mediators.

7.3. Future Directions

7.3.1. Functional assessment of murine colonoid monolayers exposed to DSS±P110

In order to more appropriately examine the effects of DSS±P110 *in-vitro*, future experiments could utilize 2D monolayers established from the isolation of murine colonic crypts[298]. Preparation of isolated colonocytes into murine colonoid monolayers could allow epithelial barrier function (transepithelial resistance) to be assessed under DSS±P110 conditions. These findings could then be supplemented with mitochondrial bioenergetic data and build a more holistic picture of how mitochondrial function/dysfunction affects epithelial barrier maintenance/deterioration. 2D monolayers also exhibit microarchitecture and cellular composition that is more representative of *in-vivo* conditions[298]. Fresh isolation of murine crypts also ensures that genetic drift and risk of malignancy is limited, thereby making the model more phenotypically representative in comparison to immortalized cultured cells.

7.3.2. Application of P110 to IBD human colonoids with active and inactive disease

It has been previously demonstrated that human colon crypts can be isolated and cultured into monolayers for *in-vitro* experimentation[299]. This technique could possibly be utilized to examine P110's effect on human colonoid monolayers from individuals with active and inactive disease, ideally from the same patients. While this *in-vitro* model would still lack *in-vivo* features like: gut microbiota, supporting structures and cell types to the epithelium (blood and lymph vessels, neurons, smooth muscle) and the presence of inflammation (active disease), it provides greater ease in translating the results of P110's effect on the colon epithelium to human IBD.

7.3.3. Measurement of steady-state ATP and NADH production after DSS±P110 treatments

In exploring several metabolic pathways with the O2k we identified potentially important bioenergetic disparities between DSS and DSS+P110 treated cells during beta oxidation. While we did not find improvements in intracellular ATP content with P110 in DSS treated cells, our specific respirometric measures do suggest that there would be differences in steady-state ATP production between DSS and DSS+P110 cells during beta oxidation. To examine this more closely, a fluorescent biosensor could be utilized to measure steady-state ATP production after DSS±P110 treatments in the presence of beta oxidation linked substrates[300,301]. Additionally, by pairing this technique with the measurement of NADH production by fluorescence microscopy, results could be obtained that bridge the gap between the observed respiratory changes and potential bioenergetic consequences with DSS±P110[302].

Bibliography

1. Yu, Y. R. & Rodriguez, R. J. Clinical presentation of Crohn's, ulcerative colitis, and indeterminate colitis: Symptoms, extraintestinal manifestations, and disease phenotypes. *Seminars in Pediatric Surgery* **26,** 349–355 (2017).

2. Paine, E. & Shen, B. Endoscopic therapy in inflammatory bowel diseases (with videos). *Gastrointestinal Endoscopy* **78,** 819–835 (2013).

3. Peyrin-Biroulet, L., Jr, E. V., Colombel, J.-F. & Sandborn, W. J. The natural history of adult Crohn's disease in population-based cohorts. *The American Journal of Gastroenterology* **105,** ajg2009579 (2009).

4. Scaringi, S. *et al.* New perspectives on the long-term outcome of segmental colectomy for Crohn's colitis: an observational study on 200 patients. *International Journal of Colorectal Disease* **33,** 479–485 (2018).

5. Dulai, P. S. & Jairath, V. Acute severe ulcerative colitis: latest evidence and therapeutic implications. *Therapeutic Advances in Chronic Diseases* **9,** 65–72 (2017).

6. Ott, C. & Schölmerich, J. Extraintestinal manifestations and complications in IBD. *Nature Reviews Gastroenterology & Hepatology* **10,** 585 (2013).

7. Burisch, J., Jess, T., Martinato, M. & Lakatos, P. L. The burden of inflammatory bowel disease in Europe. *Journal of Crohn's and Colitis* **7,** 322–337 (2013).

8. Rocchi, A. *et al.* Inflammatory bowel disease: A Canadian burden of illness review. *Canadian Journal of Gastroenterology and Hepatology* **26,** 811–817 (2012).

9. Bernstein, C. N. *et al.* The Epidemiology of Inflammatory Bowel Disease in Canada: A Population-Based Study. *The American Journal of Gastroenterology* **101,** ajg2006291 (2006).

10. Benchimol, E. I. *et al.* Trends in Epidemiology of Pediatric Inflammatory Bowel Disease in Canada: Distributed Network Analysis of Multiple Population-Based Provincial Health Administrative Databases. *The American Journal of Gastroenterology* **112,** 1120 (2017).

11. Kaplan, G. G. The global burden of IBD: from 2015 to 2025. *Nature Reviews Gastroenterology & Hepatology* **12,** 720 (2015).

12. Okamoto, R. & Watanabe, M. Role of epithelial cells in the pathogenesis and treatment of inflammatory bowel disease. *Journal of Gastroenterology* **51,** 11–21 (2016).

13. Luo, F., Herrup, K., Qi, X. & Yang, Y. Inhibition of Drp1 hyper-activation is protective in animal models of experimental multiple sclerosis. *Experimental Neurology* **292,** 21–34 (2017).

14. Filichia, E., Hoffer, B., Qi, X. & Luo, Y. Inhibition of Drp1 mitochondrial translocation provides neural protection in dopaminergic system in a Parkinson's disease model induced by MPTP. *Scientific Reports* **6,** srep32656 (2016).

15. Disatnik, M. *et al.* Acute Inhibition of excessive mitochondrial fission after myocardial infarction prevents long-term cardiac dysfunction. *Journal of the American Heart Association* **2,** (2013).

16. Tian, L. *et al.* Ischemia-induced Drp1 and Fis1-mediated mitochondrial fission and right ventricular dysfunction in pulmonary hypertension. *Journal of Molecular Medicine* **95,** 381–393 (2017).

17. Joshi, A. U. *et al.* Inhibition of Drp1/Fis1 interaction slows progression of amyotrophic lateral sclerosis. *EMBO Molecular Medicine* **10,** e8166 (2018).

18. Guo, X. *et al.* Inhibition of mitochondrial fragmentation diminishes Huntington's disease–associated neurodegeneration. *Journal of Clinical Investigation* **123,** 5371–5388 (2013).

19. Joshi, A. U., Saw, N. L., Shamloo, M. & Mochly-Rosen, D. Drp1/Fis1 interaction mediates mitochondrial dysfunction, bioenergetic failure and cognitive decline in Alzheimer's disease. *Oncotarget* **9,** 6128–6143 (2017).

20. Novak, E. A. & Mollen, K. P. Mitochondrial dysfunction in inflammatory bowel disease. *Frontiers in Cell and Developmental Biology* 3, 62 (2015).

21. Krauss, S. Mitochondria: structure and role in respiration. *Encyclopedia Of Life Sciences* (2001). doi:10.1038/npg.els.0001380

22. de Brito, O. & Scorrano, L. An intimate liaison: spatial organization of the endoplasmic reticulum–mitochondria relationship. *The EMBO Journal* **29,** 2715–2723 (2010).

23. Longo, D. L. & Archer, S. L. Mitochondrial dynamics — mitochondrial fission and fusion in human diseases. *The New England Journal of Medicine* **369,** 2236–2251 (2013).

24. Webster, K. A. Evolution of the coordinate regulation of glycolytic enzyme genes by hypoxia. *Journal of Experimental Biology* **206,** 2911–2922 (2003).

25. Scrutton, M. & Utter, M. The regulation of glycolysis and gluconeogenesis in animal tissues. *Annual Review of Biochemistry* **37,** 249–302 (1968).

26. Bartlett, K. & Eaton, S. Mitochondrial β-oxidation. *European Journal of Biochemistry* **271,** 462–469 (2004).

27. Kerner, J. & Hoppel, C. Fatty acid import into mitochondria. *Biochimica et Biophysica Acta - Molecular and Cell Biology of Lipids* **1486,** 1–17 (2000).

28. Sivaprakasam, S., Bhutia, Y. D., Yang, S. & Ganapathy, V. Short-chain fatty acid transporters: role in colonic homeostasis. *Comprehensive Physiology* **8,** 299–314 (2018).

29. Schönfeld, P. & Wojtczak, L. Short- and medium-chain fatty acids in energy metabolism: the cellular perspective. *Journal of Lipid Research* **57,** 943–954 (2016).

30. Houten, S. & Wanders, R. J. A general introduction to the biochemistry of mitochondrial fatty acid β-oxidation. *Journal of Inherited Metabolic Disease* **33,** 469–477 (2010).

31. Akram, M. Citric acid cycle and role of its intermediates in metabolism. *Cell Biochemistry and Biophysics* **68,** 475–478 (2014).

32. Schultz, B. E. & Chan, S. I. Structures and proton-pumping strategies of mitochondrial respiratory enzymes. *Annual Review of Biophysics and Biomolecular Structure* **30,** 23–65 (2001).

33. Chance, B. & William, G. Respiratory enzymes in oxidative phosphorylation. III. The steady state. *Journal of Biological Chemistry* **217,** 409–27 (1955).

34. Nakamoto, R. K., Scanlon, J. A. & Al-Shawi, M. K. The rotary mechanism of the ATP synthase. *Archives of Biochemistry and Biophysics* **476,** 43–50 (2008).

35. von Ballmoos, C., Wiedenmann, A. & Dimroth, P. Essentials for ATP synthesis by F1F0 ATP synthases. *Biochemistry* **78,** 649–672 (2009).

36. Watt, I. N., Montgomery, M. G., Runswick, M. J., Leslie, A. G. & Walker, J. E. Bioenergetic cost of making an adenosine triphosphate molecule in animal mitochondria. *Proceedings of the National Academy of Sciences* **107,** (2010).

37. Dimroth, P., Kaim, G. & Matthey, U. Crucial role of the membrane potential for ATP synthesis by F(1)F(o) ATP synthases. *Journal of Experimental Biology* **203,** 51–9 (2000).

38. Kaim, G. & Dimroth, P. ATP synthesis by F-type ATP synthase is obligatorily dependent on the transmembrane voltage. *The EMBO Journal* **18,** 4118–4127 (1999).

39. Alberts, B., Johnson, A., Lewis, J., Raff, M., Roberts, K & Walter, P. Molecular biology of the cell. 4th edition. New York, *Garland Science*, ISBN 0-8153-3218-1 (2002).

40. Han, Y., Kim, S., Kim, S. & Park, W. Carbonyl cyanide p-(trifluoromethoxy) phenylhydrazone (FCCP) as an O2− generator induces apoptosis via the depletion of intracellular GSH contents in Calu-6 cells. *Lung Cancer* **63,** 201–209 (2009).

41. Narendra, D., Tanaka, A., Suen, D.-F. & Youle, R. J. Parkin is recruited selectively to impaired mitochondria and promotes their autophagy. *Journal of Cell Biology* **183,** 795–803 (2008).

42. Anderson, N. M., Mucka, P., Kern, J. G. & Feng, H. The emerging role and targetability of the TCA cycle in cancer metabolism. *Protein Cell* **9,** 216–237 (2018).

43. Letts, J. A. & Sazanov, L. A. Clarifying the supercomplex: the higher-order organization of the mitochondrial electron transport chain. *Nature Structural and Molecular Biology* **24,** nsmb.3460 (2017).

44. Nicholls, D. G. The non-ohmic proton leak—25 years on. *Bioscience Reports* **17,** 251–257 (1997).

45. Rolfe, D., Hulbert, A. J. & Brand, M. D. Characteristics of mitochondrial proton leak and control of oxidative phosphorylation in the major oxygen-consuming tissues of the rat. *Biochimica et Biophysica Acta - Bioenergetics* **1188,** 405–416 (1994).

46. Nobes, C., Brown, G., Olive, P. & Brand. Non-ohmic proton conductance of the mitochondrial inner membrane in hepatocytes. *Journal of Biological Chemistry* **265,** 12903–9 (1990).

47. Benz, R. & McLaughlin, S. The molecular mechanism of action of the proton ionophore FCCP (carbonylcyanide p-trifluoromethoxyphenylhydrazone). *Biophysical Journal* **41,** 381–398 (1983).

48. Mlejnek, P. & Dolezel, P. Loss of mitochondrial transmembrane potential and glutathione depletion are not sufficient to account for induction of apoptosis by carbonyl cyanide 4-(trifluoromethoxy) phenylhydrazone in human leukemia K562 cells. *Chemico-Biological Interactions* **239,** 100–110 (2015).

49. Perry, S., Norman, J., Barbieri, J., Brown, E. & Gelbard, H. Mitochondrial membrane potential probes and the proton gradient: a practical usage guide. *Biotechniques* **50,** 98–115 (2011).

50. Perl, A., Gergely, P., Nagy, G., Koncz, A. & Banki, K. Mitochondrial hyperpolarization: a checkpoint of T-cell life, death and autoimmunity. *Trends in Immunology* **25,** 360–367 (2004).

51. Sanderson, T. H., Reynolds, C. A., Kumar, R., Przyklenk, K. & Hüttemann, M. Molecular mechanisms of ischemia–reperfusion injury in brain: pivotal role of the mitochondrial membrane potential in reactive oxygen species generation. *Molecular Neurobiology* **47,** 9–23 (2013).

52. Gergely, P. *et al.* Persistent mitochondrial hyperpolarization, increased reactive oxygen intermediate production, and cytoplasmic alkalinization characterize altered IL-10 signaling in patients with systemic lupus erythematosus. *Journal of Immunology* **169,** 1092–1101 (2002).

53. Matsuda, N. *et al.* PINK1 stabilized by mitochondrial depolarization recruits Parkin to damaged mitochondria and activates latent Parkin for mitophagy. *The Journal of Cell Biology* **189,** 211–221 (2010).

54. Narendra, D. P. *et al.* PINK1 is selectively stabilized on impaired mitochondria to activate parkin. *PLoS Biology* **8,** e1000298 (2010).

55. Murphy, M. P. How mitochondria produce reactive oxygen species. *Biochemical Journal* **417,** 1–13 (2009).

56. Brand, M. D. The sites and topology of mitochondrial superoxide production. *Experimental Gerontology* **45,** 466–472 (2010).

57. Fridovich, I. Superoxide anion radical ($O^{\cdot -}$), Superoxide dismutases, and related matters. *Journal of Biological Chemistry* **272,** 18515–18517 (1997).

58. Glorieux, C., Zamocky, M., Sandoval, J., Verrax, J. & Calderon, P. Regulation of catalase expression in healthy and cancerous cells. *Free Radical Biology and Medicine* **87,** 84–97 (2015).

59. Guptasarma, P., Balasubramanian, D., Matsugo, S. & Saito, I. Hydroxyl radical mediated damage to proteins, with special reference to the crystallins. *Biochemistry* **31,** 4296–303 (1992).

60. Valko, M. *et al.* Free radicals and antioxidants in normal physiological functions and human disease. *International Journal of Biochemistry and Cell Biology* **39,** 44–84 (2007).

61. Murata, M., Thanan, R., Ma, N. & Kawanishi, S. Role of nitrative and oxidative DNA damage in inflammation-related carcinogenesis. *Journal of Biomedicine and Biotechnology* **2012,** 623019 (2012).

62 Dukan, S. *et al.* Protein oxidation in response to increased transcriptional or translational errors. *Proceedings of the National Academy of Science* **97,** 5746–5749 (2000).

63. Zarkovic, N., Cipak, A., Jaganjac, M., Borovic, S. & Zarkovic, K. Pathophysiological relevance of aldehydic protein modifications. *Journal of Proteomics* **92,** 239–247 (2013).

64. Kawanishi, S. & Hiraku, Y. Oxidative and nitrative DNA damage as biomarker for carcinogenesis with special reference to inflammation. *Antioxidant Redox Signalling* **8,** 1047–58 (2006).

65. Deponte, M. Glutathione catalysis and the reaction mechanisms of glutathione-dependent enzymes. *Biochimica et Biophysica Acta (BBA) - General Subjects* **1830,** 3217–3266 (2013).

66. Zemirli, N., Morel, E. & Molino, D. Mitochondrial dynamics in basal and stressful conditions. *International Journal of Molecular Sciences* **19,** 564 (2018).

67. Ni, H.-M., Williams, J. A. & Ding, W.-X. Mitochondrial dynamics and mitochondrial quality control. *Redox Biology* **4,** 6–13 (2015).

68. Rambold, A. S. & Pearce, E. L. Mitochondrial dynamics at the interface of immune cell metabolism and function. *Trends in Immunology* **39**, 6–18 (2018).

69. Roy, M., Reddy, H. P., Iijima, M. & Sesaki, H. Mitochondrial division and fusion in metabolism. *Current Opinion in Cell Biology* **33,** 111–118 (2015).

70. Rambold, A. S., Kostelecky, B., Elia, N. & Lippincott-Schwartz, J. Tubular network formation protects mitochondria from autophagosomal degradation during nutrient starvation. *Proceedings of the National Academy of Sciences* **108,** 10190–10195 (2011).

71. Tondera, D. *et al.* SLP-2 is required for stress-induced mitochondrial hyperfusion. *The EMBO Journal* **28,** 1589–1600 (2009).

72. Ono, T., Isobe, K., Nakada, K. & Hayashi, J.-I. Human cells are protected from mitochondrial dysfunction by complementation of DNA products in fused mitochondria. *Nature Genetics* **28,** 272–275 (2001).

73. Nakada, K. *et al.* Inter-mitochondrial complementation: Mitochondria-specific system preventing mice from expression of disease phenotypes by mutant mtDNA. *Nature Medicine* **7,** nm0801_934 (2001).

74. Chen, H. *et al.* Mitochondrial fusion is required for mtDNA stability in skeletal muscle and tolerance of mtDNA mutations. *Cell* **141,** 280–289 (2010).

75. Mishra, P. & Chan, D. C. Metabolic regulation of mitochondrial dynamics. *Journal of Cell Biology* **212,** 379–387 (2016).

76. Chen, H., Chomyn, A. & Chan, D. C. Disruption of fusion results in mitochondrial heterogeneity and dysfunction. *Journal of Biological Chemistry* **280,** 26185–26192 (2005).

77. Rahn, J. J., Stackley, K. D. & Chan, S. S. Opa1 is required for proper mitochondrial metabolism in early development. *PLoS ONE* **8**, e59218 (2013).

78. Lee, S. et al. Mitofusin 2 is necessary for striatal axonal projections of midbrain dopamine neurons. *Human Molecular Genetics* **21**, 4827–4835 (2012).

79. Papanicolaou, K. N. et al. Mitofusins 1 and 2 are essential for postnatal metabolic remodeling in heart. *Circulatory Research* **111,** 1012–1026 (2012).

80. Tilokani, L., Nagashima, S., Paupe, V. & Prudent, J. Mitochondrial dynamics: overview of molecular mechanisms. *Essays In Biochemistry* **62,** 341–360 (2018).

81. Wakabayashi, J. *et al.* The dynamin-related GTPase Drp1 is required for embryonic and brain development in mice. *The Journal of Cell Biology* **186,** 805–816 (2009).

82. Parone, P. A. *et al.* Preventing mitochondrial fission impairs mitochondrial function and leads to loss of mitochondrial DNA. *PLoS ONE* **3,** e3257 (2008).

83. Shirihai, O. S., Song, M. & Gerald, D. How mitochondrial dynamism orchestrates mitophagy. *Circulation Research* **116,** 1835–1849 (2015).

84. Rath, E., Moschetta, A. & Haller, D. Mitochondrial function — gatekeeper of intestinal epithelial cell homeostasis. *Nature Reviews Gastroenterology* **15**, 497–516 (2018).

85. Ming, S. C. & Goldman, H. Pathology of gastrointestinal tract. William and Wilkins 13–33 (1998).

86. Rao, J. N. & Wang, J. Y. Regulation of gastrointestinal mucosal growth. Morgan and Claypool (2010).

87. Johansson, M. E., Sjövall, H. & Hansson, G. C. The gastrointestinal mucus system in health and disease. *Nature Reviews Gastroenterology & Hepatology* **10,** 352 (2013).

88. Johansson, M. E. et al. The inner of the two Muc2 mucin-dependent mucus layers in colon is devoid of bacteria. *Proceedings of the National Academy of Science* **105,** 15064–15069 (2008).

89. Mastroianni, J. R. & Ouellette, A. J. α-Defensins in enteric innate immunity functional Paneth cell α-Defensins in mouse colonic lumen. *Journal of Biological Chemistry* **284**, 27848–27856 (2009).

90. Fehlbaum, P., Rao, M., Zasloff, M. & Anderson, M. G. An essential amino acid induces epithelial β-defensin expression. *Proceedings of the National Academy of Sciences* **97**, 12723–12728 (2000).

91. Abreu, M. T., Fukata, M. & Arditi, M. TLR Signaling in the gut in health and disease. *The Journal of Immunology* **174**, 4453–4460 (2005).

92. Feldman, N., Rotter-Maskowitz, A. & Okun, E. DAMPs as mediators of sterile inflammation in aging-related pathologies. *Ageing Research Reviews* **24**, 29–39 (2015).

93. Fukata, M. & Arditi, M. The role of pattern recognition receptors in intestinal inflammation. *Mucosal Immunology* **6**, 451 (2013).

94. Pasparakis, M. Role of NF-κB in epithelial biology. *Immunology Reviews* **246**, 346–358 (2012).

95. Osaki, L. H. & Gama, P. MAPKs and signal transduction in the control of gastrointestinal epithelial cell proliferation and differentiation. *International Journal of Molecular Sciences* **14**, 10143–10161 (2013).

96. Farache, J., Zigmond, E., Shakhar, G. & Jung, S. Contributions of dendritic cells and macrophages to intestinal homeostasis and immune defense. *Immunology and Cell Biology* **91**, 232 (2013).

97. Pabst, O. & Bernhardt, G. The puzzle of intestinal lamina propria dendritic cells and macrophages. *European Journal of Immunology* **40**, 2107–2111 (2010).

98. Mann, E. R. & Li, X. Intestinal antigen-presenting cells in mucosal immune homeostasis: Crosstalk between dendritic cells, macrophages and B-cells. *World Journal of Gastroenterology* **20**, 9653–9664 (2014).

99. Reber, L., Sibilano, R., Mukai, K. & Galli, S. Potential effector and immunoregulatory functions of mast cells in mucosal immunity. *Mucosal Immunology* **8**, 444 (2015).

100. Parra, J. et al. Memory of natural killer cells: a new chance against Mycobacterium tuberculosis? *Frontiers in Immunology* **8**, 967 (2017).

101. Roediger, W. E. . The colonic epithelium in ulcerative colitis: an energy-deficiency disease? *The Lancet* **316**, 712–715 (1980).

102. Wang, A. *et al.* Targeting mitochondria-derived reactive oxygen species to reduce epithelial barrier dysfunction and colitis. *The American Journal of Pathology* **184,** 2516–2527 (2014).

103. Nazli, A. *et al.* Epithelia under metabolic stress perceive commensal bacteria as a threat. *The American Journal of Pathology* **164,** 947–957 (2004).

104. Bär, F. *et al.* Mitochondrial gene polymorphisms that protect mice from colitis. *Gastroenterology* **145,** 1055-1063.e3 (2013).

105. Rodríguez-Colman, M. J. *et al.* Interplay between metabolic identities in the intestinal crypt supports stem cell function. *Nature* **543,** 424 (2017).

106. Schell, J. C. *et al.* Control of intestinal stem cell function and proliferation by mitochondrial pyruvate metabolism. *Nature Cell Biology* **19,** 1027–1036 (2017).

107. Kaiko, G. E. *et al.* The colonic crypt protects stem cells from microbiota-derived metabolites. *Cell* **165,** 1708–1720 (2016).

108. Laass, M. W., Roggenbuck, D. & Conrad, K. Diagnosis and classification of Crohn's disease. *Autoimmunity Reviews* **13,** 467–471 (2014).

109. Conrad, K., Roggenbuck, D. & Laass, M. W. Diagnosis and classification of ulcerative colitis. *Autoimmunity Reviews* **13,** 463–466 (2014).

110. Levine, A. *et al.* Pediatric modification of the Montreal classification for inflammatory bowel disease: the Paris classification. *Inflammatory Bowel Diseases* **17,** 1314 (2011).

111. Jostins, L. *et al.* Host–microbe interactions have shaped the genetic architecture of inflammatory bowel disease. *Nature* **491,** 119 (2012).

112. Liu, J. Z. *et al.* Association analyses identify 38 susceptibility loci for inflammatory bowel disease and highlight shared genetic risk across populations. *Nature Genetics* **47,** 979–986 (2015).

113. Ogura, Y. *et al.* A frameshift mutation in NOD2 associated with susceptibility to Crohn's disease. *Nature* **411,** 603 (2001).

114. Cooney, R. *et al.* NOD2 stimulation induces autophagy in dendritic cells influencing bacterial handling and antigen presentation. *Nature Medicine* **16,** 90–97 (2009).

115. Travassos, L. H. *et al.* Nod1 and Nod2 direct autophagy by recruiting ATG16L1 to the plasma membrane at the site of bacterial entry. *Nature Immunology* **11,** ni.1823 (2009).

116. Matsuzawa-Ishimoto, Y. *et al.* Autophagy protein ATG16L1 prevents necroptosis in the intestinal epithelium. *Journal of Experimental Medicine* **214,** jem.20170558 (2017).

117. Alegre-Abarrategui, J. & Wade-Martins, R. Parkinson disease, LRRK2 and the endocytic-autophagic pathway. *Autophagy* **5,** 1208–10 (2009).

118. Liu, Z. *et al.* The kinase LRRK2 is a regulator of the transcription factor NFAT that modulates the severity of inflammatory bowel disease. *Nature Immunology* **12,** 1063 (2011).

119. Brest, P. *et al.* A synonymous variant in IRGM alters a binding site for miR-196 and causes deregulation of IRGM-dependent xenophagy in Crohn's disease. *Nature Genetics* **43,** 242 (2011).

120. Roy, S. *et al.* Villin-1 and gelsolin regulate changes in actin dynamics that affect cell survival signaling pathways and intestinal inflammation. *Gastroenterology* **154,** (2018).

121. Karayiannakis, A. J. *et al.* Expression of catenins and E-cadherin during epithelial restitution in inflammatory bowel disease. *Journal of Pathology* **185,** 413–418 (1998).

122. Chen, W. *et al.* Disruption of the HNF-4 gene, expressed in visceral endoderm, leads to cell death in embryonic ectoderm and impaired gastrulation of mouse embryos. *Genes & Development* **8,** 2466–2477 (1994).

123. Cattin, A.-L. *et al.* Hepatocyte nuclear factor 4α, a key factor for homeostasis, cell architecture, and barrier function of the adult intestinal epithelium. *Molecular Cell Biology* **29,** 6294–6308 (2009).

124. Pickard, J. M., Zeng, M. Y., Caruso, R. & Núñez, G. Gut microbiota: role in pathogen colonization, immune responses, and inflammatory disease. *Immunological Reviews* **279,** 70–89 (2017).

125. Lewis, J. D. *et al.* Inflammation, antibiotics, and diet as environmental stressors of the gut microbiome in pediatric Crohn's disease. *Cell Host & Microbe* **18,** 489–500 (2015).

126. Palmela, C. *et al.* Adherent-invasive Escherichia coli in inflammatory bowel disease. *Gut* **67,** 574–587 (2018).

127. Hall, A. *et al.* A novel Ruminococcus gnavus clade enriched in inflammatory bowel disease patients. *Genome Medicine* **9,** 103 (2017).

128. Ananthakrishnan, A. N. *et al.* Environmental triggers in IBD: a review of progress and evidence. *Nature Reviews Gastroenterology and Hepatology* **15,** 39 (2017).

129. Solomon, L. *et al.* The dextran sulphate sodium (DSS) model of colitis: an overview. *Comparative Clinical Pathology* **19,** 235–239 (2010).

130. Kitajima, S., Takuma, S. & Morimoto, M. Histological Analysis of murine colitis induced by dextran sulfate sodium of different molecular weights. *Experimental Animals* **49,** 9–15 (2000).

131. Okayasu, I. et al. A novel method in the induction of reliable experimental acute and chronic ulcerative colitis in mice. *Gastroenterology* **98**, 694–702 (1990).

132. Ni, J., Chen, S. & Hollander, D. Effects of dextran sulphate sodium on intestinal epithelial cells and intestinal lymphocytes. *Gut* **39,** 234–241 (1996).

133. Laroui, H. *et al.* Dextran sodium sulfate (DSS) induces colitis in mice by forming nano-lipocomplexes with medium-chain-length fatty acids in the colon. *PLoS ONE* **7,** e32084 (2012).

134. Hawkins, J. V. *et al.* Protease Activity in a hapten-induced model of ulcerative colitis in rats. *Digestive Diseases and Sciences* **42,** 1969–1980 (1997).

135. Vasina, V. et al. Effects of the non-peptidyl low molecular weight radical scavenger IAC in DNBS-induced colitis in rats. *European Journal of Pharmacology* **614**, 137–145 (2009).

136. Haj-Mirzaian, A. et al. Anxiety- and depressive-like behaviors are associated with altered hippocampal energy and inflammatory status in a mouse model of Crohn's disease. *Neuroscience* **366**, 124–137 (2017).

137. Chapman, M. et al. Butyrate oxidation is impaired in the colonic mucosa of sufferers of quiescent ulcerative colitis. *Gut* **35**, 73–76 (1994).

138. Duffy, M. et al. Mucosal metabolism in ulcerative colitis and Crohn's disease. *Diseases of the Colon & Rectum* **41**, 1399 (1998).

139. Roediger, W. & Nance, S. Metabolic induction of experimental ulcerative colitis by inhibition of fatty acid oxidation. *British Journal of Experimental Pathology* **67**, 773–82 (1986).

140. Shekhawat, P. S. et al. Spontaneous development of intestinal and colonic atrophy and inflammation in the carnitine-deficient jvs (OCTN2−/−) mice. *Molecular Genetics and Metabolism* **92**, 315–324 (2007).

141. Santhanam, S. *et al.* Mitochondrial electron transport chain complex dysfunction in the colonic mucosa in ulcerative colitis. *Inflammatory Bowel Diseases* **18,** 2158 (2012).

142. Gillis, L. A. & Sokol, R. J. Gastrointestinal manifestations of mitochondrial disease. *Gastroenterology Clinics of North America* **32**, 789–817 (2003).

143. Rahman, S. Gastrointestinal and hepatic manifestations of mitochondrial disorders. *Journal of Inherited Metabolic Diseases* **36**, 659–673 (2013).

144. Chitkara, D. K., Nurko, S., offner, J., Buie, T. & Flores, A. Abnormalities in gastrointestinal motility are associated with diseases of oxidative phosphorylation in children. *American Journal of Gastroenterology* **98**, ajg2003204 (2003).

145. Cruz, C. S. & Kang, M.-J. Mitochondrial dysfunction and damage associated molecular patterns (DAMPs) in chronic inflammatory diseases. *Mitochondrion* **41**, 37–44 (2017).

146. Liu, Q., Zhang, D., Hu, D., Zhou, X. & Zhou, Y. The role of mitochondria in NLRP3 inflammasome activation. *Molecular Immunology* **103**, 115–124 (2018).

147. Mao, L. et al. Loss-of-function CARD8 mutation causes NLRP3 inflammasome activation and Crohn's disease. *Journal of Clinical Investigation* **128**, 1793–1806 (2018).

148. Hazeldine, J., Hampson, P., Opoku, F., Foster, M. & Lord, J. M. N-Formyl peptides drive mitochondrial damage associated molecular pattern induced neutrophil activation through ERK1/2 and P38 MAP kinase signalling pathways. *Injury* **46**, 975–984 (2015).

149. Boyapati, R. K. et al. Mitochondrial DNA Is a Pro-Inflammatory Damage-Associated Molecular Pattern Released During Active IBD. *Inflammatory Bowel Diseases* (2018). doi:10.1093/ibd/izy095

150. Qi, X., Qvit, N., Su, Y.-C. & Mochly-Rosen, D. A novel Drp1 inhibitor diminishes aberrant mitochondrial fission and neurotoxicity. *Journal of Cell Science* **126,** 789–802 (2013).

151. Chang, J. et al. Impaired intestinal permeability contributes to ongoing bowel symptoms in patients with inflammatory bowel disease and mucosal healing. *Gastroenterology* **153**, 723-731.e1 (2017).

152. Shavrov, A. et al. A pilot study of confocal laser endomicroscopy to predict barrier dysfunction and relapse in pediatric inflammatory bowel disease. *Journal of Pediatric Gastroenterology & Nutrition* **62**, 873–878 (2016).

153. Tornai, T. et al. Gut barrier failure biomarkers are associated with poor disease outcome in patients with primary sclerosing cholangitis. *World Journal of Gastroenterology* **23**, 5412–5421 (2017).

154. Yu, L. Microbiota dysbiosis and barrier dysfunction in inflammatory bowel disease and colorectal cancers: exploring a common ground hypothesis. *Journal of Biomedical Science* **25**, 79 (2018).

155. Lee, J. Y. et al. Molecular pathophysiology of epithelial barrier dysfunction in inflammatory bowel diseases. *Proteomes* **6**, 17 (2018).

156. Khalili, H. et al. The role of diet in the aetiopathogenesis of inflammatory bowel disease. *Nature Reviews Gastroenterology & Hepatology* **15**, 1–11 (2018).

157. Mehta, M., Ahmed, S. & Dryden, G. Immunopathophysiology of inflammatory bowel disease: how genetics link barrier dysfunction and innate immunity to inflammation. *Innate Immunity* **23**, 497–505 (2017).

158. Shawki, A. & McCole, D. F. Mechanisms of intestinal epithelial barrier dysfunction by adherent-invasive Escherichia coli. *CMGH Cellular and Molecular Gastroenterology and Hepatology* **3**, 41–50 (2017).

159. Lee, J.-H. et al. Mitochondrial respiratory dysfunction induces claudin-1 expression via reactive oxygen species-mediated heat shock factor 1 activation, leading to hepatoma cell invasiveness. *Journal of Biological Chemistry* **290**, 21421–21431 (2015).

160. Suenaert, P. et al. Anti-tumor necrosis factor treatment restores the gut barrier in Crohn's disease. *The American Journal of Gastroenterology* **97**, 2000–4 (2002).

161. Carlsson, A. H. et al. Faecalibacterium prausnitzii supernatant improves intestinal barrier function in mice DSS colitis. *Scandinavian Journal of Gastroenterology* **48**, 1136–1144 (2013).

162. Fischer, A. et al. Adalimumab prevents barrier dysfunction and antagonizes distinct effects of TNF-α on tight junction proteins and signaling pathways in intestinal epithelial cells. *American Journal of Physiology Gastrointestinal and Liver Physiology* **304**, G970–G979 (2013).

163. Terciolo, C. et al. Saccharomyces boulardii CNCM I-745 restores intestinal barrier integrity by regulation of E-cadherin recycling. *Journal of Crohn's & Colitis* (2017). doi:10.1093/ecco-jcc/jjx030

164. Woo, J. et al. Fermented barley and soybean (BS) mixture enhances intestinal barrier function in dextran sulfate sodium (DSS)-induced colitis mouse model. *BMC Complementary and Alternative Medicine* **16**, 498 (2016).

165. JanssenDuijghuijsen, L. M. et al. Mitochondrial ATP depletion disrupts Caco-2 monolayer integrity and internalizes claudin 7. *Frontiers in Physiology* **8**, 794 (2017).

166. Brand, M. D. & Nicholls, D. G. Assessing mitochondrial dysfunction in cells. *Biochemistry Journal* **435**, 297–312 (2011).

167. Makrecka-Kuka, M., Krumschnabel, G. & Gnaiger, E. High-resolution respirometry for simultaneous measurement of oxygen and hydrogen peroxide fluxes in permeabilized cells, tissue homogenate and isolated mitochondria. *Biomolecules **l*** **5**, 1319–1338 (2015).

168. Gnaiger E. Mitochondrial pathways and respiratory control. An introduction to OXPHOS analysis. 4th ed. *Mitochondrial Physiology Network* 19.12. Oroboros MiPNet Publications, Innsbruck:80 pp. (2014)

169. Gnaiger E. O2k Quality Control 1: Polarographic oxygen sensors and accuracy of calibration. *Mitochondrial Physiology Network* 06.03(17):1-20. (2018)

170. Kuznetsov, A. V. et al. Analysis of mitochondrial function in situ in permeabilized muscle fibers, tissues and cells. *Nature Protocols* **3**, nprot.2008.61 (2008).

171. Renner K, Amberger A, Konwalinka G, Kofler R, Gnaiger E (2003) Changes of mitochondrial respiration, mitochondrial content and cell size after induction of apoptosis in leukemia cells. *Biochim Biophys Acta* 1642:115–123

172. Steinlechner-Maran R, Eberl T, Kunc M, Schrocksnadel H, Margreiter R, Gnaiger E (1997) Respiratory defect as an early event in preservation/reoxygenation injury in endothelial cells. *Transplantation* **63**:136–142

173. Harris, E. & Manger, J. Intersubstrate competitions and evidence for compartmentation in mitochondria. *Biochemical Journal* **113**, 617–628 (1969).

174. Stepanova, A., Shurubor, Y., Valsecchi, F., Manfredi, G. & Galkin, A. Differential susceptibility of mitochondrial complex II to inhibition by oxaloacetate in brain and heart. *Biochimica et Biophysica Acta (BBA) - Bioenergetics* **1857**, 1561–1568 (2016).

175. Doerrier C., Garcia-Souza L.F., Krumschnabel G., Wohlfarter Y., Mészáros A.T., Gnaiger E. High-resolution fluorespirometry and OXPHOS protocols for human cells, permeabilized fibers from small biopsies of muscle, and isolated mitochondria. In: Palmeira C., Moreno A. (eds) Mitochondrial Bioenergetics. *Methods in Molecular Biology*, vol 1782. Humana Press, New York, NY (2018).

176. Andriamihaja, M., Chaumontet, C., Tome, D. & Blachier, F. Butyrate metabolism in human colon carcinoma cells: Implications concerning its growth-inhibitory effect. *Journal of Cell Physiology* **218,** 58–65 (2009).

177. Wiki.oroboros.at. *O2k-Publications: Topics - Bioblast*. [online] Available at: http://wiki.oroboros.at/index.php/O2k-Publications:_Topics [Accessed 19 Mar. 2019].

178. Noble, C. L. *et al.* The contribution of OCTN1/2 variants within the IBD5 locus to disease susceptibility and severity in Crohn's disease. *Gastroenterology* **129,** 1854–1864 (2005).

179. Patlevič, P., Vašková, J., Švorc, P., Vaško, L. & Švorc, P. Reactive oxygen species and antioxidant defense in human gastrointestinal diseases. *Integrative Medicine Research* **5**, 250–258 (2016).

180. Eichele, D. D. & Kharbanda, K. K. Dextran sodium sulfate colitis murine model: An indispensable tool for advancing our understanding of inflammatory bowel diseases pathogenesis. *World Journal of Gastroenterology* **23**, 6016–6029 (2017).

181. Araki, Y. et al. Dextran sulfate sodium administered orally is depolymerized in the stomach and induces cell cycle arrest plus apoptosis in the colon in early mouse colitis. *Oncology Reports* **28**, 1597–1605 (2012).

182. Damiani, C. R. et al. Oxidative stress and metabolism in animal model of colitis induced by dextran sulfate sodium. *Journal of Gastroenterology and Hepatology* **22**, 1846–1851 (2007).

183. Yeganeh, R. P. et al. Apple peel polyphenols reduce mitochondrial dysfunction in mice with DSS-induced ulcerative colitis. *Journal of Nutritional Biochemistry* **57**, 56–66 (2018).

184. Matondo, A. & Kim, S. Targeted-mitochondria antioxidants therapeutic implications in inflammatory bowel disease. *Journal of Drug Targeting* 1–30 (2017). doi:10.1080/1061186X.2017.1339196

185. Ramos, E., Larsson, N.-G. & Mourier, A. Bioenergetic roles of mitochondrial fusion. *Biochimica et Biophysica Acta (BBA) - Bioenergetics* **1857**, 1277–1283 (2016).

186. Meyer, J. N., Leuthner, T. C. & Luz, A. L. Mitochondrial fusion, fission, and mitochondrial toxicity. *Toxicology* **391**, 42–53 (2017).

187. Joshi, A. U., Ebert, A. E., Haileselassie, B. & Mochly-Rosen, D. Drp1/Fis1-mediated mitochondrial fragmentation leads to lysosomal dysfunction in cardiac models of Huntington's disease. *Journal of Molecular and Cellular Cardiology* (2018). doi:10.1016/j.yjmcc.2018.12.004

188. Su, Y.-C. & Qi, X. Inhibition of excessive mitochondrial fission reduced aberrant autophagy and neuronal damage caused by LRRK2 G2019S mutation. *Human Molecular Genetics* **22**, 4545–4561 (2013).

189. Zhao, Y., Sun, X. & Qi, X. Inhibition of Drp1 hyperactivation reduces neuropathology and behavioral deficits in zQ175 knock-in mouse model of Huntington's disease. *Biochemical and Biophysical Research Communications* **507,** 319–323 (2018).

190. Li, X., Jevnikar, A. M. & Grant, D. R. Expression of functional ICAM-1 and VCAM-1 adhesion molecules by an immortalized epithelial cell clone derived from the small intestine. *Cellular Immunology* **175**, 58–66 (1997).

191. Eilenberger, C. et al. Optimized alamarBlue assay protocol for drug dose-response determination of 3D tumor spheroids. *MethodsX* **5**, 781–787 (2018).

192. O'Brien, J., Wilson, I., Orton, T. & Pognan, F. Investigation of the Alamar Blue (resazurin) fluorescent dye for the assessment of mammalian cell cytotoxicity. *European Journal of Biochemistry* 267, 5421–5426 (2000).

193. Mitrakas, A. G., Kalamida, D. & Koukourakis, M. I. Effect of mitochondrial metabolism-interfering agents on cancer cell mitochondrial function and radio/chemosensitivity. *Anti-Cancer Drugs* 25, 1182 (2014).

194. Kuepper, J., Zobel, S., Wierckx, N. & Blank, L. M. A rapid method to estimate NADH regeneration rates in living cells. *Journal of Microbiological Methods* 130, 92–94 (2016).

195. Doerrier, C., Sumbalova, Z., Krumschnabel, G. & Gnaiger, E. SUIT reference protocol for OXPHOS analysis by high-resolution respirometry. *Mitochondrial Physiology Network* 1–12

196. Ojuka, E. et al. Measurement of β-oxidation capacity of biological samples by respirometry: a review of principles and substrates. *American Journal of Physiology Endocrinology and Metabolism* **310**, E715–E723 (2016).

197. Chatel-Chaix, L. et al. Dengue virus perturbs mitochondrial morpho dynamics to dampen innate immune responses. *Cell Host Microbe* (2016). doi:10.1016/j.chom.2016.07.008

198. Toyama, E. Q. et al. Metabolism. AMP-activated protein kinase mediates mitochondrial fission in response to energy stress. *Science* **351**, 275–281 (2016).

199. Fan, F. & Wood, K. V. Bioluminescent assays for high-throughput screening. *Assay and Drug Development Technologies* **5**, 127–136 (2007).

200. Scaduto, R. C. & Grotyohann, L. W. Measurement of mitochondrial membrane potential using fluorescent rhodamine derivatives. *Biophysical Journal* **76**, 469–477 (1999).

201. Rambold, A. S., Cohen, S. & Lippincott-Schwartz, J. Fatty acid trafficking in starved cells: regulation by lipid droplet lipolysis, autophagy, and mitochondrial fusion dynamics. *Developmental Cell* **32**, 678–692 (2015).

202. Sedlackova, L. & Korolchuk, V. I. Mitochondrial quality control as a key determinant of cell survival. *Biochimica Et Biophysica Acta BBA - Molecular Cell Research* (2018). doi:10.1016/j.bbamcr.2018.12.012

203. Gergely, P. et al. Mitochondrial hyperpolarization and ATP depletion in patients with systemic lupus erythematosus. *Arthritis & Rheumatism* **46**, 175–190 (2002).

204. Eberhardson, M. *et al.* Toward improved control of inflammatory bowel disease. *Scandinavian Journal of Immunology* e12745 (2018). doi:10.1111/sji.12745

205. Neurath, M. F. Current and emerging therapeutic targets for IBD. *Nature Reviews Gastroenterology* **14**, 269–278 (2017).

206. Rezaie, A., Kuenzig, M. & Benchimol, E. Budesonide for induction of remission in Crohn's disease. *Cochrane Database* (2015). doi:10.1002/14651858.cd000296.pub4/abstract

207. Waljee, A. K. et al. Corticosteroid use and complications in a US inflammatory bowel disease cohort. *PLOS ONE* **11**, e0158017 (2016).

208. Lichtenstein, G. R., Abreu, M. T., Cohen, R., Tremaine, W. American Gastroenterological Association Institute technical review on corticosteroids, immunomodulators, and infliximab in inflammatory bowel disease. *Gastroenterology* **130**, 940–987 (2006).

209. Marinkovi, G., Hamers, A. A., de Vries, C. J. & de Waard, V. 6-Mercaptopurine reduces macrophage activation and gut epithelium proliferation through inhibition of GTPase Rac1. *Inflammatory Bowel Diseases* **20,** 1487–1495 (2014).

210. Tiede, I. et al. CD28-dependent Rac1 activation is the molecular target of azathioprine in primary human CD4+ T lymphocytes. *The Journal of Clinical Investigation* **111**, (2003).

211. Steiner, S. *et al.* Cyclosporine A regulates pro-inflammatory cytokine production in ulcerative colitis. *Archivum Immunologiae et Therapiae Experimentalis* **63,** 53–63 (2015).

212. Nielsen, C., Albertsen, L., Bendtzen, K. & Baslund, B. Methotrexate induces poly(ADP-ribose) polymerase-dependent, caspase 3-independent apoptosis in subsets of proliferating CD4+ T cells. *Clinical & Experimental Immunology* **148**, 288–295 (2007).

213. Wessels, J., Huizinga, T. & Guchelaar, H.-J. Recent insights in the pharmacological actions of methotrexate in the treatment of rheumatoid arthritis. *Rheumatology* **47,** 249–255 (2008).

214. Colombel, J. *et al.* Early mucosal healing with infliximab is associated with improved long-term clinical outcomes in ulcerative colitis. *Gastroenterology* **141,** 1194–201 (2011).

215. Schnitzler, F. *et al.* Mucosal healing predicts long-term outcome of maintenance therapy with infliximab in Crohn's disease. *Inflammatory Bowel Diseases* **15,** 1295–1301 (2009).

216. Colombel, J. *et al.* Adalimumab induces deep remission in patients with Crohn's disease. *Clinical Gastroenterology and Hepatology* **12,** (2014).

217. Sandborn, W. J. *et al.* Adalimumab induces and maintains clinical remission in patients with moderate-to-severe ulcerative colitis. *Gastroenterology* **142,** 257-265.e3 (2012).

218. Peyrin–Biroulet, L. et al. Efficacy and safety of tumor necrosis factor antagonists in Crohn's disease: meta-analysis of placebo-controlled trials. *Clinical Gastroenterology and Hepatology* **6**, 644–653 (2008).

219. Dubinsky, M. C. *et al.* 6-MP metabolite profiles provide a biochemical explanation for 6-MP resistance in patients with inflammatory bowel disease. *Gastroenterology* **122,** 904–915 (2002).

220. Odenwald, M. A. & Turner, J. R. The intestinal epithelial barrier: a therapeutic target? *Nature Reviews Gastroenterology & Hepatology* **14,** 9–21 (2016).

221. Michielan, A. & D'Incà, R. Intestinal permeability in inflammatory bowel disease: pathogenesis, clinical evaluation, and therapy of leaky gut. *Mediators of Inflammation*, 1–10 (2015).

222. Ukabam, S. O., Clamp, J. R. & Cooper, B. T. Abnormal small intestinal permeability to sugars in patients with Crohn's disease of the terminal ileum and colon. *Digestion* **27**, 70–74 (1983).

223. Pearson, A., Eastham, E., Laker, M., Craft, A. & Nelson, R. Intestinal permeability in children with Crohn's disease and coeliac disease. *British Medical Journal Clinical Research* Ed **285**, 20 (1982).

224. Martini, E., Krug, S. M., Siegmund, B., Neurath, M. F. & Becker, C. Mend your fences the epithelial barrier and its relationship with mucosal immunity in inflammatory bowel disease. *Cell and Molecular Gastroenterology Hepatology* **4**, 33–46 (2017).

225. Guo, W. et al. Asiatic acid ameliorates dextran sulfate sodium-induced murine experimental colitis via suppressing mitochondria-mediated NLRP3 inflammasome activation. *International Immunopharmacology* **24**, 232–238 (2015).

226. Dashdorj, A. et al. Mitochondria-targeted antioxidant MitoQ ameliorates experimental mouse colitis by suppressing NLRP3 inflammasome-mediated inflammatory cytokines. *BMC Medicine* **11**, 178 (2013).

227. Liu, X. et al. Dimethyl fumarate ameliorates dextran sulfate sodium-induced murine experimental colitis by activating Nrf2 and suppressing NLRP3 inflammasome activation. *Biochemical Pharmacology* **112**, 37–49 (2016).

228. Liu, L. et al. The pathogenic role of NLRP3 inflammasome activation in inflammatory bowel diseases of both mice and humans. *Journal of Crohn's and Colitis* (2016). doi:10.1093/ecco-jcc/jjw219

229. Ruiz, P. A. et al. Titanium dioxide nanoparticles exacerbate DSS-induced colitis: role of the NLRP3 inflammasome. *Gut* **66**, 1216 (2017).

230. Feng, Y., Wang, Y., Wang, P., Huang, Y. & Wang, F. Short-chain fatty acids manifest stimulative and protective effects on intestinal barrier function through the inhibition of NLRP3 inflammasome and autophagy. *Cellular Physiology and Biochemistry* **49**, 190–205 (2018).

231. Storr, M. et al. Differential effects of CB1 neutral antagonists and inverse agonists on gastrointestinal motility in mice. *Neurogastroenterology & Motility* **22**, 787-e223 (2010).

232. Arai, T., Lopes, F., Shute, A., Wang, A. & McKay, D. M. Young mice expel the tapeworm Hymenolepis diminuta and are protected from colitis by triggering a memory response with worm antigen. *American Journal of Physiology Gastrointestinal and Liver Physiology* (2018). doi:10.1152/ajpgi.00295.2017

233. Park, C. M., Reid, P. E., Walker, D. C. & MacPherson, B. R. A simple, practical 'swiss roll' method of preparing tissues for paraffin or methacrylate embedding. *Journal of Microscopy* **145**, 115–120 (1987).

234. Khan, A. A., Alsahli, M. A. & Rahmani, A. H. Myeloperoxidase as an active disease biomarker: recent biochemical and pathological perspectives. *Medical Sciences* **6**, 33 (2018).

235. Diaz-Granados, N., Howe, K., Lu, J. & McKay, D. M. Dextran sulfate sodium-induced colonic histopathology, but not altered epithelial ion transport, is reduced by inhibition of phosphodiesterase activity. *The American Journal of Pathology* **156**, 2169–2177 (2000).

236. Dulai, P. S., Singh, S., Casteele, N. V., Boland, B. S. & Sandborn, W. J. How will evolving future therapies and strategies change how we position the use of biologics in moderate to severely active inflammatory bowel disease. *Inflammatory Bowel Diseases* **22**, 998–1009 (2016).

237. Matsuoka, K. et al. Evidence-based clinical practice guidelines for inflammatory bowel disease. *Journal of Gastroenterology* **53**, 305–353 (2018).

238. Trottier, M. D., Irwin, R., Li, Y., McCabe, L. R. & Fraker, P. J. Enhanced production of early lineages of monocytic and granulocytic cells in mice with colitis. *Proceedings of the National Academy of Science* **109**, 16594–16599 (2012).

239. Morampudi, V. et al. DNBS/TNBS colitis models: providing insights into inflammatory bowel disease and effects of dietary fat. *Journal of Visualized Experiments* (2014). doi:10.3791/51297

240. Dothel, G., Vasina, V., Barbara, G. & Ponti, F. Animal models of chemically induced intestinal inflammation: predictivity and ethical issues. *Pharmacology and Therapeutics* **139**, 71–86 (2013).

241. Hussein, R. M. & Saleh, H. Promising therapeutic effect of gold nanoparticles against dinitrobenzene sulfonic acid-induced colitis in rats. *Nanomedicine* (2018). doi:10.2217/nnm-2018-0009

242. Casili, G. et al. Dimethyl fumarate reduces inflammatory responses in experimental colitis. *Journal of Crohn's and Colitis* **10**, 472–483 (2016).

243. Khairy, H., Saleh, H., Badr, A. M. & Marie, M.-A. S. Therapeutic efficacy of osthole against dinitrobenzene sulphonic acid induced-colitis in rats. *Biomedicine and Pharmacotherapy* **100**, 42–51 (2018).

244. Cunningham, K. E. et al. Peroxisome proliferator-activated receptor-γ coactivator 1-α (PGC1α) protects against experimental murine colitis. *Journal of Biological Chemistry* **291**, 10184–10200 (2016).

245. Amrouche-Mekkioui, I. & Djerdjouri, B. N-acetylcysteine improves redox status, mitochondrial dysfunction, mucin-depleted crypts and epithelial hyperplasia in dextran sulfate sodium-induced oxidative colitis in mice. *European Journal of Pharmacology* **691**, 209–217 (2012).

246. Murthy, S. K., James, P. D., Antonova, L., Chalifoux, M. & Tanuseputro, P. High end of life health care costs and hospitalization burden in inflammatory bowel disease patients: A population-based study. *PLoS One* **12**, e0177211 (2017).

247. Becker, H. M. et al. Living with inflammatory bowel disease: A Crohns and colitis Canada survey. *Canadian Journal of Gastroenterology and Hepatology* **29**, 77–84 (2015).

248. Chang, S. & Hanauer, S. Optimizing pharmacologic management of inflammatory bowel disease. *Expert Review of Clinical Pharmacology* 1–13 (2017). doi:10.1080/17512433.2017.1318062

249. Renna, S., Cottone, M. & Orlando, A. Optimization of the treatment with immunosuppressants and biologics in inflammatory bowel disease. *World Journal of Gastroenterology* **20**, 9675–9690 (2014).

250. Martinez-Montiel, María et al. Pharmacologic therapy for inflammatory bowel disease refractory to steroids. *Clinical and Experimental Gastroenterology* Volume **8**, 257–269 (2015).

251. Danese, S., Vuitton, L. & Peyrin-Biroulet, L. Biologic agents for IBD: practical insights. *Nature Reviews Gastroenterology* **12**, 537–545 (2015).

252. Digitonin. *Digitonin – Bioblast* Available at: http://wiki.oroboros.at/index.php/Digitonin. (Accessed: 29th March 2019)

253. Leonel, A. J. & Alvarez-Leite, J. I. Butyrate: implications for intestinal function. *Current Opinion in Clinical Nutrition and Metabolic Care* **15**, 474–479 (2012).

254. Zhang, L. et al. Sodium butyrate protects against high fat diet-induced cardiac dysfunction and metabolic disorders in type II diabetic mice. *Journal of Cellular Biochemistry* **118**, 2395–2408 (2017).

255. Negroni, A., Cucchiara, S. & Stronati, L. Apoptosis, necrosis, and necroptosis in the gut and intestinal homeostasis. *Mediators of Inflammation* 1–10 (2015).

256. Skulachev, V. Bioenergetic aspects of apoptosis, necrosis and mitoptosis. *Apoptosis* **11**, 473–485 (2006).

257. Poritz, L. S. et al. Loss of the tight junction protein ZO-1 in dextran sulfate sodium induced colitis. *Journal of Surgical Research* **140**, 12–19 (2007).

258. Kitajima, S., Takuma, S. & Morimoto, M. Changes in colonic mucosal permeability in mouse colitis induced with dextran sulfate sodium. *Experimental Animal* **48**, 137–143 (1999).

259. Ahmad et al. Butyrate and glucose metabolism by colonocytes in experimental colitis in mice. *Gut* **46**, 493–499 (2000).

260. Valdez, L. B., Zaobornyj, T. & Boveris, A. Mitochondrial metabolic states and membrane potential modulate mtNOS activity. *Biochimica et Biophysica Acta BBA - Bioenergetics* **1757,** 166–172 (2006).

261. Zorova, L. D. et al. Mitochondrial membrane potential. *Analytical Biochemistry* **552**, (2018).

262. Samak, G. et al. Calcium/Ask1/MKK7/JNK2/c-Src signalling cascade mediates disruption of intestinal epithelial tight junctions by dextran sulfate sodium. *Biochemical Journal* **465**, 503–515 (2015).

263. Gangwar, R. et al. Calcium-mediated oxidative stress: a common mechanism in tight junction disruption by different types of cellular stress. *Biochemical Journal* **474**, 731–749 (2017).

264. Patron, M. et al. The mitochondrial calcium uniporter (MCU): molecular identity and physiological roles. *Journal of Biological Chemistry* **288**, 10750–10758 (2013).

265. Wu, K. et al. Perturbation of Akt Signaling, mitochondrial potential, and ADP/ATP ratio in acidosis-challenged rat cortical astrocytes. *Journal of Cellular Biochemistry* **118**, 1108–1117 (2017).

266. Liu, M.-J., Wang, Z., Ju, Y., Wong, R. & Wu, Q.-Y. Diosgenin induces cell cycle arrest and apoptosis in human leukemia K562 cells with the disruption of Ca2+ homeostasis. *Cancer Chemotherapy and Pharmacology* **55**, 79–90 (2005).

267. Liu, M.-J., Yue, P., Wang, Z. & Wong, R. Methyl protodioscin induces G2/M arrest and apoptosis in K562 cells with the hyperpolarization of mitochondria. *Cancer Letters* **224**, 229–241 (2005).

268. Arbo, M. et al. In vitro neurotoxicity evaluation of piperazine designer drugs in differentiated human neuroblastoma SH-SY5Y cells. *Journal of Applied Toxicology* **36**, 121–130 (2016).

269. Matarrese, P. et al. Clostridium difficile toxin B causes apoptosis in epithelial cells by thrilling mitochondria involvement of ATP-sensitive mitochondrial potassium channels. *Journal of Biological Chemistry* **282**, 9029–9041 (2007).

270. Tanaka, K. et al. Ca^{2+} buffering capacity of mitochondria after oxygen-glucose deprivation in hippocampal neurons. *Neurochemical Research* **34**, 221–226 (2009).

271. Iijima, T. et al. Calcium loading capacity and morphological changes in mitochondria in an ischemic preconditioned model. *Neuroscience Letters* **448**, 268–272 (2008).

272. Hurst, S., Hoek, J. & Sheu, S.-S. Mitochondrial Ca^{2+} and regulation of the permeability transition pore. *Journal of Bioenergetics and Biomembranes* **49**, 27–47 (2017).

273. Zorov, D. B., Juhaszova, M. & Sollott, S. J. Mitochondrial ROS-induced ROS release: An update and review. *Biochimica et Biophysica Acta BBA - Bioenergetics* **1757**, 509–517 (2006).

274. Huang, Q. et al. Mitochondrial fission forms a positive feedback loop with cytosolic calcium signaling pathway to promote autophagy in hepatocellular carcinoma cells. *Cancer Letters* **403**, (2017).

275. Matarrese, P. et al. Galectin-1 sensitizes resting human T lymphocytes to Fas (CD95)-mediated cell death via mitochondrial hyperpolarization, budding, and fission. *Journal of Biological Chemistry* **280**, 6969–6985 (2005).

276. Kaddour-Djebbar, I. et al. Specific mitochondrial calcium overload induces mitochondrial fission in prostate cancer cells. *International Journal of Oncology* **36**, (2010).

277. Strober, W. Why study animal models of IBD. *Inflammatory Bowel Diseases* **14**, S129–S131 (2008).

278. Kiesler, P., Fuss, I. J. & Strober, W. Experimental models of inflammatory bowel diseases. *CMGH Cellular and Molecular Gastroenterology and Hepatology* **1**, 154–170 (2015).

279. Wirtz, S. et al. Chemically induced mouse models of acute and chronic intestinal inflammation. *Nature Protocols* **12**, 1295–1309 (2017).

280. Mizoguchi, E., Nguyen, D. & Low, D. Animal models of ulcerative colitis and their application in drug research. *Drug Design, Development and The*rapy **7**, 1341–1357 (2013).

281. Lukas, G., Brindle, S. & Greengard, P. The route of absorption of intraperitoneally administered compounds. *Journal of Pharmacology and Experimental Therapeutics* **178**, 562–4 (1971).

282. Marco, D. T. & Levine, R. Role of the lymphatics in the intestinal absorption and distribution of drugs. *Journal of Pharmacology and Experimental Therapeutics* **169**, 142–51 (1969).

283. Banks, W. A. From blood–brain barrier to blood–brain interface: new opportunities for CNS drug delivery. *Nature Reviews Drug Discovery* **15**, nrd.2015.21 (2016).

284. Serlin, Y., Shelef, I., Knyazer, B. & Friedman, A. Anatomy and physiology of the blood–brain barrier. *Seminars in Cell and Developmental Biology* **38**, 2–6 (2015).

285. Latorre, R., Sternini, C., Giorgio, D. R. & Meerveld, G. B. Enteroendocrine cells: a review of their role in brain–gut communication. *Neurogastroenterology and Motility* **28**, 620–630 (2016).

286. Powell, N., Walker, M. M. & Talley, N. J. The mucosal immune system: master regulator of bidirectional gut-brain communications. *Nature Reviews Gastroenterology* **14**, 143–159 (2017).

287. Reichmann, F. et al. Dextran sulfate sodium-induced colitis alters stress-associated behaviour and neuropeptide gene expression in the amygdala-hippocampus network of mice. *Scientific Reports* **5**, 9970 (2015).

288. Jain, P. et al. Behavioral and molecular processing of visceral pain in the brain of mice: impact of colitis and psychological stress. *Frontiers in Behavioral Neuroscience* **9**, 177 (2015).

289. Nyuyki, K. D., Cluny, N. L., Swain, M. G., Sharkey, K. A. & Pittman, Q. J. Altered Brain Excitability and Increased Anxiety in Mice with Experimental Colitis: Consideration of Hyperalgesia and Sex Differences. *Frontiers in Behavioral Neuroscience* **12**, 58 (2018).

290. Do, J. & Woo, J. From gut to brain: alteration in inflammation markers in the brain of dextran sodium sulfate-induced colitis model mice. *Clinical Psychopharmocology and Neuroscience* **16**, 422–433 (2018).

291. Heiden, M. G., Cantley, L. C. & Thompson, C. B. Understanding the Warburg effect: the metabolic requirements of cell proliferation. *Science* **324**, 1029–1033 (2009).

292. Kalyanaraman, B. Teaching the basics of cancer metabolism: developing antitumor strategies by exploiting the differences between normal and cancer cell metabolism. *Redox Biology* **12**, 833–842 (2017).

293. Mollica, M. *et al.* Butyrate regulates liver mitochondrial function, efficiency, and dynamic, in insulin resistant obese mice. *Diabetes* **66,** db160924 (2017).

294. Harwig, M. C. *et al.* Methods for imaging mammalian mitochondrial morphology: a prospective on MitoGraph. *Analytical Biochemistry* **552,** 81–99 (2018).

295. Bento, A. et al. Evaluation of chemical mediators and cellular response during acute and chronic gut inflammatory response induced by dextran sodium sulfate in mice. *Biochemical Pharmacology* **84**, 1459–1469 (2012).

296. Bolhassani, A., Jafarzade, B. & Mardani, G. In vitro and in vivo delivery of therapeutic proteins using cell penetrating peptides. *Peptides* **87**, 50–63 (2017).

297. Li, H., Tsui, T. & Ma, W. Intracellular delivery of molecular cargo using cell-penetrating peptides and the combination strategies. *International Journal of Molecular Sciences* **16**, 19518–19536 (2015).

298. Fernando, E. H. et al. A simple, cost-effective method for generating murine colonic 3D enteroids and 2D monolayers for studies of primary epithelial cell function. *American Journal of Physiology Gastroenterology and Liver Physiology* **313**, G467–G475 (2017).

299. In, J. et al. Enterohemorrhagic Escherichia coli reduces mucus and intermicrovillar bridges in human stem cell-derived colonoids. *CMGH Cellular and Molecular Gastroenterology and Hepatology* **2**, 48-62.e3 (2016).

300. Vancraenenbroeck, R. & Webb, M. R. A Fluorescent, Reagentless Biosensor for ATP, Based on Malonyl-Coenzyme A Synthetase. *ACS Chemical Biology* **10**, 2650–2657 (2015).

301. Vancraenenbroeck, R., Kunzelmann, S. & Webb, M. R. Development of a range of fluorescent reagentless biosensors for ATP, based on malonyl-coenzyme A synthetase. *PLoS One* **12**, e0179547 (2017).

302. Bartolomé F., Abramov A.Y. (2015) Measurement of Mitochondrial NADH and FAD Autofluorescence in Live Cells. In: Weissig V., Edeas M. (eds) Mitochondrial Medicine. *Methods in Molecular Biology*, vol 1264. Humana Press, New York, NY

Appendix A

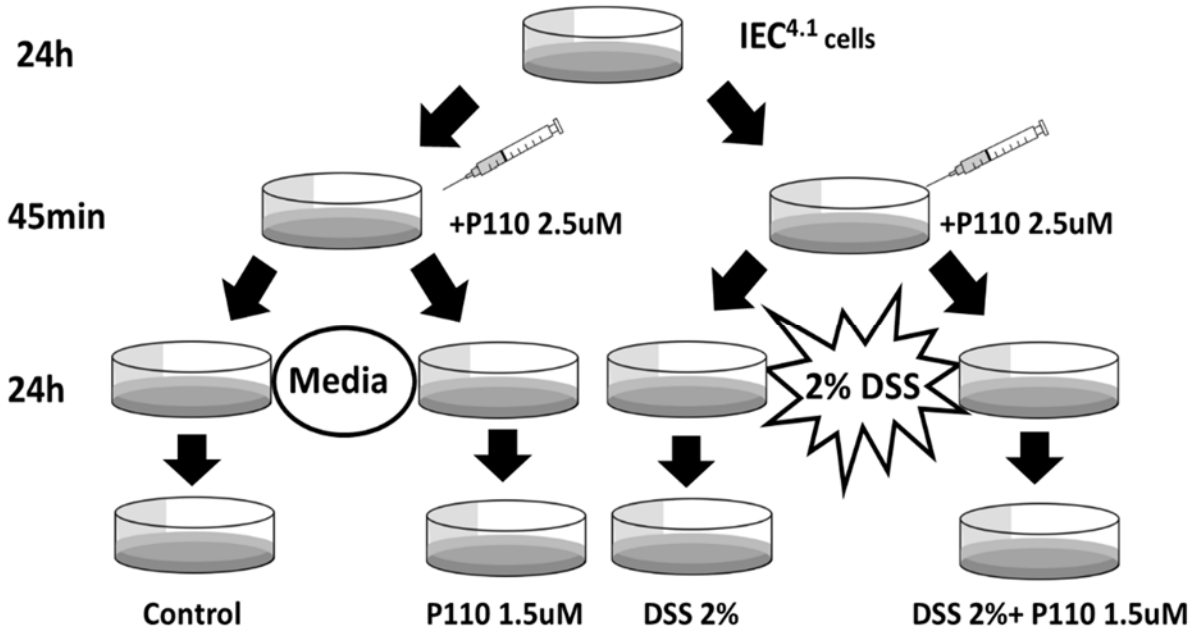

Figure A.1: Schematic of *in-vitro* DSS±P110 treatment regime for IEC$^{4.1}$ cells prior to further experimentation. Cells were seeded at 62 500 cells/cm^2.

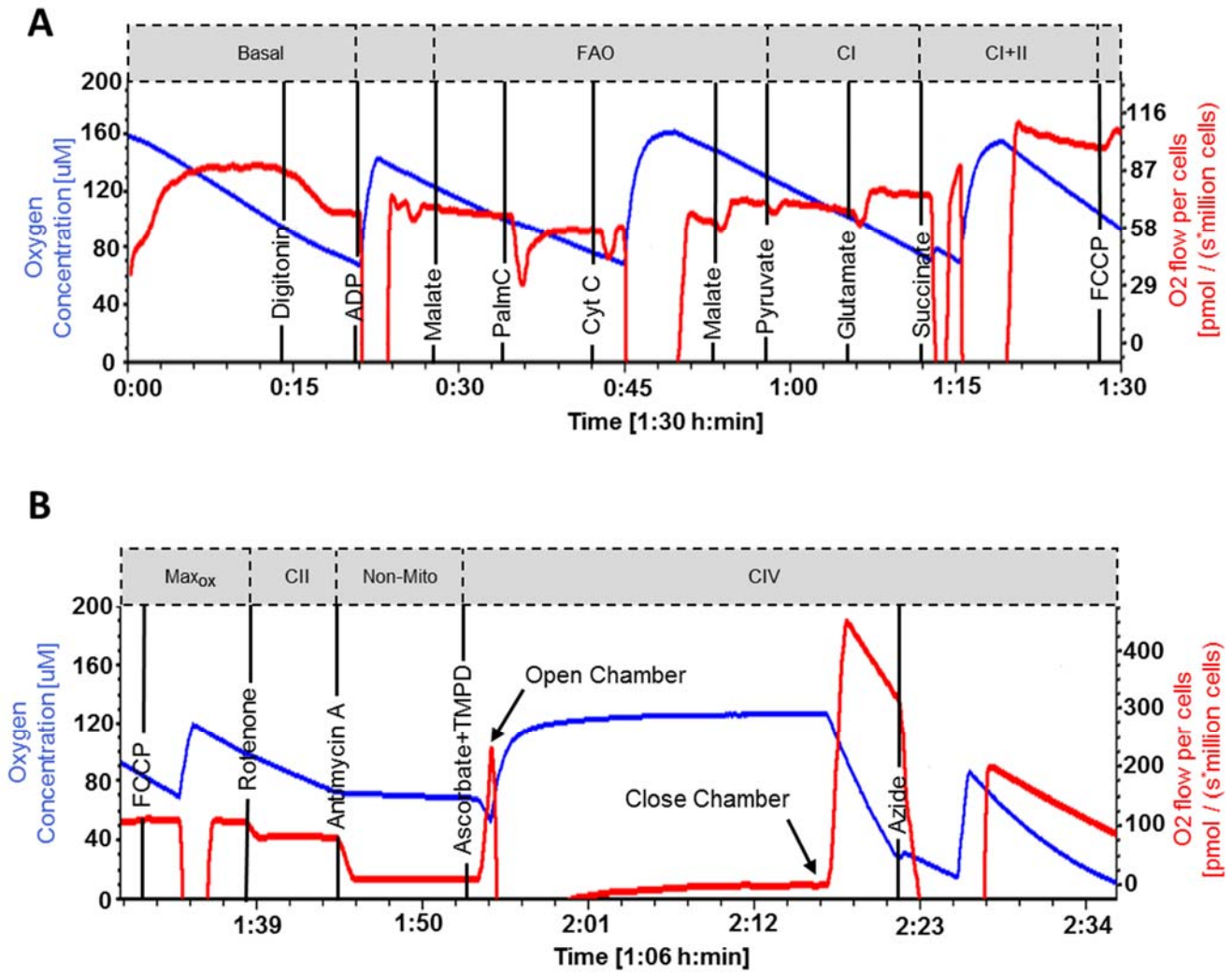

Figure A.2: Control cell representative tracing during the modified SUIT-002 protocol for analysis of mitochondrial respiration in IEC[4.1] cells treated with DSS±P110. Protocol begins with Panel A and is continued in Panel B. Panel A shows respirometric changes associated with permeabilization, fatty acid oxidation (FAO), CI and CII linked titrations, while Panel B shows respirometric changes during maximum oxidative phosphorylation (MAXOX), non-mitochondrial respiration (Non-Mito) and CIV assessment. Cells were permeabilized with digitonin (4µg/mL) and allowed to respire for 5 mins prior to further titrations. This was followed by ADP (2.5mM) to ensure state 3 respiration for future substrates. Long chain fatty acid oxidation (FAO) was examined next with titrations of malate (0.1mM) and palmitoylcarnitine (PalmC, 50µM). Cytochrome c (5mM) was then added to identify if OMM damage occurred from digitonin permeabilization. Saturating concentrations of malate (2mM) allowed maximal FAO to be

examined, at the expense of some CI involvement. Titrations of pyruvate (5mM) and glutamate (10mM) were added to saturate NADH linked substrates and associated CI activity. Addition of succinate (>10mM) saturates $FADH_2$ linked respiration associated with CII. Sequential titrations of FCCP (μM) allow Max OXPHOS to be identified. Rotenone (0.5μM) allows the CII exclusive respiration to be identified by inhibiting CI. After rotenone, titration of antimycin A (2.5μM) leads to mitochondrial respiratory inhibition. Activity of mitochondrial complex IV can be determined by the titration of ascorbate (2mM) and (TMPD, 0.5mM). Due to dramatic shifts in oxygen consumption from autoxidation of ascorbate/TMPD and activity of CIV, the Oxygraph-2k chambers were opened for 20 mins to limit hypoxia. After 20 mins, Oxygraph-2k chambers were closed and oxygen consumption related to CIV+ ascorbate autoxidation was allowed to proceed for 4-5 mins. To correct for auto-oxidation of ascorbate and TMPD, sodium azide (100mM) was titrated to inhibit CIV. Once inhibited oxygen consumption related to ascorbate and TMPD autoxidation can be isolated and subtracted from oxygen consumption obtained during CIV+ascorbate+TMPD to get CIV activity.

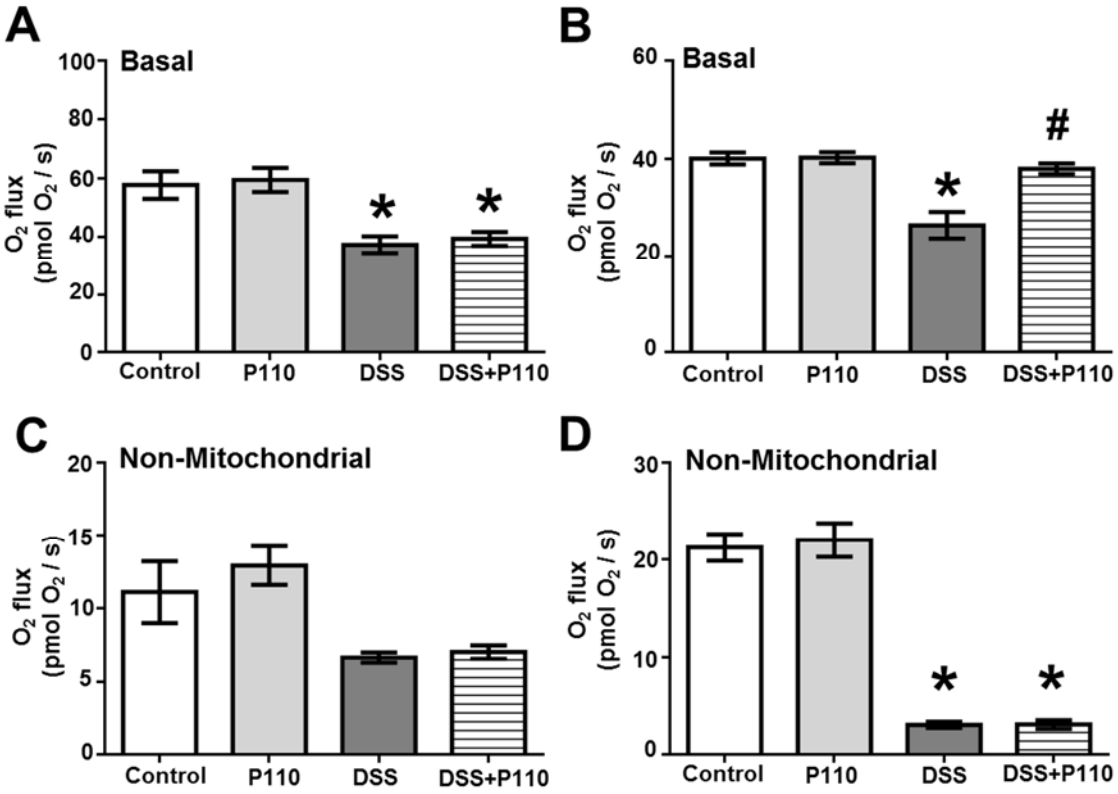

Figure A.3: O_2 flux of $IEC^{4.1}$ cells during basal and non-mitochondrial respiration after 24h DSS±P110 treatments. Graphs A & B represent O_2 flux of cells after digitonin permeabilization (basal) for the modified SUIT-002 and SCFA protocols respectively. Graph C & D show O_2 flux of cells after rotenone and antimycin A titrations (Non-mitochondrial respiration) for the modified SUIT-002 and SCFA protocols respectively. Data is represented as mean ± SEM, Graphs A & C, n = 6-8 replicates from 3 independent experiments; Graphs B & D, n = 6-8 replicates from 2-3 independent experiments. *Represents significant differences between the control group, #Represents significant differences between the DSS groups, $p<0.05$, One-Way ANOVA, Tukey's multiple comparison test.

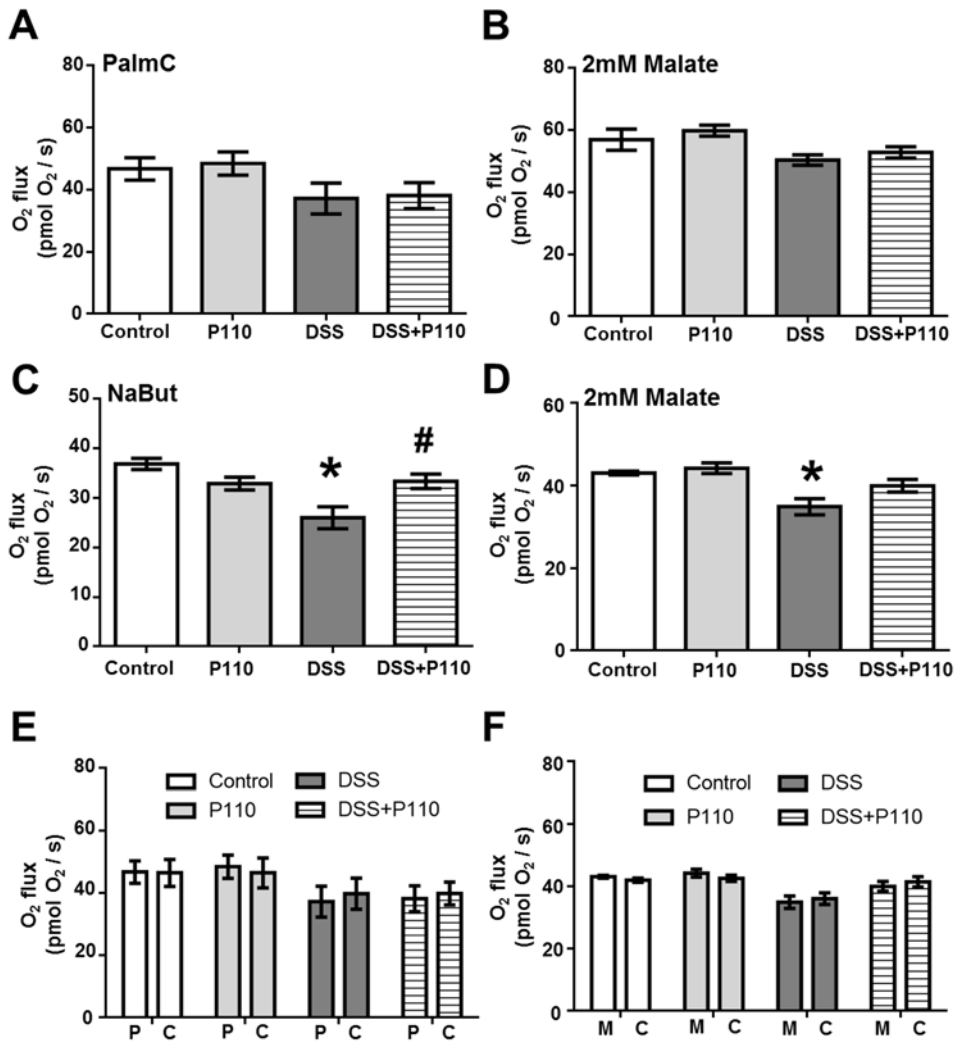

Figure A.4: O_2 flux of IEC$^{4.1}$ cells during LCFA/SCFA beta oxidation after 24h DSS±P110 treatments. Graphs A, B & E represents O_2 flux of cells during the LCFA component of the SUIT-002 protocol: A) 0.05mM PalmC B) 2mM malate E) cytochrome C test. Graphs C, D & F represents the O_2 flux of cells during a separate SCFA protocol C) 2mM sodium butyrate (NaBut) D) 2mM malate F) cytochrome C test. Graphs E & F present O_2 flux of cells after titrations of (P) PalmC and (C) cytochrome c or (M) malate and (C) cytochrome c. Data is represented as mean ± SEM, Graphs A, B & E, n = 6-8 replicates from 3 independent experiments; Graphs C, D, F, n = 6-8 replicates from 2-3 independent experiments. *Represents significant differences between the control group, #Represents significant differences between the DSS groups, $p<0.05$, A-D) One-Way ANOVA, Tukey's multiple comparison test, E & F) Repeated measures Two-Way ANOVA, Sidak's multiple comparison test.

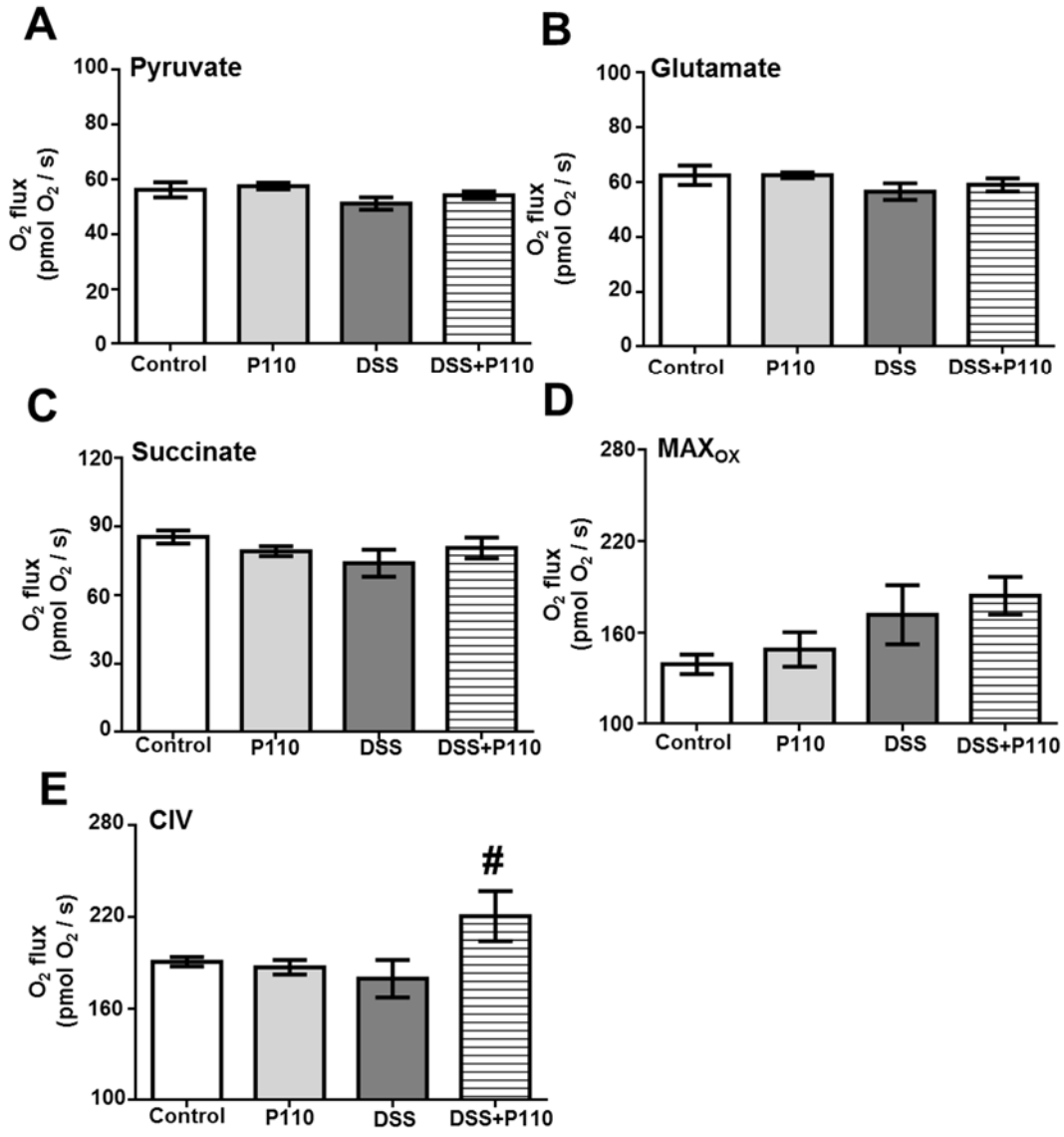

Figure A.5: O_2 flux of 24h DSS±P110 treated IEC$^{4.1}$ cells in the presence of chemicals linked to CI, CII, MAX_{OX} & CIV during the modified SUIT-002 protocol. Graphs represent O_2 flux of cells after the following titrations: A) 5mM pyruvate B) 10mM glutamate C) 10mM succinate D) 0.3-0.6µM FCCP. Graph E) represents O_2 flux in the presence of 2mM ascorbate & 0.5mM TMPD subtracted by the O_2 flux after CIV inhibition with 100mM sodium azide. Data is represented as mean ± SEM, n = 6-8 replicates from 3 independent experiments. *Represents significant differences between the control group, #Represents significant differences between the DSS groups, $p<0.05$, One-Way ANOVA, Tukey's multiple comparison test.

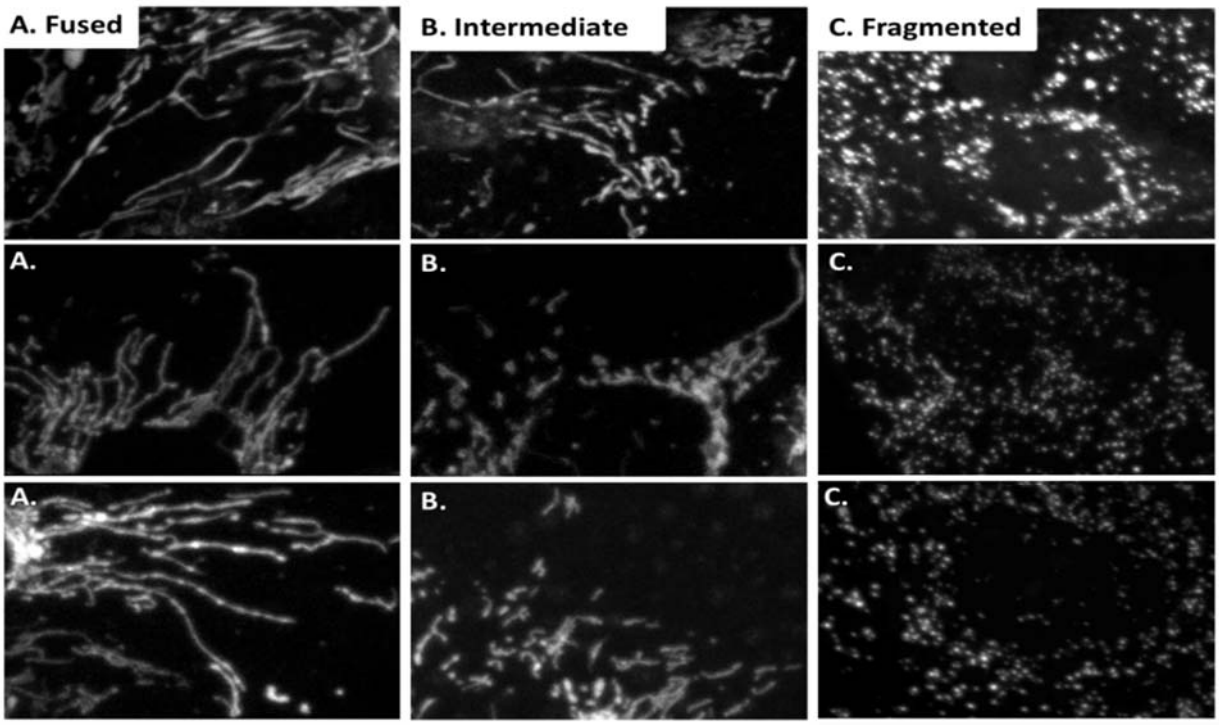

Figure A.6: Representative images for the categorization of mitochondrial networks: A) Fused B) Intermediate C) Fragmented. Images were taken and provided by Nicole Mancini.

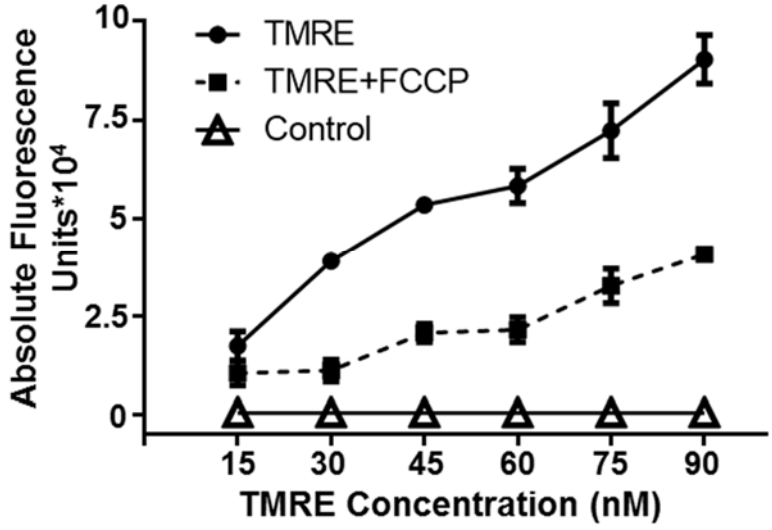

Figure A.7: Optimization of TMRE dye concentration to ensure limited non-specific binding of TMRE[49]